Towards Convex Economic Model Predictive Individual Pitch Control for Wind Turbine Load Mitigation

R.T.O. Dinkla

Master of Science Thesis

TU Delft Delft University of Technology

Delft Center for Systems and Control

Towards Convex Economic Model Predictive Individual Pitch Control for Wind Turbine Load Mitigation

Master of Science Thesis

For the degree of Master of Science in Systems and Control at Delft University of Technology

R.T.O. Dinkla

April 16, 2021

Faculty of Mechanical, Maritime and Materials Engineering (3mE) · Delft University of Technology

Delft University of Technology
Department of
Delft Center for Systems and Control (dcsc)

The undersigned hereby certify that they have read and recommend to the Faculty of Mechanical, Maritime and Materials Engineering (3mE) for acceptance a thesis entitled

Towards Convex Economic Model Predictive Individual Pitch Control for Wind Turbine Load Mitigation

by

R.T.O. Dinkla

in partial fulfillment of the requirements for the degree of

Master of Science Systems and Control

Dated: April 16, 2021

Supervisor(s):

Prof. dr. ir. Jan-Willem van Wingerden

Ir. Atindriyo K. Pamososuryo

Reader(s):

Dr. Riccardo M. G. Ferrari

Abstract

Wind turbines offer an appealing method for power generation. In the fight against global warming wind energy helps realise green house gas emission reduction targets. Moreover, given a globally increasing demand for energy, the role of wind energy is set to become even more important. Historically, the cost of wind energy has decreased significantly, making it more competitive with respect to fossil fuels. This trend is set to continue thanks in part to a driving factor, which is the increasing size of wind turbines.

However, there are several impediments to the upscaling of wind turbine sizes. The larger, more flexible wind turbine components experience greater loads. To mitigate increasing fatigue loading, which limits the lifetime of components, thereby increasing the cost of wind energy, smart control methodologies are needed.

The existing literature indicates that individual pitch control (IPC) offers good perspectives for fatigue load mitigation. An interesting approach to performing IPC is by means of model predictive control (MPC). Unlike conventional IPC implementations, MPC offers the designer a more intuitive way to evaluate trade-offs between, e.g., power generation and load mitigation. In addition, an important advantage of MPC is its ability to handle constraints explicitly.

A particularly interesting application of MPC for wind turbine operation concerns convex economic model predictive control (CEMPC). By means of a simple change of variables, the normally troublesome nonlinear dynamics are transformed into linear dynamics. As a result, relevant optimization problems can be reformulated in a convex fashion. The formulation of such a convex optimization problem is useful because such problems enable a global optimum to be found, and can be solved relatively efficiently.

Unfortunately, the existing CEMPC framework is limited to collective pitch control (CPC). To facilitate further load reduction, it would be useful to extend the CEMPC framework to the domain of IPC. This thesis therefore seeks to investigate how the existing CEMPC framework can be extended to the domain of IPC for the purpose of wind turbine load mitigation. It is shown that an improved CPC implementation of CEMPC can be extended to IPC by considering a blade-effective wind speed and CPC-equivalent aerodynamic power for each blade. With regards to load reduction, a case study of out-of-plane blade root bending

moment fatigue load mitigation indicates several important difficulties that require further investigation. Arguably the most important impediment for future load reduction prospects within CEMPC using IPC is the inability to consider the pitch, which is an important variable to minimize various sorts of loading, as a free optimization variable.

Table of Contents

List of Figures

List of Tables

Acknowledgements

For all of the help and encouragement that I have received throughout my thesis several words of thanks are in order. First and foremost, I would like to thank ir. Atindriyo Pamososuryo for the many hours he has taken to answer my questions and provide me with invaluable feedback. In addition, I would like to express my gratitude towards prof. dr. ir. Jan-Willem van Wingerden for all of the counsel he has provided me with during the course of this thesis. My thanks also go out to dr. ir. Sebastiaan Mulders for reaching out to me about this thesis project and his help with the preceding literature survey.

Met deze thesis brei ik ook een einde aan mijn studententijd. Ik zou graag de Boze Mannen van de Raamstraat willen bedanken voor de vele intrigerende discussies en het nodige vertier dat mij altijd bij zal blijven. Mijn clubgenoten wil ik bedanken voor hun gouden vriendschap en de vele mooie herinneringen die ik nu al hieraan over heb gehouden. Hartelijk dank ook aan de heren van de Da Costastraat die gedurende mijn thesis mij op allerlei manieren, bewust of onbewust, hebben weten te motiveren ondanks alle corona-beperkingen. Met name Sjoerd Gnodde wil ik bij dezen bedanken voor het leveren van nuttige feedback op dit document. Ten slotte wil ik nog mijn familie - Cor, Carla en Marlou - bedanken voor het koesteren van mijn nieuwschierigheid en alle steun en liefde die ze mij altijd hebben geboden.

Delft, University of Technology — R.T.O. Dinkla
April 16, 2021

"I would rather have questions that can't be answered than answers that can't be questioned."

— *Richard P. Feynman*

Chapter 1

Introduction

One of the most significant problems that humankind is currently faced with is global warming. The disastrous consequences of globally increasing temperatures include rising ocean levels, oceanic acidification, large-scale biodiversity loss, and increased risks from extreme weather phenomena in the form of, e.g., heavy precipitation, heat waves, and flooding of coastal areas [1]. To reduce the risks of the changes that result from global warming, countries signed the Paris Agreement in 2015. The agreement attempts to limit the global average temperature rise to 2°C relative to pre-industrial temperatures, and calls on its signatories to try to limit this temperature increase further to 1.5°C [2]. Unfortunately, in one of its most recent reports, the Intergovernmental Panel on Climate Change (IPCC) indicates that not enough progress is being made to accomplish the aforementioned goals; the required changes are unrivalled in terms of both scale and scope [3].

One of these necessary changes concerns the transition from fossil fuels to renewable energy sources like wind energy. To comply with the Paris Agreement, the growth of installed wind power capacity needs to be accelerated. Relative to 2018, total onshore installed wind power capacity needs to triple by 2030, and offshore installed wind power capacity needs to become ten times larger in the same timeframe [4].

One of the main drivers of installed wind power capacity growth are cost reductions, which, in turn, is largely due to increasing wind turbine sizes. This phenomenon is refered to as upscaling, and it is clearly shown in Figure 1-1. There are several reasons why larger wind turbine sizes contribute to decreasing costs. Since the aerodynamic power is proportional to the rotor's swept area and (approximately proportional to) the cube of the wind speed, increasing rotor sizes and hub heights (the latter of which gives access to the greater wind speeds found at higher elevations) allow larger turbines to extract more power from the wind. The smaller number of turbines needed to produce the same amount of power also reduces costs related to, e.g., maintenance and cabling [5].

Unfortunately, there are several impediments to the upscaling process and the cost reductions it can effectuate. For instance, as wind turbines become larger, loads on the turbine's larger components increase. Wind turbine blade loading arises from, for example, gravity,

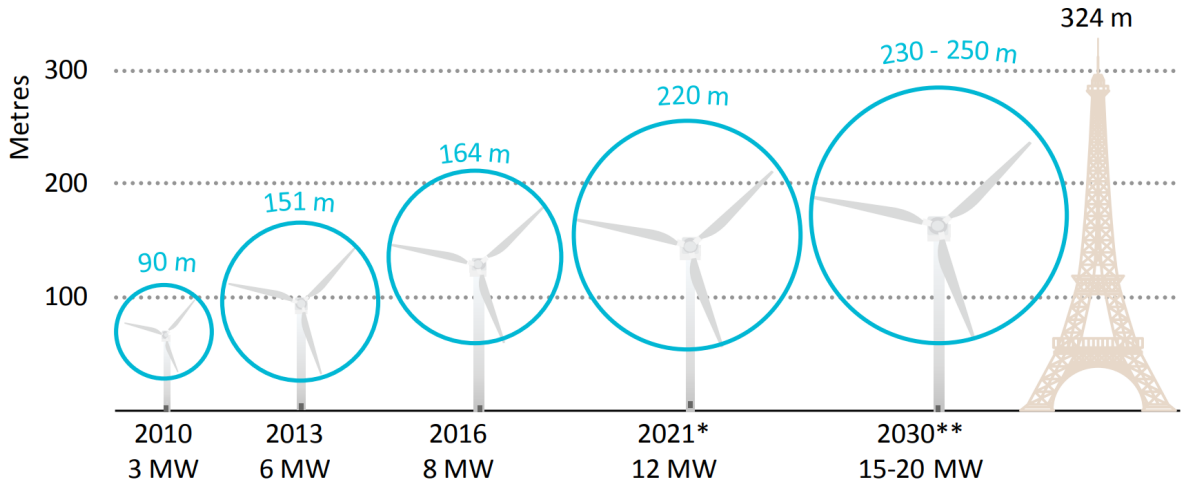

Figure 1-1: Upscaling of wind turbines over time has reduced costs. Larger rotor areas allow more power to be extracted from more wind, and higher hub heights let turbines experience greater average wind speeds. Figure was acquired from [6].

yaw misalignment, as well as (the rotational sampling of) turbulence, wind shear and tower shadow [7]. As blade sizes increase relative to the size of typical turbulence phenomena, the spatial variability of loads along the blades becomes more significant [8]. The increased, more variable loading is particularly problematic because the resulting increase in fatigue damage limits component lifetimes, increasing costs. Moreover, the drive to produce larger parts whilst minimizing material costs has lead turbine components to become more flexible [9]. Besides clear difficulties arising from the combination of larger loads on more flexible structures (larger deflections), the increased component flexibility also increases the coupling between different modes of the turbine's structure [10]. Hence, to facilitate and accelerate the upscaling process, smart control strategies are needed to address the (combination of) increasing component loads and flexibility. The next section will present a literature review of several such smart control methods.

1-1 Literature Review

An active area of research concerns pitch[1] control. In the past, blades were designed to stall during high wind speeds. No pitch actuation was therefore needed. However, this passive form of pitch control placed a relatively large load on wind turbine components and caused fairly large power oscillations [11]. Hence, modern turbines now feature (typically either electric or hydraulic) pitch actuators to provide so called 'active' pitch control [12].

There are two important types of active pitch control, the first of which is named collective pitch control (CPC). This pitching method entails that each of the wind turbine's blades is sent identical pitching commands. CPC has been widely implemented by the wind turbine industry [13] and typically implements a gain-scheduled proportional-integral-derivative (PID) pitch controller to handle the nonlinear wind turbine dynamics [11].

[1] A blade's pitch is the degree of rotation that it has around its own axis. By pitching a blade, the controller makes use of the blade's changing aerodynamic properties at different pitch angles.

The second type of active pitch control is called individual pitch control (IPC). Unlike is the case with CPC, with IPC the pitch signal that is sent to each blade may differ. IPC offers particularly promising perspectives for load reduction because it is especially well-suited to reduce asymetric loading across the rotor, which becomes increasingly significant due to wind turbine upscaling [15]. An example of a typical controller design that makes use of IPC is shown in Figure 1-2. A CPC loop is used to regulate the rotational speed (and thereby power), whilst a complementary IPC feedback loop is used to minimize loading.

The rest of this literature review will focus on IPC because of its beforementioned potential to substantially reduce loads on wind turbine components. In Section 1-1-1, the conventional IPC method, which is based on the multi-blade coordinate (MBC) transformation, is discussed. Section 1-1-2 subsequently presents state-of-the-art alternatives to this conventional form of IPC. Given the limitations of the discussed IPC methods, a particularly promising method called convex economic model predictive control (CEMPC) will be introduced here.

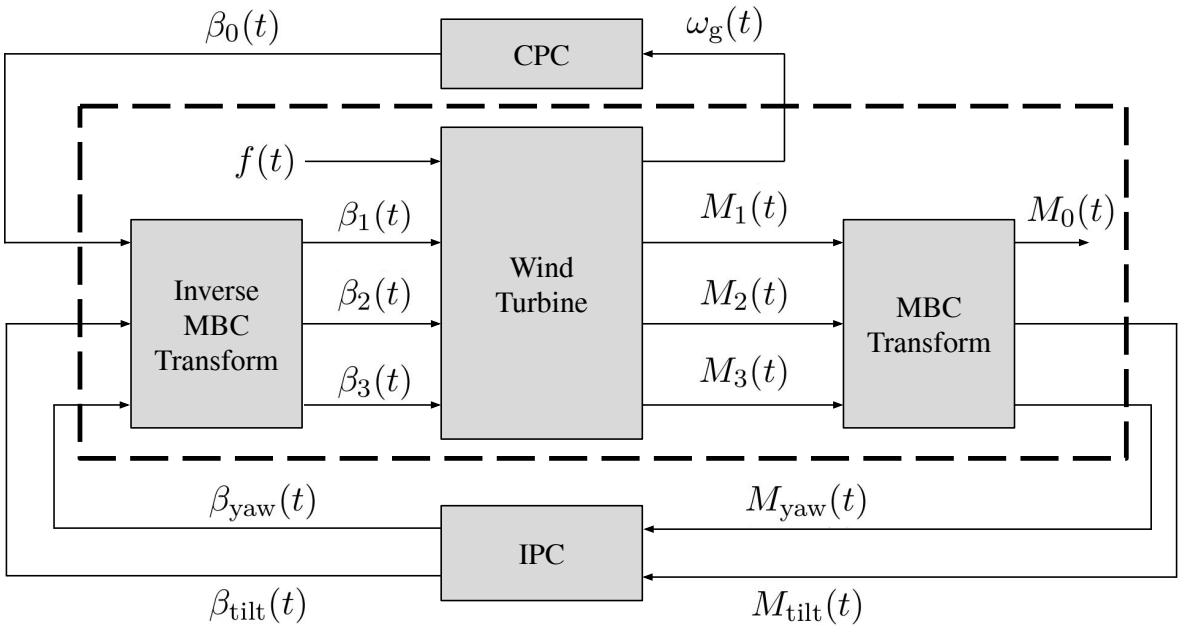

Figure 1-2: A typical individual pitch control (IPC) implementation that makes use of the forward and inverse MBC transformations to minimize loading. The resulting IPC feedback loop complements a CPC loop that regulates the generator speed $\omega_g(t)$ (and thereby the power) by means of a collective pitch $\beta_0(t)$. The MBC transformation transforms the out-of-plane blade root bending moments of the three blades ($M_1(t)$, $M_2(t)$, $M_3(t)$) from the rotating frame to their fixed frame equivalents: an average moment $M_0(t)$, a yaw moment $M_{yaw}(t)$, and a tilt moment $M_{tilt}(t)$. An IPC controller then uses the tilt and yaw moments to produce tilt and yaw pitch signals (β_{tilt} and β_{yaw} respectively). These tilt and yaw pitch angles are subsequently used together with the collective pitch to yield the individual pitch angles of the three blades β_1, β_2, and β_3 via the inverse MBC transformation. Influences on the turbine that are not independently shown in this figure (like the wind speed and generator torque) are represented by $f(t)$. If the turbine dynamics are linearized, the MBC-IPC approach reduces the periodicity of the system within the dashed lines to such an extent that it is often modelled by a linear time-invariant (LTI) system. Figure was adapted from [14].

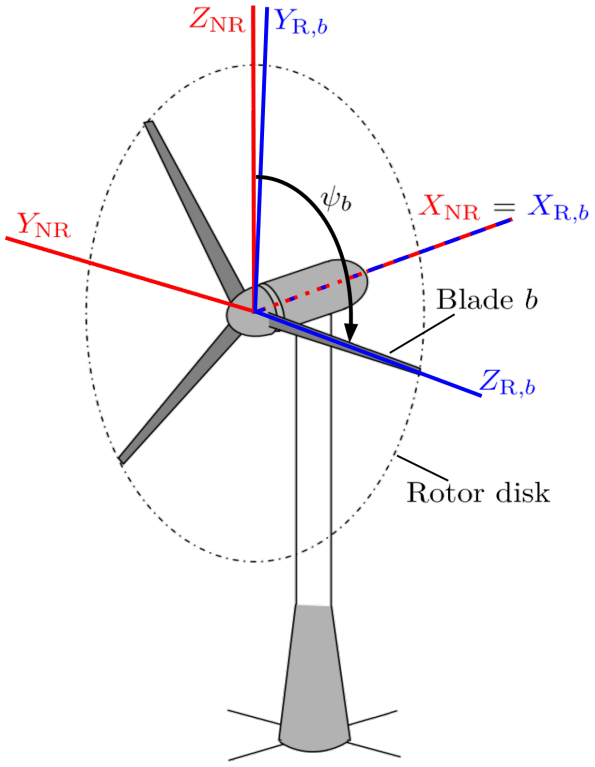

Figure 1-3: The MBC transformation transforms coordinates from the rotating frames of reference of each blade b (one of the three such rotating frames is shown in blue, denoted by subscript 'R,b') to the nonrotating frame of reference (shown in red, denoted by subscript 'NR'). The rotation of each rotating frame of reference is described in terms of the azimuth position ψ_b of its corresponding blade b. The inverse MBC transformation transforms the coordinates from the fixed frame of reference to the rotating frames of reference. The Z_{NR} and Y_{NR} axes are often respectively called the 'yaw' and 'tilt' axes. Figure was inspired by [16] and was adapted from [17].

1-1-1 Conventional IPC: Using the MBC Transformations

Although several IPC methods exist, most IPC methods currently use the multi-blade coordinate (MBC) transformations [14, 15], as shown in Figure 1-2. From this point onwards, this method will be referred to as conventional IPC in this thesis. In effect, the MBC transformations are used to transform Cartesian coordinates between a nonrotating frame of reference and the rotating frames of reference of the individual turbine blades, as shown in Figure 1-3.

The IPC controller in Figure 1-2 often takes the form of two independent proportional-integral (PI) (or even simply integral) controllers. To minimize the coupling between the tilt and yaw axes (Y_{NR} and Z_{NR} respectively in Figure 1-3) an azimuth-offset in the inverse MBC transformation can be applied [18]. A nice feature of the conventional IPC implementation is that upon linearizing the turbine dynamics, the resulting system within the dashed lines of Figure 1-2 has a strongly reduced periodicity with respect to the linearized turbine, and may even be modelled by an LTI system[2]. This is a clear benefit of this method because

[2]For state-of-the-art averaging techniques to obtain such an LTI system, the interested reader may consult [19].

LTI systems are well-understood, and effective control methods for such systems are readily available.

However, the conventional IPC implementation also has several downsides. Notably, it is incapable of handling constraints. Moreover, it is difficult to evaluate trade-offs between competing objectives such as power production and load mitigation because these trade-offs are not described explicitly in the conventional IPC framework.

1-1-2 State-of-the-Art in IPC

Besides applications of the conventional IPC method, multiple other IPC implementations can be found in the existing literature. The trend towards larger, increasingly flexible turbine components makes decoupling of structural modes more difficult, thereby making a clear case for multiple-input multiple-output (MIMO) wind turbine control strategies [20]. Examples of multivariable IPC implementations that have been investigated make use of linear quadratic regulator (LQR) control [21] and linear quadratic Gaussian (LQG) control [22], robust methods like $\mathcal{H}_\infty$ control [23], or ℓ_1-optimal control [24]. Often, such multivariable control implementations still make use of the MBC transformations, in which case they offer an improvement over the conventional IPC framework because they are able to account for the tilt-yaw axis coupling. An important advantage that the above IPC applications have with respect to the conventional IPC method is that objectives are defined explicitly, thereby giving more insight into the various trade-offs that are made [25].

Model Predictive Control for IPC

Another method that has attracted much attention within the domain of IPC is model predictive control (MPC). The MPC framework is illustrated by Figure 1-4 and comprises of four important components [26, 27]:

1. a plant model that is used to be able to make predictions of optimal inputs, states, and outputs for a certain number of steps into the future (the prediction horizon),
2. a cost function to be able to evaluate the performance of a certain sequence of inputs,
3. an optimization algorithm to find the input sequence that corresponds to the lowest cost in accordance with the cost function, and
4. a receding horizon strategy, whereby the first input of the input sequence is implemented and the beginning of the prediction horizon moves ahead to the next time step, from which the process is repeated.

Since the nonlinear dynamics of a wind turbines is often modelled directly in MPC, this method is often used without the MBC transformations. However, MPC applications within the domain of IPC that rely on (multiple) linear models may still opt to employ the MBC transformations to (as is done in [28]) reduce the periodicity of the linear models with respect to the azimuth position.

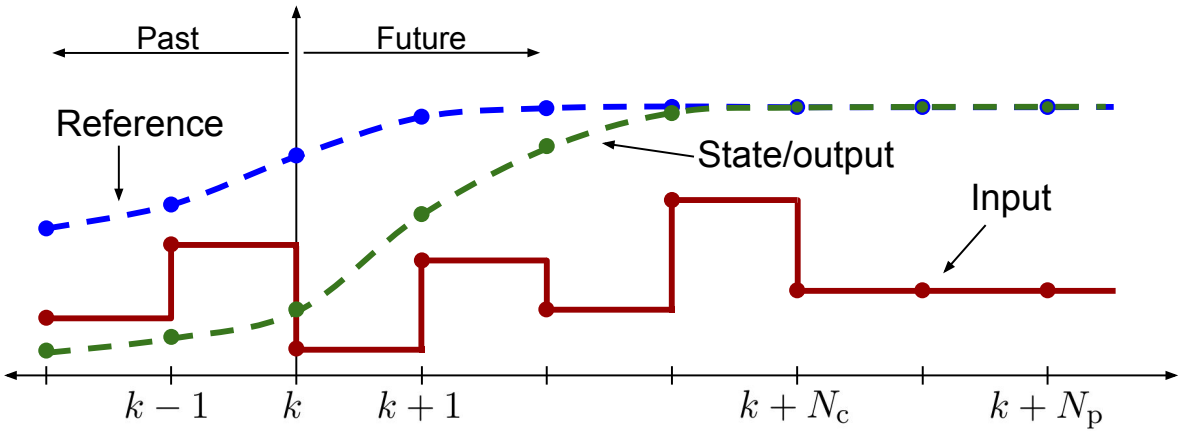

Figure 1-4: An illustration of several MPC components. At time step k, the controller uses an optimization algorithm to optimize the system input trajectory over the prediction horizon, which stretches N_p time steps into the future. A plant model is used during the optimization process to provide a relationship between inputs and other optimization variables such as system states or outputs. The cost function is often defined in terms of the deviation from some reference trajectory. A so called 'receding horizon strategy' is used by implementing the first control input, shifting the prediction horizon, and repeating the process again from the next time step ($k+1 \rightarrow k$). One may decide to keep a certain number of inputs of the last section of the prediction horizon constant. The first N_c inputs that are allowed to vary from one input to the next are part of the control horizon.

Just like the previously discussed alternatives to the conventional IPC framework, MPC can easily accomodate multivariable problems. Moreover, MPC also makes use of an objective function that allows one to explicitly control the way in which trade-offs between competing objectives (like power maximization and load mitigation) are made. Unlike for example $\mathcal{H}_\infty$ control, and ℓ_1-optimal control, the objective functions in MPC are typically formulated in the time-domain instead of the frequency-domain. A significant additional benefit of MPC that distinguishes it from the beforementioned control methods is that it also allows one to implement both hard and soft constraints on the system's inputs, outputs and states. These aspects of MPC are particularly relevant given that concerns over increased pitch actuator loading as a result of IPC [29] probably explain, at least in part, why IPC does not yet see large-scale deployment in the field [18]. Unlike with the conventional IPC framework, MPC would allow for the pitching activity to be accounted for directly or indirectly in the objective function, or, alternatively, it could be limited by imposing constraints.

As described earlier, MPC is inherently model-based. This allows MPC applications of IPC to make use of information on future wind speeds as provided by, e.g., light detection and ranging (LIDAR) systems[3]. The anticipative ability provided by feedforward control based on wind speed previewing can provide noteworthy benefits in terms of both load mitigation and rotational speed regulation [30].

[3]It may be noted that integration of LIDAR technology in MPC applications for IPC is an active area of research. Although LIDAR technology is not typically implemented in commercial wind turbine applications, perhaps in part due to the uncertainties associated with the LIDAR measurements, the potential advantages of feedforward control that it would enable make control methods that are able to take into account future wind speeds, like MPC, attractive control methods [11].

The models that are used in MPC applications for IPC are of different degrees of complexity. In particular, the nonlinear nature of wind turbine dynamics is problematic for two reasons in MPC. Firstly, it gives rise to an important trade-off between model complexity and accuracy. Nonlinear models can accurately describe the wind turbine dynamics, but their large computation time hinders their real-time implementation [31]. By comparison, a single linearized model is beneficial from the point of view of computational tractability, but it is typically unsuitable for the entire operating regime [32]. Secondly, the nonlinear optimization problem that arises from nonlinear MPC is typically nonconvex, and as such, the solution may not be a global optimum.

Convex Model Predictive Control Frameworks

There are several sources of nonlinearities that can be troubling for MPC applications in wind turbine control. Petrović, Jelavić, and Baotić demonstrate in [28] that even if the nonlinear wind turbine dynamics are linearized, and the MBC transformations are applied as shown in Figure 1-2, input constraints on the pitch angles in the resulting fixed reference frame become nonconvex and dependent on the azimuth position. Both of these issues are subsequently tackled by the authors by introducing some additional conservatism and formalizing convex cone constraints that are not dependent on the azimuth position.

With regards to the problems that the nonlinear wind turbine dynamics pose for MPC, the recent development of a state-of-the-art convex economic model predictive control (CEMPC) framework for wind turbine control [33, 34] seems very promising. The developed method is able to circumvent the typical nonlinear wind turbine model by using a change of variables that renders the wind turbine dynamics linear. As a result of this change of variables, the resulting optimization problem that has to be solved becomes convex. This offers perspectives for wind turbine controllers that use an accurate turbine model that is both computationally tractable and provides a globally optimal solution. Moreover, whereas conventional MPC applications typically involve set-point tracking, in economic model predictive control (EMPC) there is no set-point[4]. Set-points typically reflect the relevant optimal steady state, but are usually picked without regard for how this equilibrium should be reached (i.e. the dynamic performance). As a result, particularly processes in which the set-point may change quickly and frequently compared to the relevant state may exhibit suboptimal performance when controlled by conventional MPC methods [35]. Instead of set-point tracking, EMPC therefore simply attempts to optimize a cost function that reflects real costs and benefits.

Although the linear dynamics of the CEMPC method is very promising, the existing framework has only been applied using CPC. Perhaps because IPC is typically used in literature to achieve load reductions [36], only tower base fore-aft bending moment fatigue load mitigation has yet been considered within the CEMPC framework (see [34]). In order to facilitate other forms of fatigue load mitigation using CEMPC, such as those arising from out-of-plane blade bending, it would be valuable to extend the current CEMPC framework to the domain of IPC.

[4] As will become clear in Section 3-2 the existing CEMPC framework does in fact penalize deviation from a set-point, which prompts the removal of this objective. On a more philosophical note, where for example, costs are minimized, one may argue that EMPC does perform reference tracking with respect to zero. In this thesis, this is still considered EMPC because the cost function does reflect actual costs.

1-1-3 Summary

In this section, a short summary is given of the literature review in light of the relevant societal challenges. Cost reductions, which drive the global installed wind power capacity growth that is needed to limit global warming, are realized by means of wind turbine upscaling. IPC plays an important role in minimizing loading to enable this upscaling process.

Conventional IPC makes use of the MBC transformations. Although this is an elegant solution, the conventional IPC method lacks the ability to explicitly account for constraints and trade-offs between competing objectives. MPC appears to be particularly promising for IPC, in large part because it can explicitly account for both objective trade-offs and constraints. However, the nonlinear dynamics of wind turbines is problematic for MPC applications in wind turbine control because the resulting optimization problem quickly becomes computationally demanding and offers no guarantees for global optimality.

Thankfully, a state-of-the-art CEMPC framework is able to accomodate the nonlinear dynamics by means of a change of variables that renders the resulting optimization problem convex. This offers perspectives for computationally tractable, accurate models that can be solved for the global optimum. However, the existing CEMPC theory is currently limited to the domain of CPC, using which only tower base fore-aft bending moment fatigue has yet been studied. To facilitate further load mitigation using CEMPC it would be useful to extend this framework to the domain of IPC. How this can be done remains an open question.

1-2 Research Question

This sets the stage for the subject of this thesis, which concerns the extension of the CEMPC framework to the domain of IPC. The corresponding research question is:

How can the existing CEMPC framework be extended to the domain of IPC for the purpose of wind turbine load mitigation?

Since out-of-plane blade root bending moment fatigue load mitigation is a typical application of IPC, this thesis will specifically consider out-of-plane blade root bending moment fatigue loading. Further, to answer this research question, this thesis seeks to answer the following sub-questions:

1. How does the existing CEMPC method for wind turbine control work?
2. How may the existing CEMPC framework be altered to realize a both theoretically and practically suitable application for CPC?
3. How can the newly developed CPC implementation of CEMPC be extended to the domain of IPC?
4. How can out-of-plane blade root bending moment fatigue load mitigation - a specific example of wind turbine loads - be incorporated within the developed IPC-CEMPC framework?

5. How do the developed CPC-based and IPC-based CEMPC frameworks perform compared to a respective benchmark controller when using a high-fidelity wind turbine simulator?

1-2-1 Main Contributions

Since the answer to the first sub-question inherently depends on existing knowledge, the main contributions of this thesis are formed by the answers to sub-questions two and three. The main contributions of this thesis are:

1. *The reformulation of the aerodynamic power constraints to also reflect pitching rate constraints;*
   The existing CEMPC framework does not take into account pitching rate constraints. These rate constraints are important to take into account because pitch actuators have their physical limitations. However, the existing CEMPC literature does not consider such pitching rate limitations. Whilst for sufficiently large time steps, such as 10 s in [33], pitching rate constraints may never be active, one would definitely expect them to play a meaningful role with considerably smaller time steps such as 0.2 s in [34].

2. *The extension of the CEMPC framework to the domain of IPC;*
   As mentioned earlier, IPC is an important control methodology for load reduction in wind turbines. By extending the CEMPC framework to the domain of IPC, this thesis facilitates future research into possible load reduction prospects using the CEMPC framework.

1-3 Thesis Outline

This thesis is composed of six chapters. Following this first chapter that has provided an introduction, Chapter 2 will present and explain the existing CEMPC framework, thereby answering the first sub-question. To appreciate the value of the CEMPC framework it is first shown how even the simple objective of power maximization leads to a non-convex optimization problem using a typical wind turbine description. Within the existing CEMPC framework it is subsequently shown how the same objective of power maximization leads to a convex optimization problem.

Chapter 3 is dedicated to answering sub-question two. The relevant part of the optimization problem that is implemented in [34] forms the starting point for the development of a viable and useful CPC implementation of CEMPC. In a stepwise fashion, several points of improvement are identified, and the optimization problem is altered accordingly. With regards to the existing literature the most noteworthy changes are the incorporation of pitching rate constraints and the reformulation of the optimization problem as a quadratic programming (QP) problem.

Chapter 4 subsequently extends the developed CPC implementation to the domain of IPC, thereby providing an answer to sub-question three. The basis of the extension to IPC is formed by considering blade-effective wind speeds, which are determined based on an estimated

rotor-effective wind speed that is augmented by a simple vertical wind shear model. Using such a formulation, the concepts used for CPC can fairly simply be repurposed for IPC. To answer sub-question four, Chapter 4 subsequently develops an out-of-plane blade root bending moment model that is amenable to the developed CEMPC framework. Two different out-of-plane blade root bending moment fatigue load mitigation strategies are explained that both make use of tilt and yaw moment mitigation, as is the case with the conventional IPC implementation.

Next, Chapter 5 concentrates on answering sub-question five. Simulations are performed using a high-fidelity wind turbine plane model for two wind speed profiles. The first wind speed profile is used to demonstrate several features of the developed CEMPC framework. The second wind speed profile spans a large part of the operating regime of the wind turbine. During this simulation case, results obtained using CEMPC both for CPC and IPC are compared against those that are obtained using a relevant benchmark controller. For both CPC and IPC a qualitative analysis first discusses the observed performance of the controllers. Following such a qualitative analysis, several performance metrics are used to be able to better asses and compare the performance of the controllers with respect to pitch actuation, out-of-plane blade root bending moment fatigue damage, and energy capture.

Lastly, in Chapter 6, the research question is revisited. The sub-questions that were stipulated to help answer this research question are addressed step by step, leading to a clear conclusion. Given, for example, the various challenges that were encountered, this thesis will end by providing several recommendations for future work.

Chapter 2

Convex Economic MPC for Wind Turbines: Theoretical Overview

The inherent nonlinearity of wind turbine dynamics typically means that a nonlinear optimization problem has to be solved for each new model predictive control (MPC) time step. The computational tractability of these optimization problems is restricted by their nonlinear nature [31], and becomes particularly critical for real-time implementations. Moreover, there is generally no guarantee that the obtained solution of the nonlinear optimization problem is in fact a global optimum. This chapter describes an existing convex economic model predictive control (CEMPC) framework, which seems promising because its convex nature ensures global optimality. Moreover, the CEMPC approach arguably offers better perspectives for limiting computational demand, thereby helping to realise real-time implementations.

In Section 2-1 a typical nonlinear wind turbine model is provided, and it is explained how this description leads to a nonlinear optimization problem. Subsequently, in Section 2-2 the nonlinear optimization problem is transformed into a convex problem by means of a change of variables.

2-1 The Nonlinear Wind Turbine Framework

2-1-1 Wind Turbine Model

The simplified dynamics of a wind turbine can be represented by

$$\dot{\omega}_{\mathrm{g}} = \frac{1}{J}\left(\frac{T_{\mathrm{r}}}{N} - T_{\mathrm{g}}\right), \tag{2-1}$$

in which ω_{g} is the generator's rotational speed, the dot ($\dot{}$) indicates that the differential with respect to time ($\frac{d}{dt}$) is taken, T_{r} is the rotor torque, T_{g} is the generator torque, N is the gearbox ratio, and J is the rotational inertia of the drive train as seen by the generator.

The total wind power that is extracted by a wind turbine is given by

$$P_{\mathrm{w}} = \frac{1}{2}\rho A C_{\mathrm{P}}(\beta, \lambda) v^3, \tag{2-2}$$

in which P_{w} represents the aerodynamic power that is extracted from the wind, ρ is the air density, $A = \pi R^2$ is the rotor area of the rotor with a radius of length R, C_{P} is the power coefficient, β is the (collective[1]) pitch angle, v is the effective wind speed, and λ is the tip speed ratio. This ratio is defined by

$$\lambda = \frac{\omega_{\mathrm{r}} R}{v}, \tag{2-3}$$

in which ω_{r} is the rotational speed of the rotor. By assuming a stiff drivetrain, the relationship between the rotational speed of the rotor and generator is given by

$$\omega_{\mathrm{g}} = \omega_{\mathrm{r}} N. \tag{2-4}$$

In Eq. (2-2) the dependency of the power coefficient C_{P} on the tip speed ratio λ and the pitch angle β is markedly nonlinear, as is shown by Figure 2-1.

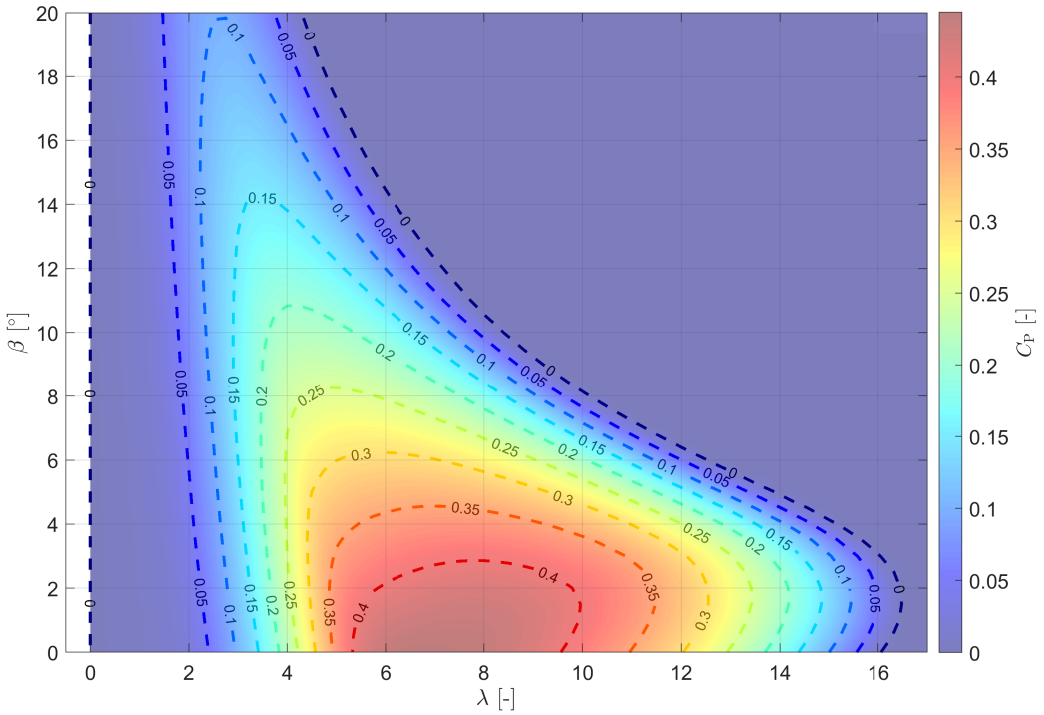

Figure 2-1: The $C_{\mathrm{P}}(\beta, \lambda)$ characteristic of the NREL 5 MW reference turbine [37].

By dividing the aerodynamic power P_{w} from Eq. (2-2) by the rotational speed of the rotor ω_{r}, and by noting that the power coefficient is in fact dependent on the pitch angle β, the

[1]The collective pitch angle is the mean pitch angle of all of the turbine's blades.

rotor speed ω_r, and the wind speed v due to the dependency on the tip speed ratio as shown in Eq. (2-3), the rotor torque is found to be

$$T_r = \frac{1}{2}\rho A \frac{C_P(v, \omega_r, \beta)v^3}{\omega_r}. \tag{2-5}$$

Unlike the rotor torque T_r, the generator torque T_g can (by approximation) be determined directly by the controller, and together with the rotational speed of the generator ω_g and the generator efficiency η_g, it determines the generator's output power P_g:

$$P_g = \eta_g T_g \omega_g.$$

By substituting Eq. (2-5) into Eq. (2-1) and using Eq. (2-4), this model can be written in state-space form as follows:

$$\begin{cases} \dot{\omega}_g &= \frac{1}{2J}\rho A \frac{C_P(v, \omega_g, \beta)v^3}{\omega_g} - \frac{T_g}{J}, & (2\text{-}6) \\ P_g &= \eta_g T_g \omega_g, & (2\text{-}7) \end{cases}$$

in which the state is the generator speed ω_g, the inputs are the pitch angle β and the generator torque T_g, the disturbance is the wind speed v, and the output is the generator output power P_g. Note that the system is clearly nonlinear because of the nonlinear term $\frac{C_P(v, \omega_g, \beta)v^3}{\omega_g}$ in Eq. (2-6), and the product between the state ω_g and the input T_g that is required to determine the output (generator power) in Eq. (2-7).

2-1-2 Optimization Problem: Power Maximization

To demonstrate the nonlinear nature of the optimization problem that arises from the relatively simple wind turbine model presented above, consider a simplified case in which the controller only attempts to maximize the energy capture of the wind turbine. The optimization problem then looks as follows:

$$\max_{\beta(t), T_g(t)} \int_{t_0}^{t_1} P_g(t)dt \tag{2-8}$$

$$\text{s.t.} \quad \dot{\omega}_g = \frac{1}{2J}\rho A \frac{C_P(v, \omega_g, \beta)v^3}{\omega_g} - \frac{T_g}{J}, \tag{2-6}$$

$$P_g = \eta_g T_g \omega_g, \tag{2-7}$$

$$\omega_{g,\min} \leq \omega_g(t) \leq \omega_{g,\max}, \tag{2-9}$$

$$T_{g,\min} \leq T_g(t) \leq T_{g,\max}, \tag{2-10}$$

$$P_{\min} \leq P_g(t) \leq P_{\text{rated}}, \tag{2-11}$$

$$\beta_{\min} \leq \beta(t) \leq \beta_{\max}, \tag{2-12}$$

in which the dependence on time t has been temporarily shown explicitly to emphasize that the optimization occurs over the prediction horizon (from t_0 to t_1), and the meaning of the maximum and minimum values of the inequalities provided by Eq. (2-9) - Eq. (2-12) are

defined in Table 2-1. Eq. (2-6) and Eq. (2-7) have been restated in the above optimization problem for the sake of clarity.

Within the above framework, the objective function Eq. (2-8) as well as the inequality constraints posed by Eq. (2-9) - Eq. (2-12) all take a linear form. However, the equality constraints imposed by Eq. (2-6) and Eq. (2-7) are decidedly nonlinear, which makes this a nonlinear optimization problem.

Table 2-1: Summary of constants relevant to the definition of a simple wind turbine model and a generator power maximization optimization problem.

Parameter	Description
$\omega_{\mathrm{g,min}}$	Minimum generator rotational speed
$\omega_{\mathrm{g,max}}$	Maximum generator rotational speed
$T_{\mathrm{g,min}}$	Minimum generator torque
$T_{\mathrm{g,max}}$	Maximum generator torque
P_{min}	Minimum generator output power
P_{rated}	Rated generator output power
β_{min}	Minimum pitch angle
β_{max}	Maximum pitch angle
N	Gearbox ratio
J	Mass moment of inertia of the drive train as seen by the generator
η_{g}	Generator efficiency
R	Rotor radius
ρ	Density of air

2-2 The Convex Economic Model Predictive Control Framework

This section describes the existing convex economic model predictive control (CEMPC) framework. By rewriting the nonlinear optimization problem in terms of energies and powers it is recast as a convex optimization problem. Such an optimization problem has the following form [38]:

$$\min_{x} f(x) \tag{2-13}$$

$$\text{s.t. } g_i(x) \leq 0, \quad \forall i, \tag{2-14}$$

$$h_k(x) = 0, \quad \forall k, \tag{2-15}$$

in which x represents the variables over which the optimization occurs, the functions g_i and f are convex, and each function h_k is affine.

The derivation of this convex framework, as provided below, is based on the pioneering work of Hovgaard, Boyd, and Jørgensen as presented in [33]. The essential change of variables that lies at the heart of this work is described by

$$\left.\begin{array}{ll} \mathbf{x} & = \omega_{\mathrm{g}} \\ \mathbf{u} & = [T_{\mathrm{g}}\ \beta]^{\top} \\ d & = v \end{array}\right\} \longrightarrow \left\{\begin{array}{ll} \mathbf{x} & = K \\ \mathbf{u} & = [P_{\mathrm{g}}\ P_{\mathrm{w}}]^{\top} \\ d & = v \end{array}\right. , \tag{2-16}$$

in which the old variables are on the left hand side, the new variables are on the right hand side, $\mathbf{x}$ represents the system's state, $\mathbf{u}$ represents the system's inputs, d represents a disturbance and K is the rotational kinetic energy of the drivetrain.

2-2-1 Transforming the System Dynamics

To see how these sets of variables are interchangeable, first consider the simple relationship between the rotational kinetic energy of the (stiff) drivetrain K and the generator speed ω_{g}:

$$K = \frac{1}{2} J \omega_{\mathrm{g}}^2. \tag{2-17}$$

The dynamics of the new system representation is found by taking the derivative with respect to time of Eq. (2-17) and combining the result with Eq. (2-1) to arrive at

$$\dot{K} = P_{\mathrm{w}} - \frac{P_{\mathrm{g}}}{\eta_{\mathrm{g}}}. \tag{2-18}$$

Note that in terms of the new variables (as described by Eq. (2-16)), Eq. (2-18) represents linear dynamics, as opposed to the nonlinear dynamics evident with the old variables in Eq. (2-6).

2-2-2 Transforming the Inequality Constraints

Having transformed the constraint posed by the dynamics in Eq. (2-6), the rest of the constraints posed by Eq. (2-9) to Eq. (2-12) are transformed here.

To start, when Eq. (2-17) is applied to the inequality constraint posed by Eq. (2-9), the state constraint on the rotational kinetic energy becomes

$$0 \leq K \leq K_{\max}, \tag{2-19}$$

in which the left hand side is zero because $K_{\min} = \frac{J}{2}\omega_{\mathrm{g,min}}^2$, and the minimum generator rotational speed is considered zero to enable the wind turbine to rotate in only one direction. The maximum kinetic energy is given by $K_{\max} = \frac{J}{2}\omega_{\mathrm{g,max}}^2$.

With respect to the new input constraints, the existing constraint on the generator power given by Eq. (2-11) is refined further by applying Eq. (2-7) to Eq. (2-10) to obtain

$$\max\left\{\eta_{\mathrm{g}} T_{\mathrm{g,min}} \omega_{\mathrm{g}}, P_{\min}\right\} \leq P_{\mathrm{g}} \leq \min\left\{\eta_{\mathrm{g}} T_{\mathrm{g,max}} \omega_{\mathrm{g}}, P_{\mathrm{rated}}\right\}. \tag{2-20}$$

To ensure that the wind turbine does not extract power from the grid, the minimum generator power $P_{\min}$ and torque $T_{\mathrm{g,min}}$ are zero. Using Eq. (2-17) and the corresponding values of zero for $T_{\mathrm{g,min}}$ and $P_{\min}$, Eq. (2-20) can be rewritten in terms of the new variables as

$$0 \leq P_{\mathrm{g}} \leq \min\left\{\eta_{\mathrm{g}} T_{\mathrm{g,max}} \sqrt{\frac{2K}{J}}, P_{\mathrm{rated}}\right\}. \tag{2-21}$$

The new constraints for the other input - the aerodynamic power - are given by

$$0 \leq P_{\mathrm{w}} \leq \hat{P}_{\mathrm{av}}(v, K), \tag{2-22}$$

in which the inequality on the left hand side represents the fact that the aerodynamic power cannot be negative, and $\hat{P}_{\mathrm{av}}(v, K)$ represents an approximation of the (maximum) available aerodynamic power P_{av} at a certain wind speed and kinetic energy, as defined by

$$P_{\mathrm{av}}(v, K) = \max_{\beta_{\min} \leq \beta \leq \beta_{\max}} \frac{1}{2} \rho A C_{\mathrm{P}}(\beta, K, v) v^3. \tag{2-23}$$

As can be seen from Eq. (2-23), the last remaining original inequality constraint Eq. (2-12) is used to define the upper bound on the aerodynamic power P_{w}.

By inspection of Eq. (2-19) and Eq. (2-21) it is clear that these inequalities are respectively linear and convex when rewritten in the form shown by Eq. (2-14). Similarly, Eq. (2-18) corresponds with the affine form[2] demanded of a convex optimization problem as specified by Eq. (2-15). At present, it is not evident how - or even if - Eq. (2-22) is in conformance with the convex optimization problem form, for which the approximated available power $\hat{P}_{\mathrm{av}}$ from Eq. (2-22) would need to be concave.

2-2-3 Approximating the Available Power

This section is dedicated to show that the available power can in fact accurately be approximated as a concave function. To this end, consider Figure 2-2, in which the available power P_{av}, normalised by v^3 for the purpose of graphical clarity, is displayed as a function of the kinetic energy K for different wind speeds between typical cut-in and cut-out wind speeds of respectively 3 m/s and 25 m/s. The figure suggests that for any specific wind speed between the cut-in and cut-out wind speed v_i, the available power curve $P_{\mathrm{av}}(v = v_i, K)$ can accurately be approximated by a concave function.

For a specific wind speed v_i such a concave approximation is taken to be of a piecewise linear form:

$$\hat{P}_{\mathrm{av},i}(K) = \min\{a_1 K + b_1, \ldots, a_{n_{\mathrm{w}}} K + b_{n_{\mathrm{w}}}\} v_i^3, \tag{2-24}$$

in which the a and b constants form part of affine functions that each provide a local approximation of the actual available power curve, and n_{w} is the total number of such affine functions. To calculate these affine functions the method described in [39] was followed to minimize the root-mean-square error. As Figure 2-3 indicates, the approximation that can be made with $n_{\mathrm{w}} = 15$ is very good since the absolute value of the percentage error is typically very small.

By means of linear interpolation between two neighbouring wind speeds v_1 and v_2 for which a function of the form shown by Eq. (2-24) is available, a concave approximation of the available wind power can be constructed:

$$\hat{P}_{\mathrm{av}}(v, K) = \left(1 - \frac{v - v_1}{v_2 - v_1}\right) \hat{P}_{\mathrm{av},1}(K) + \left(\frac{v - v_1}{v_2 - v_1}\right) \hat{P}_{\mathrm{av},2}(K). \tag{2-25}$$

[2] Those who find the fact that the dynamics are represented by a linear *differential* equation troubling may be reassured by the fact that the implemented MPC algorithm uses a discretization scheme for these dynamics (see Section 3-4), thereby yielding a simple linear algebraic equation.

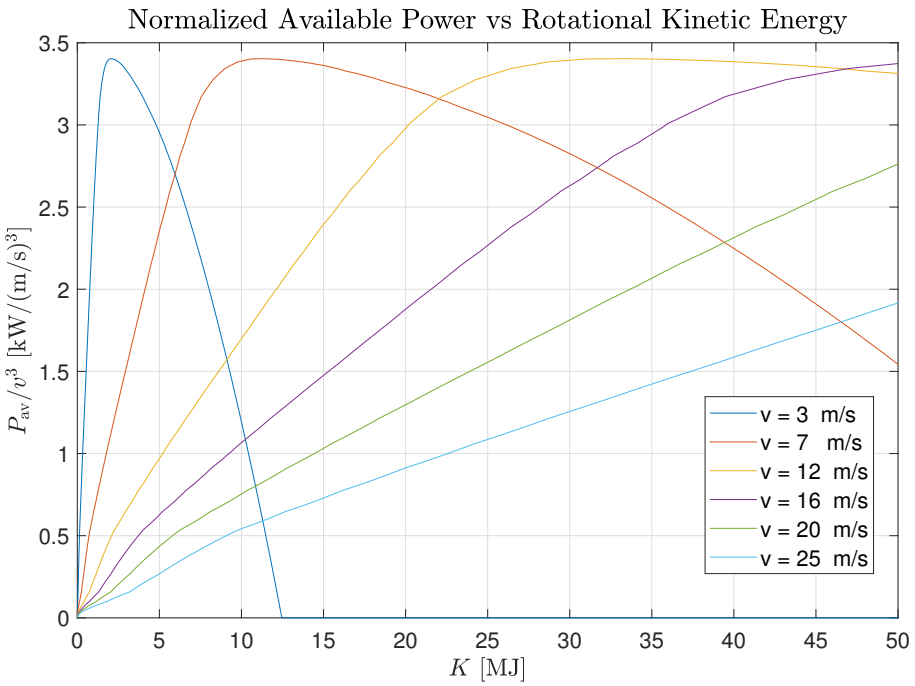

Figure 2-2: The available power P_{av}, normalised by v^3, as a function of the rotational kinetic energy K for different wind speeds between a cut-in wind speed of 3 m/s and cut-out wind speed of 25 m/s. Note that for each wind speed, the relationship looks almost concave.

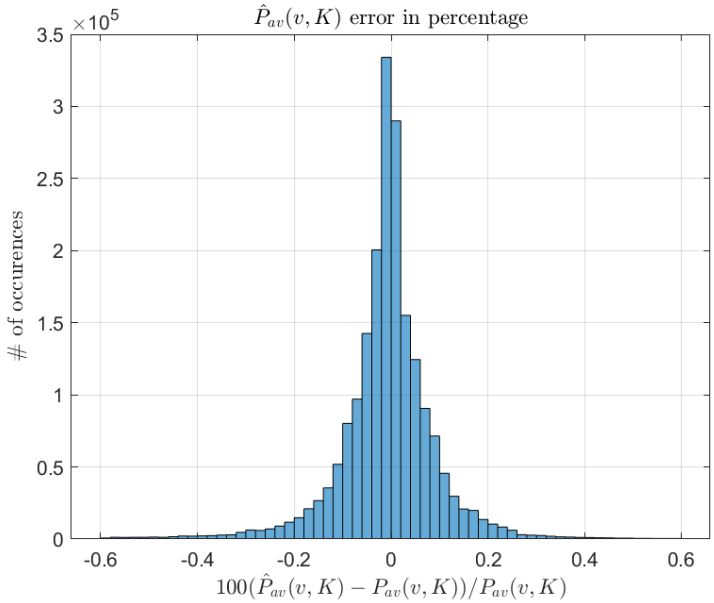

Figure 2-3: A histogram of the percentage error of the approximated available power as obtained by following the method from [39] with 15 piecewise-linear approximations per wind speed, aggregated over all wind speeds between a cut-in wind speed of 3 m/s and cut-out wind speed of 25 m/s.

Note that the resulting expression for $\hat{P}_{\text{av}}$ is concave because the sum of two concave functions remains a concave function.

2-2-4 Optimization Problem: Power Maximization

Using the new variables in terms of powers and energies, the resulting optimization problem from Section 2-1-2 becomes convex. The simple objective of power maximization now gives rise to the following optimization problem:

$$\max_{P_{\text{w}}(t),P_{\text{g}}(t)} \int_{t_0}^{t_1} P_{\text{g}}(t)dt \tag{2-26}$$

$$\text{s.t.} \quad \dot{K}(t) = P_{\text{w}}(t) - \frac{P_{\text{g}}(t)}{\eta_{\text{g}}} \tag{2-18}$$

$$0 \leq K(t) \leq K_{\max}, \tag{2-19}$$

$$0 \leq P_{\text{w}}(t) \leq \hat{P}_{\text{av}}(v(t), K(t)), \tag{2-22}$$

$$0 \leq P_{\text{g}}(t) \leq \eta_{\text{g}} T_{\text{g,max}} \sqrt{\frac{2K(t)}{J}}, \tag{2-27}$$

$$P_{\text{g}}(t) \leq P_{\text{rated}}, \tag{2-28}$$

in which the dependence of the different variables on time t has again been included temporarily to stress that the optimization occurs over the prediction horizon. Eq. (2-18), Eq. (2-19), and Eq. (2-22) have been restated for the sake of clarity. Eq. (2-27) and Eq. (2-28) follow from Eq. (2-21). By inspection, the presented optimization problem is convex because the objective of the maximization problem (Eq. (2-26)) is of an affine form (and thereby concave), the equality constraint is linear, and of the inequalities, only the right hand sides of Eq. (2-22) and Eq. (2-27) are concave instead of linear.

2-2-5 Retrieving the Original Input Variables

Although the above optimization problem is convex, the computed solution also needs to be transferable to the old input variables (pitch β and generator torque T_{g}) in order to control the turbine. After all, it is typically a generator torque that one gives as an input to the generator, not a generator output power. Likewise, one ultimately sends a signal to the blade actuators for the blade pitch, not of the aerodynamic power.

To start with the generator power, consider the generator rotational speed constraints posed by Eq. (2-9), and the definition of the kinetic rotational energy provided by Eq. (2-17). The left hand side of Eq. (2-9) renders Eq. (2-17) a one-to-one correspondence between K and ω_{g}

$$\omega_{\text{g}} = \sqrt{\frac{2K}{J}}. \tag{2-29}$$

Substituting this into the definition of the generator output power provided by Eq. (2-7) and rewriting the result for T_{g} yields

$$T_{\mathrm{g}} = \frac{P_{\mathrm{g}}}{\eta_{\mathrm{g}}}\sqrt{\frac{J}{2K}}. \tag{2-30}$$

To find the pitch angle β from the new variables, consider its role in determining the aerodynamic power P_{w} as described by Eq. (2-2). Assuming that the wind speed is known from, e.g., light detection and ranging (LIDAR) measurements, this allows for the power coefficient C_{P} to be calculated, which is dependent on both the pitch and tip speed ratio. The tip speed ratio can be computed by combining Eq. (2-29) and the definition of the tip speed ratio provided by Eq. (2-3), and by taking into account the transmission ratio of the gearbox

$$\lambda = \frac{R}{vN}\sqrt{\frac{2K}{J}}. \tag{2-31}$$

Knowing the power coefficient and the tip speed ratio, a corresponding pitch angle may be obtained using the power coefficient data shown in Figure 2-1. By searching for intersections between the line corresponding to a certain tip speed ratio and the contour line corresponding to the found power coefficient, one or more possible pitch angles may be found. If there are multiple pitch angle candidate solutions, any pitch angles that do not satisfy the pitch constraints posed by Eq. (2-12) should be discarded. In this way, a lookup table β_{lut} can be constructed to find the pitch angle from a calculated power coefficient and tip speed ratio, which in turn have been calculated from the aerodynamic power, wind speed, and kinetic energy of the drivetrain:

$$\beta = \beta_{\mathrm{lut}}(C_{\mathrm{P}}(P_{\mathrm{w}}, v), \lambda(K, v)). \tag{2-32}$$

2-2-6 Modelling the Aerodynamic Thrust

Whilst the power maximization objective employed in Section 2-1-2 and Section 2-2-4 nicely illustrates how the change of variables leads to a convex optimization problem, it does not reflect the objective of load mitigation. Noting that load mitigation is not considered in the above convex framework, in [34], Shaltout, Ma and Chen extend the above CEMPC framework by including the mitigation of tower base fore-aft bending moment fatigue. The authors modelled the tower motion as a second order mass-spring-damper system that is driven by the aerodynamic thrust. Since the relationship between the thrust that acts on a blade and the blade root bending moment is approximately linear [40], the way that the thrust has been modelled in the existing CEMPC framework is of particular relevance to this thesis, and is described here.

The thrust that acts on a wind turbine's rotor is given by

$$F_{\mathrm{T}}(v, \beta, \lambda) = \frac{1}{2}\rho A C_{\mathrm{T}}(\beta, \lambda) v^2, \tag{2-33}$$

in which C_{T} is the thrust coefficient, which is dependent nonlinearly on the collective pitch and the tip speed ratio. This relationship presents two significant challenges for its implementation within the existing CEMPC framework. Firstly, a convex problem description requires

affine equality constraints, quite unlike the nonlinear relationship above. Secondly, Eq. (2-33) defines the thrust in terms of the 'old', nonlinear wind turbine framework.

To solve these problems, the thrust force is therefore replaced by an affine approximation thereof with respect to the inputs and states of the new, convex framework. To arrive at such an approximation, it is assumed once more that the wind speed v is known during the prediction horizon. This obviates the need for any linearizations of the thrust with respect to the wind speed. The remaining nonlinearity derives from the thrust coefficient C_{T}. Note that according to Eq. (2-31), the thrust coefficient can also be defined in terms of the wind speed, kinetic energy, and the pitch angle. Linearizing this expression with respect to the pitch angle and the kinetic energy of the drivetrain yields

$$C_{\mathrm{T}}(\beta, K, v; \beta^*, K^*) = \frac{\partial C_{\mathrm{T}}}{\partial \beta}\bigg|_{\beta^*,K^*,v} (\beta - \beta^*) + \frac{\partial C_{\mathrm{T}}}{\partial K}\bigg|_{\beta^*,K^*,v} (K - K^*) + C_{\mathrm{T}}(\beta^*, K^*, v), \tag{2-34}$$

$$= q_{\mathrm{t}}(\beta - \beta^*) + r_{\mathrm{t}} K + s_{\mathrm{t}}, \tag{2-35}$$

in which the superscript * denotes the point where the linearization is applied[3], and the constants q_{t}, r_{t} and s_{t} from Eq. (2-35) can be found by analyzing Eq. (2-34).

In the convex framework the pitch angle is determined from the aerodynamic power, kinetic energy, and wind speed according to the lookup table described by Eq. (2-32), which is a nonlinear relationship. The nonlinear nature of this equation makes it unsuitable for substitution in Eq. (2-34). As an alternative, the change in pitch angle is approximated by using a linearization of the power coefficient, which will ultimately allow the thrust coefficient (and the thrust force) to be rewritten as an affine function of the aerodynamic power and kinetic energy.

The linearized power coefficient is given by the relationship

$$C_{\mathrm{P}}(\beta, K, v; \beta^*, K^*) = \frac{\partial C_{\mathrm{P}}}{\partial \beta}\bigg|_{\beta^*,K^*,v} (\beta - \beta^*) + \frac{\partial C_{\mathrm{P}}}{\partial K}\bigg|_{\beta^*,K^*,v} (K - K^*) + C_{\mathrm{P}}(\beta^*, K^*, v), \tag{2-36}$$

$$= q_{\mathrm{p}}(\beta - \beta^*) + r_{\mathrm{p}} K + s_{\mathrm{p}}, \tag{2-37}$$

in which the constants q_{p}, r_{p} and s_{p} from Eq. (2-37) can be found by analyzing Eq. (2-36)[4]. Combining Eq. (2-35) and Eq. (2-37) to remove the term $(\beta - \beta^*)$ yields

$$C_{\mathrm{T}}(\beta, K, v; \beta^*, K^*) = \frac{q_{\mathrm{t}}}{q_{\mathrm{p}}} C_{\mathrm{P}}(\beta, K, v) + \left(r_{\mathrm{t}} - r_{\mathrm{p}} \frac{q_{\mathrm{t}}}{q_{\mathrm{p}}} \right) K + \left(s_{\mathrm{t}} - s_{\mathrm{p}} \frac{q_{\mathrm{t}}}{q_{\mathrm{p}}} \right). \tag{2-38}$$

To rewrite this in terms of an approximation of the thrust force $\hat{F}_{\mathrm{T}}$ that is affine in the aerodynamic power and the kinetic energy one needs to apply the definition of the aerodynamic power (Eq. (2-2)) and the definition of the thrust force (Eq. (2-33)) to Eq. (2-38) to find

[3] To see why linearization with respect to a known wind speed is not necessary, consider that the resulting contribution to Eq. (2-34) would be $\frac{\partial C_{\mathrm{T}}}{\partial v}\Big|_{\beta^*,K^*,v^*} (v - v^*) = 0$ because one can choose to linearize at the known wind speed $v^* = v$.

[4] In [34] the constants s_{t} and s_{p} are defined slightly differently in order to remove β instead of the term $\beta - \beta^*$, but the resulting affine approximation of the thrust force is the same.

$$\hat{F}_{\mathrm{T}}(v, P_{\mathrm{w}}, K; \beta^*, K^*) = \left(\frac{q_{\mathrm{t}}}{v q_{\mathrm{p}}}\right) P_{\mathrm{w}} + \frac{1}{2}\rho A v^2 \left(r_{\mathrm{t}} - r_{\mathrm{p}}\frac{q_{\mathrm{t}}}{q_{\mathrm{p}}}\right) K + \frac{1}{2}\rho A v^2 \left(s_{\mathrm{t}} - s_{\mathrm{p}}\frac{q_{\mathrm{t}}}{q_{\mathrm{p}}}\right). \quad (2\text{-}39)$$

This approximation of the thrust can be rewritten as

$$\hat{F}_{\mathrm{T}}(P_{\mathrm{w}}, K; v, \beta^*, K^*) = Q_{\mathrm{T}}(v, \beta^*, K^*)P_{\mathrm{w}} + R_{\mathrm{T}}(v, \beta^*, K^*)K + S_{\mathrm{T}}(v, \beta^*, K^*), \quad (2\text{-}40)$$

for which the meaning of Q_{T}, R_{T}, and S_{T} can be found by comparing Eq. (2-39) with Eq. (2-40). Each of these terms is dependent on the wind speed as well as the pitch and rotational kinetic energy linearization points. One can determine a value of Q_{T}, R_{T}, and S_{T} for each time step within the prediction horizon by using the available wind speed information and initial measurements of the pitch angle and kinetic rotational energy as linearization points.

As Shaltout, Ma and Chen note in [34], the accuracy of the affine thrust approximation is dependent on two important factors. Firstly, it depens on the accuracy of the used wind speed. Secondly, the accuracy of the approximation depends on the the magnitude of the changes in pitch angle ($\beta - \beta^*$) and kinetic energy ($K - K^*$) from their respective linearization point. If these changes are too large, the accuracy of the approximation will likely decrease.

Since one may anticipate substantial deviations from the initial pitch and kinetic rotational energy measurements, particularly for long prediction horizons, it seems odd that the authors chose not to use estimates of future pitch and kinetic energies as linearization points. Moreover, since the authors use simulated LIDAR measurements, the wind speed v will be variable throughout the prediction horizon, and therefore require multiple linearizations of the power and thrust coefficients anyway. To increase the accuracy of the predictions, (at least initially) one may need an iterative solution procedure if multiple, different linearization points are chosen for the pitch and kinetic energy [41]. Perhaps this explains why only a single linearization point is used for the pitch angle and the kinetic energy.

To (presumably) nonetheless limit the error that is made by the affine approximation, hard constraints are imposed on the affine thrust force:

$$0 \leq \hat{F}_{\mathrm{T}}(P_{\mathrm{w}}, K; v, \beta^*, K^*) \leq F_{\mathrm{T,max}}(v), \quad (2\text{-}41)$$

in which $F_{\mathrm{T,max}}$ is the maximum thrust force. The authors of [34] don't specify how to find this maximum thrust force, but one may use the maximum possible thrust coefficient for a certain wind speed (given constraints Eq. (2-9) and Eq. (2-12)) is used in Eq. (2-33). This approach makes the resulting maximum thrust force directly dependent on only the wind speed.

Chapter 3

Convex Economic MPC for CPC: Implementation and Practical Considerations

Having presented the existing convex economic model predictive control (CEMPC) theory in the previous chapter, this chapter will discuss the implementation of this theory for the purpose of collective pitch control (CPC). First, a suitable controller implementation is discussed in Section 3-1. Next, the complete existing optimization problem is presented in Section 3-2. Given this controller implementation and several practical and theoretical shortcomings of the presented CEMPC optimization problem, various changes to the existing CEMPC framework are subsequently discussed in Section 3-3 to Section 3-8. An overview of the resulting, implemented controller is subsequently given in Section 3-9, and the used optimization problem is finally shown in Section 3-10.

3-1 Controller Implementation

3-1-1 Convex Economic Model Predictive Controller

The convex economic model predictive controller that is implemented for CPC, and to which Section 3-2 to Section 3-10 will be dedicated, is shown in relation to other control design components and the wind turbine in Figure 3-1. The controller uses measurements of the generator and rotor rotational speed that are taken from the wind turbine, as well as an estimate of the rotor-effective wind speed. Although the internal model of the model predictive controller makes use of a stiff drivetrain, there is some flexibility to the drivetrain of an actual wind turbine. As will be explained in greater detail in Section 3-7, the rotational speed of the rotor is also used (besides the generator speed) because it more accurately describes the kinetic rotational energy. Outputs of the controller are vectors with the envisioned future collective pitch angles and generator powers.

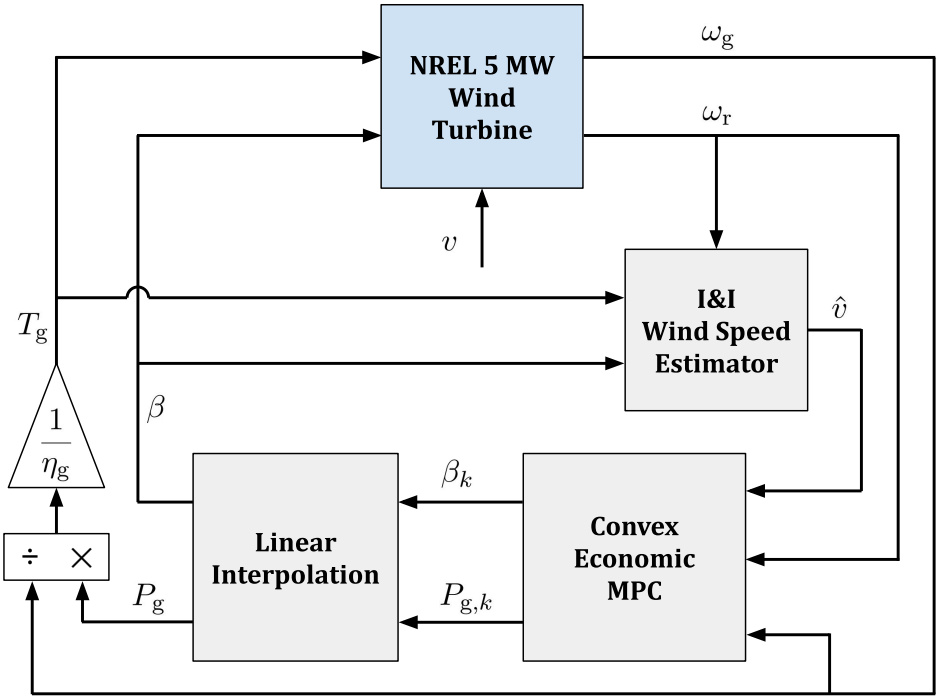

Figure 3-1: A control diagram that shows the dependencies between different control components and the investigated NREL 5 MW wind turbine in the case of CPC. A rotor-effective wind speed estimate $\hat{v}$ of the wind speed acting on the turbine v is provided to the CEMPC implementation by an immersion and invariance (I&I) wind speed estimator. Other inputs to the convex economic model predictive controller consist of the measured rotational speeds of the generator and rotor (ω_g and ω_r). The outputs of the CEMPC block consists of a solution trajectory for the pitch β_k and generator power $P_{g,k}$. These are interpolated linearly to prevent any large transients of inputs to the generator. The applied generator torque is computed from the generator power and rotational speed as shown.

3-1-2 Linear Interpolation of CEMPC Outputs

In-between model predictive control (MPC) time steps, the outputs of the controller are interpolated linearly. The most important reason for this linear interpolation is to avoid large wind turbine input transients. As will be discussed in Section 3-4, the CEMPC method can adequately account for the linear interpolation of the outputs by using a first-order-hold discretization method. The reason that the collective pitch angle is provided as an output from the controller instead of the aerodynamic power (which one might expect based on the previous chapter) is to facilitate the implementation of pitching rate constraints, which will be developed in Section 3-8-2. If the aerodynamic power were to be provided as an output of the controller and were to be interpolated linearly, the resulting piecewise-linear aerodynamic power trajectory would lead to collective pitch angles that, due to the nonlinear mapping from P_w, K, and v to β described by the pitch lookup table β_{lut} (see Eq. (2-32)), do not necessarily abide by the pitching rate constraints modelled by the controller. Moreover, such a continuous lookup of the pitch angle would be quite time consuming compared to the shown implementation.

3-1-3 Wind Turbine Plant

The wind turbine that is used during this thesis is the NREL 5 MW wind turbine [37]. Relevant parameters that characterize this wind turbine and its implementation in this thesis and the model used to describe it by the convex economic model predictive controller are given in Table 3-1. For the purpose of CPC the only inputs it uses are the collective pitch angle β and the generator torque T_{g}, and the only measured outputs are the rotational speeds of the rotor and the generator. The generator torque derives from the generator output power and the generator speed as shown in Figure 3-1.

Table 3-1: Various parameter values that are used to characterise the investigated NREL 5 MW turbine [37] in this study.

Parameter	Description	Value	Units	Source or Motivation
$\omega_{\mathrm{g,min}}$	Minimum generator rotational speed	0	rpm	Lets the rotor only turn one way
$\omega_{\mathrm{g,rated}}$	Rated generator rotational speed	1,173.7	rpm	NREL 5 MW definition document
$\omega_{\mathrm{g,max}}$	Maximum generator rotational speed	1,291.1	rpm	Taken to be $1.1(\omega_{\mathrm{g,rated}})$
$T_{\mathrm{g,min}}$	Minimum generator torque	0	N m	NREL 5 MW definition document
$T_{\mathrm{g,rated}}$	Rated generator torque	43,093.55	N m	NREL 5 MW definition document
$T_{\mathrm{g,max}}$	Maximum generator torque	43,093.55	N m	Same as $T_{\mathrm{g,rated}}$ because it fixes ω_{g} at $\omega_{\mathrm{g,rated}}$ for maximum power production[1].
P_{min}	Minimum generator output power	0	MW	Do not want to extract power from the grid
P_{rated}	Rated generator output power	5	MW	NREL 5 MW definition document
β_{min}	Minimum pitch angle	0	$^\circ$	Prevent pitching to stall
β_{max}	Maximum pitch angle	20	$^\circ$	Larger pitch angles should not be necessary during normal operation
$\dot{\beta}_{\mathrm{max}}$	Maximum absolute pitch rate	8	$^\circ$/s	NREL 5 MW definition document
N	Gearbox ratio	97	-	NREL 5 MW definition document

[1] This is useful because it prevents operation at or around natural excitation frequencies. Alternatively, using $T_{\mathrm{g,max}} = 1.1(T_{\mathrm{g,rated}})$ from the NREL 5 MW definition document, it was found that the 1st edgewise blade mode was excited by 6P vibrations at a rotor speed of approximately 11 rpm. This can be clearly seen from the Campbell Diagram depicted by Figure B-1 in Appendix B.

Table 3-1 continued from previous page

Parameter	Description	Value	Units	Source or Motivation
J_{g}	Mass moment of inertia of the generator with respect to the high-speed shaft	534.116	kg m^2	NREL 5 MW definition document
J_{hub}	Mass moment of inertia of the hub	115,926	kg m^2	NREL 5 MW definition document
J_{blade}	Mass moment of inertia of a single blade	11,776,047	kg m^2	NREL 5 MW definition document
J_{r}	Mass moment of inertia of the rotor	35,444,067	kg m^2	$J_{\mathrm{r}} = J_{\mathrm{hub}} + 3J_{\mathrm{blade}}$
J	Mass moment of inertia of the drive train as seen by the generator	4,301.2	kg m^2	$J = J_{\mathrm{g}} + \frac{J_{\mathrm{r}}}{N^2}$
η_{g}	Generator efficiency	94.4	%	NREL 5 MW definition document
v_{min}	Cut-in wind speed	3.0	m / s	NREL 5 MW definition document
v_{rated}	Rated wind speed	11.4	m / s	NREL 5 MW definition document
v_{max}	Cut-out wind speed	25.0	m / s	NREL 5 MW definition document
h_{hub}	Hub height	90	m	NREL 5 MW definition document
R	Rotor radius	63	m	NREL 5 MW definition document

3-1-4 Wind Speed Estimation

To estimate the rotor-effective wind speed v, an immersion and invariance (I&I) estimator [42] is used. In essence, the I&I estimator works by applying a smart adaptive parameter estimation technique to the model for the rotational acceleration given by Eq. (2-6). As can be seen from Figure 3-1, the I&I estimator is dependent on the measured rotor speed, the collective pitch angle, and the implemented generator torque. Under certain conditions that typically appear to be satisfied during normal wind turbine operation, the technique offers asymptotic convergence to a constant wind speed. By selecting a sufficiently high adaptation gain, this technique can also be used for variable wind speeds. To reduce the error that arises from wind speed estimation, a variant of the typical I&I estimator as provided by [43] is implemented that makes use of integral action to enhance the accuracy of the estimator. The interested reader is referred to [42, 43] for more details. To be able to make a fair comparison between controllers, some of which are incapable of using wind speed previewing, no wind speed previewing (by means of, e.g., simulated light detection and ranging (LIDAR) measurements) is used. Instead, the estimated rotor-effective wind speed $\hat{v}$ is assumed to

remain constant throughout the entire prediction horizon.

3-2 Existing Optimization Problem Formulation

The optimization problem posed by Shaltout, Ma, and Chen in [34] considers more objectives than only power maximization. The relevant optimization problem that can be distilled from their work is given by

$$\max_{P_{\mathrm{g}}(t),P_{\mathrm{w}}(t)} \int_{t_0}^{t_1} \Big[\alpha_1 P_{\mathrm{g}}(t) - \alpha_2 \dot{P}_{\mathrm{g}}(t)^2 - \alpha_3 \dot{P}_{\mathrm{w}}(t)^2 + \alpha_4 \hat{P}_{\mathrm{av}}(K(t), v(t)) - \alpha_5 \max\{K(t) - K_{\mathrm{rated}}, 0\} - \alpha_6 (K(t) - K_{\mathrm{ref}}(v(t)))^2\Big] dt, \tag{3-1}$$

$$\text{s.t.} \quad \dot{K}(t) = P_{\mathrm{w}}(t) - \frac{P_{\mathrm{g}}(t)}{\eta_{\mathrm{g}}} \tag{2-18}$$

$$0 \leq K(t) \leq K_{\max}, \tag{2-19}$$

$$0 \leq P_{\mathrm{w}}(t) \leq \hat{P}_{\mathrm{av}}(v(t), K(t)), \tag{2-22}$$

$$0 \leq P_{\mathrm{g}}(t) \leq \eta_{\mathrm{g}} T_{\mathrm{g,max}} \sqrt{\frac{2K(t)}{J}}, \tag{2-27}$$

$$P_{\mathrm{g}}(t) \leq P_{\mathrm{rated}}, \tag{2-28}$$

in which α_1 to α_6 indicate positive, weighting factors of their respective objective terms, the dependence on time is explicitly shown to emphasize the importance of variations of the objective terms within the prediction horizon. The constraints are the same as those from the convex power maximization optimization problem derived in Section 2-2-4, and are restated for the sake of clarity. Note that the estimated wind speed $\hat{v}$ does not feature in the above problem formulation because the aforementioned authors assume perfect wind speed previewing by means of LIDAR measurements. Moreover, K_{rated} represents the kinetic rotational energy at the rated rotational speed, and K_{ref} represents a reference kinetic rotational energy. This reference kinetic energy is given by

$$K_{\mathrm{ref}}(v) = \begin{cases} \frac{1}{2} J \left(\frac{N \lambda_{\mathrm{opt}} v}{R}\right)^2, & \text{if } v \leq \frac{\omega_{\mathrm{r,rated}} R}{\lambda_{\mathrm{opt}}} \\ K_{\mathrm{rated}}, & \text{otherwise} \end{cases}, \tag{3-2}$$

in which λ_{opt} is the tip speed ratio that corresponds the the maximum power coefficient and $\omega_{\mathrm{r,rated}}$ corresponds to the rated rotational speed of the rotor.

The first term of Eq. (3-1) represents the familiar power maximization objective. The second objective is meant to minimize generator power variations. The third term reflects the minimization of aerodynamic power variability. The fourth term represents the desire to maximize the available power in order to help determine the optimal kinetic rotational energy [33]. The fifth term is designed to limit overspeeding, whilst the sixth term aims to limit variations of the kinetic rotational energy with respect to a reference kinetic energy. By inspection one may conclude that this optimization problem is indeed a convex optimization problem.

The optimization problem that is used in this thesis is largely based on Eq. (3-1) and the constraints given by Eq. (2-18), Eq. (2-19), Eq. (2-22), Eq. (2-27), and Eq. (2-28). However,

there are several theoretical and practical considerations that necessitate modifications and additions to this optimization problem. These changes are first described in Section 3-3 to Section 3-8 before presenting the new optimization problem for CPC in Section 3-10.

3-3 Using Economic Model Predictive Control

Several elements do not adhere to an economic model predictive control (EMPC) framework. For example, the sixth objective aims to minimize the difference of the kinetic rotational energy with respect to a reference. As is shown by the definition of this reference kinetic energy provided by Eq. (3-2), this reference is chosen to reflect a preconceived notion of the optimal steady state based on the wind speed. As is explained in Section 1-1-2, the sixth objective is incompatible with an EMPC framework because the focus on deviations from a steady state disregard the dynamic performance, i.e., the costs and benefits associated with *how* such a steady state is reached. Hence, such objective formalisms do not accurately reflect real costs and benefits, in contrast to what is the case in EMPC.

Another problem arises from the third objective in Eq. (3-1), which attempts to minimize variations of the aerodynamic power. Since in [34] use is made of LIDAR to provide (what is assumed to be) perfect future wind speed information (which may hence be variable) it makes particularly little sense to minimize aerodynamic power variations over the prediction horizon. Given that in accordance with Eq. (2-2), $P_{\mathrm{w}} \propto C_{\mathrm{P}}(\lambda, \beta)v^3$, in order for the aerodynamic power to remain relatively constant, any changes in wind speed require relatively large changes in the power coefficient. Depending on the initial operating point and the induced change in tip speed ratio, this in turn may result in relatively large pitching rates. Given the problem of increased pitch actuator loading previously mentioned in Section 1-1-2, the third objective hence does not appear to accurately reflect the reduction of actual costs and is therefore incompatible with the EMPC framework. If however, one would like to minimize the pitching rate, one may try to do so indirectly by minimizing the variations of the power coefficient. The logic of this approach for CPC resides in the assumption that the tip speed ratio will remain fairly constant between time steps. This assumption makes sense because in this thesis, the wind speed is assumed to be constant over the entire time horizon. Hence, only changes in the rotor's rotational speed will bring about changes in the tip speed ratio. If both the tip speed ratio and the power coefficient remain relatively constant, one would then expect a minimal change in pitch.

3-4 Discretization

Discrete-time MPC formulations are typically simpler than their continuous-time counterparts, and are the most prevalent type of MPC [44]. As such, this thesis will focus on discrete-time implementations. However, the optimization problem described by Eq. (3-1) and its constraints is posed in the continuous-time framework.

First, to discretize the inequality constraints formed by Eq. (2-19), Eq. (2-22), Eq. (2-27), and Eq. (2-28), simply apply each of these equations at all of the time steps k within the prediction horizon. The mapping between the discrete and continuous time indications k

and t is given by $t = t_0 + k\Delta t_\mathrm{s}$, in which Δt_s is the MPC time step length. The resulting constraints are given by

$$K[k] \geq 0, \qquad k \in \{1, 2, \ldots, N_\mathrm{p}\}, \tag{3-3}$$
$$K[k] \leq K_\mathrm{max}, \qquad k \in \{1, 2, \ldots, N_\mathrm{p}\}, \tag{3-4}$$
$$P_\mathrm{g}[k] \geq 0, \qquad k \in \{1, 2, \ldots, N_\mathrm{p}\}, \tag{3-5}$$
$$P_\mathrm{g}[k] \leq P_\mathrm{rated}, \qquad k \in \{1, 2, \ldots, N_\mathrm{p}\}, \tag{3-6}$$
$$P_\mathrm{g}[k] \leq \eta_\mathrm{g} T_\mathrm{g,max} \sqrt{\frac{2K[k]}{J}}, \quad k \in \{1, 2, \ldots, N_\mathrm{p}\}, \tag{3-7}$$

in which the current time step at $k = 0$ is purposefully omitted because relevant equality constraints will be developed for this time step in Section 3-7 based on measurements provided as feedback signals.

Moreover, the integral can be approximated by (weighted) sums of the different terms that contribute to the objective function at the discrete intervals within the time horizon. To approximate rates of change, discrete changes between time steps are used. An exception is formed by the discretization of the state-space dynamics given by Eq. (2-18). These dynamics are discretized by means of the first-order-hold discretization method as described in [45]. The choice for the first-order-hold discretization method derives from the assumption that the inputs vary linearly from one discrete input to the next. This assumption makes sense because the inputs computed by the MPC algorithm and pitch-lookup function are also interpolated linearly from the current time step to the next[2,3]. The resulting discretized dynamics are then given by

$$x_\mathrm{d}[k+1] = A_\mathrm{d} x_\mathrm{d}[k] + B_\mathrm{d} \begin{bmatrix} P_\mathrm{w}[k] & P_\mathrm{g}[k] \end{bmatrix}^\top, \tag{3-8a}$$
$$K[k] = C_\mathrm{d} x_\mathrm{d}[k] + D_\mathrm{d} \begin{bmatrix} P_\mathrm{w}[k] & P_\mathrm{g}[k] \end{bmatrix}^\top, \tag{3-8b}$$

in which the subscript d represents the distinction 'discrete', x_d is the discrete (scalar) state that is used to describe the kinetic energy dynamics, and with reference to the continuous state-space dynamics provided by Eq. (2-18) the matrices A_d, B_d, C_d, and D_d can be obtained using the MATLAB command

`c2d(ss(0,[1 -1/`η_g`],1,[0 0]),` Δt_s `,'foh').`

Applying Eq. (3-8) to all of the $N_\mathrm{p} + 1$ points within the prediction horizon, one can derive a single matrix equality that defines all of the kinetic energies given the current, measured kinetic energy and the MPC inputs (aerodynamic power and generator power):

$$\underline{K} = \mathcal{A} K[0] + \mathcal{B}_\mathrm{w} \underline{P}_\mathrm{w} + \mathcal{B}_\mathrm{g} \underline{P}_\mathrm{g}, \tag{3-9}$$

[2] Together with the feedback constraints described in Section 3-7, this linear interpolation scheme of the inputs is used to prevent large input transients.

[3] The error of the discretization stems from the fact that the linear interpolation of the pitch will likely not produce a linearly increasing aerodynamic power due to the nonlinear dependence of the power coefficient on the pitch angle. Nonetheless, the pitch angle is interpolated linearly (instead of the aerodynamic power) because this error is assumed to be fairly small. Moreover, the linear interpolation of the pitch angle obviates the need to continuously lookup the pitch angle from the aerodynamic power.

in which $\mathcal{A}$, $\mathcal{B}_{\mathrm{w}}$, and $\mathcal{B}_{\mathrm{g}}$ are matrices that are dependent on the discrete state-space matrices from Eq. (3-8), and $\underline{K}$, $\underline{P}_{\mathrm{w}}$ and $\underline{P}_{\mathrm{g}}$ are vectors of the kinetic energy, aerodynamic power, and generator power respectively within the prediction horizon, as defined by

$$\underline{K} = \begin{bmatrix} K[0] & K[1] & K[2] & \dots & K[N_{\mathrm{p}}-1] & K[N_{\mathrm{p}}] \end{bmatrix}^{\top}, \tag{3-10}$$

$$\underline{P}_{\mathrm{w}} = \begin{bmatrix} P_{\mathrm{w}}[0] & P_{\mathrm{w}}[1] & P_{\mathrm{w}}[2] & \dots & P_{\mathrm{w}}[N_{\mathrm{p}}-1] & P_{\mathrm{w}}[N_{\mathrm{p}}] \end{bmatrix}^{\top}, \tag{3-11}$$

$$\underline{P}_{\mathrm{g}} = \begin{bmatrix} P_{\mathrm{g}}[0] & P_{\mathrm{g}}[1] & P_{\mathrm{g}}[2] & \dots & P_{\mathrm{g}}[N_{\mathrm{p}}-1] & P_{\mathrm{g}}[N_{\mathrm{p}}] \end{bmatrix}^{\top}. \tag{3-12}$$

3-4-1 Time Step Size and Horizon Length Selection

The choice of the horizon length N_{p} and time step size Δt_{s} is very important for an effective MPC implementation. Looking at the existing CEMPC framework developed in [34], the prediction horizon is comprised of 50 time steps, each with a duration of $\Delta t_{\mathrm{s}} = 0.2$ s. Although these 50 time steps include the initial time step at $k = 0$, the prediction horizon is still said to be 10 s long. Hence, the authors of the cited paper likely use a different discretization scheme. An educated guess would be their use of the zero-order hold discretization method. Given the same time step length, the first-order hold discretization scheme used in this paper requires one extra coordinate to describe the same time span as the zero-order hold discretization method.

To realize a prediction horizon length that is long enough for the controller to make meaningful predictions that, for example, are able to steer the system towards some kind of optimal steady state, the prediction horizon length of 10 s from the cited paper is used. However, to be able to more finely model dynamic behaviour[4] a time step length Δt_{s} of 0.1 s is used. Given the resulting first-order hold discretization method, the resulting number of time steps used then becomes $N_{\mathrm{p}} = 100$, which excludes the initial time step at $k = 0$. Whilst this greater number of time steps may raise concerns about the computational tractability, or any real-time implementation, this thesis does not aim to demonstrate such real-time feasibility, instead illustrating the general feasibility of the used methods themselves.

3-5 Obtaining a Quadratic Programming Problem Formulation

By comparing the optimization problem from Eq. (3-1) and the corresponding constraints to the definition of a convex optimization problem (Eq. (2-13) to Eq. (2-15)) it is clear that the optimization problem is indeed convex. However, despite the advantage of computational efficiency of convex optimization problems, in this thesis, the large problem size still posed a considerable difficulty. To overcome these obstacles, the problem was tackled by reducing its complexity by rewriting it as a quadratic programming (QP) problem[5], for which several highly efficient optimizers exist.

[4] This desire comes from, e.g., an entirely novel method designed to deal with pitching rate constraints as will be developed in Section 3-8-2. Moreover, a reduced time step length is thought to help to reduce the accumulation of model error together with an effective feedback strategy.

[5] One could alternatively rewrite the optimization problem as a second-order cone problem, but unfortunately constraint satisfaction was fairly poor.

The QP problem that is used in this thesis consists of a convex, quadratic objective function and a set of linear equality and inequality constraints:

$$\min_x f(x) = \min_x \frac{1}{2} x^\top H_{\text{qp}} x + c_{\text{qp}}^\top x \tag{3-13}$$

$$\text{s.t. } A_{\text{ineq}} x \leq b_{\text{ineq}}, \tag{3-14}$$

$$A_{\text{eq}} x = b_{\text{eq}}, \tag{3-15}$$

in which x represents a vector of optimization variables, consisting of states, inputs and outputs, A_{ineq} and b_{ineq} indicate a matrix and vector respectively for the inequality constraints, and A_{eq} and b_{eq} likewise indicate a matrix and vector for equality constraints. Moreover, H_{qp} is a positive, semi-definite matrix, and c_{qp} is a column vector. The two elements that need to be rewritten in order to realize a QP problem are the overspeeding term within Eq. (3-1), and the maximum generator torque constraint given by the right hand side of Eq. (3-7). The objective that maximizes the available power also needs to be changed, and will be reformulated in a way that is amenable to a QP optimization problem.

3-5-1 Overspeeding

In order to limit acoustic noise and centrifugal forces the controller should attempt to limit the rotational speed to the rated rotor speed [46]. The fifth objective of Eq. (3-1) therefore penalizes overspeeding by penalizing any kinetic rotational energy that is greater than the rated kinetic rotational energy. The nonlinear overspeeding objective involving the max function can be rewritten as a linear objective with linear constraints because the objective is convex [47]. This process is illustrated below.

In accordance with the discretization method described above, the relevant discrete overspeeding objective is

$$\max_{\underline{P}_{\text{w}}, \underline{P}_{\text{g}}} -\sum_{k=1}^{N_{\text{p}}} \max\{K[k] - K_{\text{rated}}, 0\}, \tag{3-16}$$

in which the sum is again taken from $k = 1$ instead of the current time step $k = 0$ because a relevant equality constraint is formulated in Section 3-7 for $K[0]$.

To reformulate this as a linear objective, consider that for two real numbers a and b

$$\max\{a, b\} = \frac{a+b}{2} + \frac{|a-b|}{2}. \tag{3-17}$$

By applying Eq. (3-17) to Eq. (3-16) the overspeeding objective can be rewritten as

$$\max_{\underline{P}_{\text{w}}, \underline{P}_{\text{g}}} -\frac{1}{2} \sum_{k=1}^{N_{\text{p}}} K[k] - K_{\text{rated}} + |K[k] - K_{\text{rated}}|. \tag{3-18}$$

Since this objective is consistent with a convex optimization problem, it is possible to replace the absolute values $|K[k] - K_{\text{rated}}|$ in Eq. (3-18) with new variables $z_{\text{K}}[k]$ (which from this point onward will be called 'overspeed' variables) and are in turn bound by new affine constraints.

The new, equivalent objective with additional constraints is then given by

$$\max_{\underline{P}_{\mathrm{w}},\underline{P}_{\mathrm{g}},\underline{z}_{\mathrm{K}}} \; -\frac{1}{2}\sum_{k=1}^{N_{\mathrm{p}}} K[k] - K_{\mathrm{rated}} + z_{\mathrm{K}}[k] \tag{3-19}$$

$$\text{s.t.} \quad \underline{K} = \mathcal{A}K[0] + \mathcal{B}_{\mathrm{w}}\underline{P}_{\mathrm{w}} + \mathcal{B}_{\mathrm{g}}\underline{P}_{\mathrm{g}}, \tag{3-9}$$

$$z_{\mathrm{K}}[k] \geq K[k] - K_{\mathrm{rated}}, \qquad k = \{1, 2, \ldots, N_{\mathrm{p}}\}, \tag{3-20}$$

$$z_{\mathrm{K}}[k] \geq -K[k] + K_{\mathrm{rated}}, \qquad k = \{1, 2, \ldots, N_{\mathrm{p}}\}, \tag{3-21}$$

in which $\underline{z}_{\mathrm{K}}$ is a vector containing all of the overspeed variables for all of the time steps within the time except $k = 0$, and Eq. (3-9) is restated for clarity. Except for the exclusion of the current time step, $\underline{z}_{\mathrm{K}}$ is defined in the same fashion as Eq. (3-10) to Eq. (3-12). The matrix equality provided by Eq. (3-9) makes sense of the above optimization problem by relating the kinetic rotational energies to the aerodynamic powers and the generator output powers.

3-5-2 Piecewise-Linear Approximation of the Maximum Torque Constraint

Having rewritten the overspeeding objective, the remaining obstacle to obtaining a QP problem structure are the nonlinear maximum torque constraints posed by Eq. (3-7). Similar to the available power constraint, the maximum torque constraint can be approximated in a piecewise-linear fashion, as illustrated by Figure 3-2a.

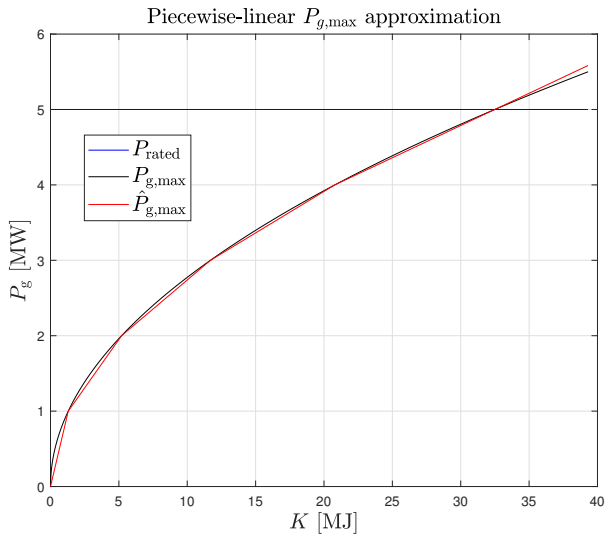

(a) The approximation of the generator power upper bound given by Eq. (3-7) for all kinetic energies between 0 J and K_{rated} using 5 linear constraints.

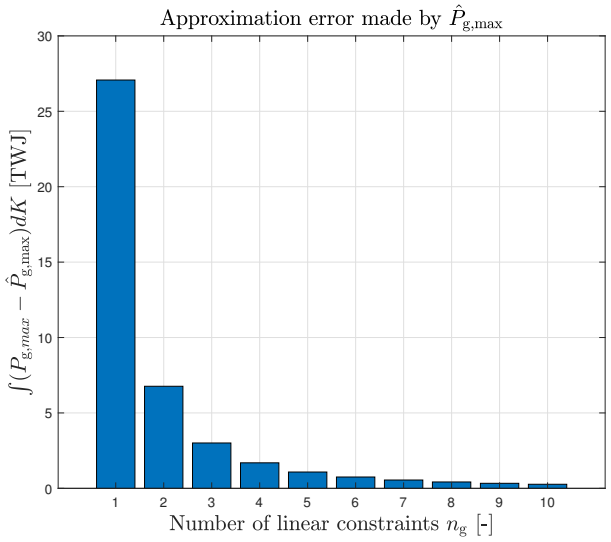

(b) The error made to approximate the nonlinear generator power upper bound, as quantified by $\int_0^{K_{\mathrm{rated}}} \left[P_{\mathrm{g,max}}(K) - \hat{P}_{\mathrm{g,max}}(K)\right] dK$, for different numbers of linear constraints used.

Figure 3-2: a) The piecewise-linear approximation of the maximum torque constraint posed by Eq. (3-7) (for all kinetic energies for which it forms a more stringent upper bound than the rated power upper bound Eq. (3-6)) using 5 linear constraints, which is used in this thesis. **b)** The marginal decrease in the approximation error decreases as the number of piecewise-linear constraints used to approximate Eq. (3-7) increases.

To obtain a good approximation, one can attempt to maximize the area under the curve of this piecewise-linear approximation such that the approximation is still less than or equal to the actual upper bound. This leads to the following optimization problem:

$$\max_{\underline{K}_{n_g+1}, \underline{\hat{P}}_{g,n_g+1}} \sum_{i=1}^{n_g} \int_{K_i}^{K_{i+1}} (a_{g,i}K + b_{g,i})dK \tag{3-22}$$

$$\text{s.t.} \quad K_1 = 0, \tag{3-23}$$

$$K_{n_g+1} = K_{\text{rated}} = \frac{1}{2} J \omega_{g,\text{rated}}^2, \tag{3-24}$$

$$K_i \leq K_{i+1}, \qquad i \in \{1, 2, \ldots, n_g - 1, n_g\}, \tag{3-25}$$

$$\hat{P}_{g,i} \leq \eta_g T_{g,\text{rated}} \sqrt{\frac{2K_i}{J}}, \quad i \in \{1, 2, \ldots, n_g - 1, n_g, n_g + 1\}, \tag{3-26}$$

$$a_{g,i} = \frac{\hat{P}_{g,i+1} - \hat{P}_{g,i}}{K_{i+1} - K_i}, \qquad i \in \{1, 2, \ldots, n_g - 1, n_g\}, \tag{3-27}$$

$$b_{g,i} = \hat{P}_{g,i} - a_i K_i, \qquad i \in \{1, 2, \ldots, n_g - 1, n_g\}, \tag{3-28}$$

in which n_g is the number of linear constraints used to approximate Eq. (3-7) for each time step in the time horizon, i is the linear constraint number, Eq. (3-27) and Eq. (3-28) define the slope and P_g-intercept ($a_{g,i}$ and $b_{g,i}$) respectively of these linear constraints, and $\underline{K}_{n_g+1}$ and $\underline{\hat{P}}_{g,n_g+1}$ are vectors that are respectively composed of all of the $(n_g + 1)$ kinetic energy and output generator power optimization variables that determine the shape of the piecewise-linear approximation.

One can further simplify this optimization problem by applying Eq. (3-27) and Eq. (3-28) to Eq. (3-22) and evaluating the objective. This leaves the constraints given by Eq. (3-23) to Eq. (3-26), which are suitable for convex optimization. Note that since the upper bound shown in black in Figure 3-2a is greater than the rated power (which forms another upper bound on the generator power) the optimization is only performed for values of K up to K_{rated}. Although the resulting objective becomes quadratic, it has a non-convex hessian. Hence, an equivalent[6] of the above optimization problem is solved using MATLAB's nonlinear solver `fmincon`.

From Figure 3-2b it is evident that the approximation error clearly decreases as the number of linear constraints used n_g increases. A clear trade-off therefore exists between a decreasing approximation error and increasing problem size (each extra linear constraint is used for each point in the prediction horizon). By looking at graphs like Figure 3-2a for different values of n_g to ensure that the difference between the approximation and the original upper bound is not too large at any value of the kinetic energy in the range given by $0 \leq K \leq K_{\text{rated}}$, and by inspection of Figure 3-2b, which shows that the marginal decrease in error decreases as n_g grows, a value of $n_g = 5$ was ultimately chosen.

3-5-3 Reformulating the Available Power Maximization Objective

Consider the objective for the maximization of the available power as presented by Eq. (3-1). Since the available aerodynamic power approximately scales with v^3 (see Eq. (2-23)), the

[6] The only difference is that Eq. (3-26) is implemented as an equality since any optimal solution should logically adhere to such an equality anyways.

contribution of the available power to the objective will be larger at greater wind speeds. The maximization of this objective is meant to help determine an optimal kinetic rotational energy trajectory since for a particular wind speed, the available aerodynamic power is only maximized at a single kinetic energy. Whilst this makes sense below the rated wind speed because a maximal available power enables the wind turbine to extract the maximum amount of power from the wind, above rated this is arguably not as useful. In the latter case, the maximum available power is often maximized at kinetic energies that fall below the rated kinetic rotational energy[7]. From Figure 3-2 it is clear that kinetic energies below K_{rated} also lead to a generator power that is below the rated power, which is clearly suboptimal from the point of view of power generation.

To prevent a large available power contribution to the objective from decreasing the output power as described above, the objective of available power maximization is reformulated in a way that is similar to the overspeeding objective. Given a particular considered trajectory of the kinetic energy, a more appropriate objective that limits the contribution of the available power is

$$\max_{\underline{\hat{P}}_{\text{av}}} \Delta t \sum_{k=1}^{N_{\text{p}}} \min \left\{ \hat{P}_{\text{av}}[k], \frac{P_{\text{rated}}}{\eta_{\text{g}}} \right\}, \tag{3-29}$$

$$\text{s.t. } \hat{P}_{\text{av}}[k] \leq a_i K[k] + b_i, \quad k \in \{1, 2, \ldots, N_{\text{p}}\}, \quad i \in \{1, 2, \ldots, n_{\text{w}}\}, \tag{3-30}$$

in which $\underline{\hat{P}}_{\text{av}}$ represents an ordered vector with all available power approximations from $k = 1$ to $k = N_{\text{p}}$. The imposed limitation of $\frac{P_{\text{rated}}}{\eta_{\text{g}}}$ reflects the *input* generator power that is needed to achieve an output generator power of P_{rated}. Envisioning steady state operation, any aerodynamic power above the imposed limit has no discernible value because the maximum generator power is limited to the rated power, hence ultimately resulting in overspeeding. Note that in Eq. (3-30) the available power approximation is treated as a 'free' optimization variable that is limited by the piecewise-linear approximations composed of the constants a_i and b_i as described in Section 2-2-3. Although there is not necessarily one unique solution to the above optimization problem, it is definitely compatible with a convex optimization framework.

Similar to Eq. (3-17), the minimum of two real numbers is described by

$$\min\{a, b\} = \frac{a + b}{2} - \frac{|a - b|}{2}. \tag{3-31}$$

Analogous to the reformulation of the overspeeding objective, let's represent the absolute value $\left|\hat{P}_{\text{av}}[k] - \frac{P_{\text{rated}}}{\eta_{\text{g}}}\right|$ by z_{P}, which will be referred to as the 'overpower' variable. By applying Eq. (3-31) to the optimization problem given by Eq. (3-29) and Eq. (3-30), the optimization problem relevant to the available aerodynamic power objective (for a given kinetic energy

[7]One may not expect this based on Figure 2-2 and with $K_{\text{rated}} \approx 32.5$ MJ, but this is a common condition for wind speeds above the rated wind speed due to the reformulation of the available power in Section 3-8. As an example one may take a look at the available power shown by Figure 3-4.

trajectory) becomes

$$\max_{\underline{\hat{P}}_{\text{av}}, \underline{z}_{\text{P}}} \frac{\Delta t}{2} \sum_{k=1}^{N_{\text{p}}} \hat{P}_{\text{av}}[k] + \frac{P_{\text{rated}}}{\eta_{\text{g}}} - z_{\text{P}}[k], \tag{3-32}$$

$$\text{s.t. } \hat{P}_{\text{av}}[k] \leq a_i K[k] + b_i, \qquad k \in \{1, 2, \ldots, N_{\text{p}}\}, \quad i \in \{1, 2, \ldots, n_{\text{w}}\}, \tag{3-30}$$

$$z_{\text{P}}[k] \geq \hat{P}_{\text{av}}[k] - \frac{P_{\text{rated}}}{\eta_{\text{g}}}, \qquad k \in \{1, 2, \ldots, N_{\text{p}}\}, \tag{3-33}$$

$$z_{\text{P}}[k] \geq -\hat{P}_{\text{av}}[k] + \frac{P_{\text{rated}}}{\eta_{\text{g}}}, \quad k \in \{1, 2, \ldots, N_{\text{p}}\}, \tag{3-34}$$

in which $\underline{z}_{\text{P}}$ is a sorted vector that contains all of the overpower variables for time steps $k = 1$ to $k = N_{\text{p}}$, and Eq. (3-30) has been restated for the purpose of clarity.

3-6 Turnpike Mitigation

A common problem that the authors of [34] do not mention in setting up their optimization problem as indicated in Section 3-2 is an issue named 'turnpike'. It refers to the fact that if one does not value the kinetic rotational energy at the end of the prediction horizon $K[N_{\text{p}}]$, the controller will increase the generator power throughout the end of the prediction horizon, decreasing the kinetic rotational energy in the process.

Clearly though, there is some merit to the kinetic rotational energy at the end of the prediction horizon. After all, this energy can be converted into usable energy in the future with an efficiency given by the generator efficiency η_{g} (assuming that there are no other sources of useful power loss like gearbox losses). It is typically possible to account for turnpike by including the a term $\eta_{\text{g}} K[N_{\text{p}}]$ that is to be maximized within the objective of the optimization problem [48].

However, such an objective also rewards any kinetic energy above the rated kinetic rotational energy. This is in direct contravention of the objective that aims to minimize overspeeding as detailed in Section 3-5-1. Hence, a modified contribution is used within the objective function that only rewards kinetic energies up to the rated rotational speed:

$$\eta_{\text{g}} \left[K[N_{\text{p}}] - \frac{1}{2}(K[N_{\text{p}}] - K_{\text{rated}} + z_{\text{K}}[N_{\text{p}}]) \right], \tag{3-35}$$

in which the term that is subtracted represents any (non-negative amount of) kinetic energy above the rated kinetic energy.

3-7 Feedback Implementation

To minimize errors that can develop over time between the implemented model and the actual wind turbine system, feedback is included in this CEMPC implementation. The measured quantities that are provided as feedback signals for CPC concern the pitch angle, generator torque, generator rotational speed, and the rotor speed.

3-7-1 Feedback Constraints

As a feedback signal, these measurements provide equality constraints that prescribe the kinetic rotational energy, aerodynamic power, and the generator output power at time step $k = 0$. These equalities are given by

$$K[0] = \frac{1}{2} J N^2 \omega_{\mathrm{r,me}}^2, \tag{3-36}$$

$$P_{\mathrm{w}}[0] = \frac{1}{2} \rho A C_{\mathrm{P}}(\beta_{\mathrm{me}}, \lambda[0]) \hat{v}^3, \tag{3-37}$$

$$P_{\mathrm{g}}[0] = \eta_{\mathrm{g}} T_{\mathrm{g,me}} \omega_{\mathrm{g,me}}, \tag{3-38}$$

in which the measured generator speed, rotor speed, pitch angle, and generator torque are respectively given by $\omega_{\mathrm{g,me}}$, $\omega_{\mathrm{r,me}}$, β_{me}, and $T_{\mathrm{g,me}}$, and the relevant tip speed ratio $\lambda[0]$ is computed by application of $K[0]$ and $\hat{v}$ to Eq. (2-31). The reason for the use of the rotor speed in Eq. (3-36) instead of the generator speed is that it provides a more accurate description of the kinetic rotational energy since the contribution of the rotor (J_{r}/N^2) to the total mass moment of inertia J is far greater than the contribution of the generator inertia J_{g}. This can be verified by studying Table 3-1.

3-7-2 Updating the Predictions from a Previous Solution

The kinetic energy obtained Eq. (3-36) and the measured pitch angle β_{me} can be used to update the predicted solution trajectories. As will be explained later on in Section 3-8-2, the predictions of these solution trajectories are important for the determination of the implemented aerodynamic power constraints (such new constraints are developed in Section 3-8). The predictions are updated based on

$$\hat{K}[k|m] = \hat{K}[k|m-1] + (K[0] - \hat{K}[0|m-1]), \qquad k \in \{0, 1, \ldots, N_{\mathrm{p}}\}, \tag{3-39}$$

$$\hat{\beta}[k|m] = \hat{\beta}[k|m-1] + (\beta_{\mathrm{me}} - \hat{\beta}[0|m-1]), \qquad k \in \{0, 1, \ldots, N_{\mathrm{p}}\}, \tag{3-40}$$

in which m represents the number of times that the prediction horizon has shifted (thereby illustrating which solution iteration the prediction originates from), and the subscript 'me' demonstrates that the relevant quantity is measured. The number m will from hereon forwards only be shown again where it is relevant to show that information is conveyed from one solution to the next, as is the case in Eq. (3-39) and Eq. (3-40).

3-8 Aerodynamic Power Constraints

The essential approximation that was made in Chapter 2 that allowed a convex optimization problem was the approximation of the available power as a piecewise-linear function. However, looking at the definition of the aerodynamic power constraints provided by Eq. (2-22), the definition of the available power in Eq. (2-23), and the approximation of the available power described in Section 2-2-3, it becomes clear that there is still some room for improvement.

3-8-1 Using a Different Fitting Method

To start, the fitting procedure used by Hovgaard, Boyd, and Jørgensen in [33] follows the method outlined in [39]. As a result of this fitting method, and as is visible from Figure 3-3 the piecewise-linear available power approximation may be greater than the actual available power. In fact, as Figure 2-3 from the previous chapter demonstrates, the approximated available power $\hat{P}_{\text{av}}$ will be larger than the actual available power P_{av} for about half of the operating conditions specified by a combination of the wind speed and kinetic rotational energy.

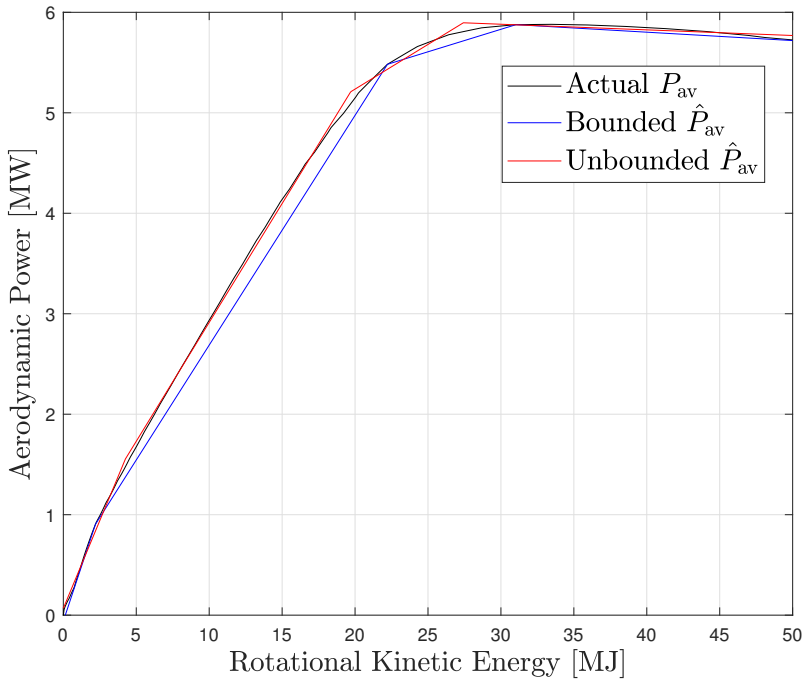

Figure 3-3: A comparison between the actual available power and two piecewise-linear, convex approximations thereof at a wind speed of 12 m/s. The unbounded approximation uses the method described in [39] and results in an approximation that at times is greater than the actual available power. In contrast, the bounded approximation does not exceed the actual available power, and is produced using the method from Appendix A. It is important to note that whilst both approximations as shown in this figure only use four linear constraints, this is only done to better illustrate the differences between the approximation methods; as the number of linear constraints increases, these differences become less noticeable.

This, at times, too high available power allows from an in reality unattainable aerodynamic power, and (therefore) power coefficient. In effect, the maximum theoretical power coefficient that corresponds with the tip speed ratio (as defined by the wind speed and kinetic energy as per Eq. (2-31)) is exceeded by the power coefficient one would calculate based on the (too high) modeled aerodynamic power. There are two practical ramifications, namely: the question of what pitch angle to implement, and the problem of introduced model error.

With respect to the first issue, one may choose the pitch angle that would maximize the

theoretical power coefficient. This would also limit the model error that results from an aerodynamic power that is greater than the actual available power, which would cause the model to predict unreachable kinetic energies at the next time step. However, it is unnecessary to introduce this model error in the first place; alternatively, one may impose the constraint that the available power approximation is less than or equal to the theoretical available power:

$$\hat{P}_{\mathrm{av}} \leq P_{\mathrm{av}}. \tag{3-41}$$

A new fitting method that is based on a simple linear programming (LP) problem that takes into account this constraint is explained in Appendix A. As can be seen from Figure 3-3, the resulting bounded, concave, piecewise-linear approximation $\hat{P}_{\mathrm{av}}$ is effectively bounded by the actual available power P_{av}.

3-8-2 Incorporating Pitching Rate Constraints

A pitching rate constraint is not modeled in the existing CEMPC literature. The original inventors of this framework in [33] use an MPC time step of 10 s since they do not focus on dynamic effects. Combining such an MPC time step size with the maximum absolute pitching rate from the NREL 5 MW wind turbine of $\dot{\beta}_{\max} = 8°/\mathrm{s}$ as provided by Table 3-1 gives rise to a very large maximal pitch deviation of 80° between time steps. With reference to the minimum and maximum pitch angles of 0° and 20° provided by Table 3-1 one can see that a pitch rate constraint makes no sense in such a setting because all pitch angles between the minimum and maximum pitch are reachable within a single time step.

However, given the time step size used in this thesis of $\Delta t_{\mathrm{s}} = 0.1$ s, this pitching rate constraint becomes more important. Since the resulting maximum pitch deviation between time steps is only 0.8°, the inclusion of only pitch angle lower and upper bounds does not properly address the pitch rate constraint. As a result, one may argue that the classical definition of the available aerodynamic power as provided by Eq. (2-23) is inadequate for applications with shorter time step lengths. The minimum aerodynamic power $P_{\mathrm{w}}^{\mathrm{lb}}$ of zero is clearly also unsuitable for the same reason. With reference to this deficiency, the available aerodynamic power P_{av} and the minimum aerodynamic power are redefined as

$$P_{\mathrm{av}}(v, K[k]; \beta[k-1]) = \max_{\beta^{\mathrm{lb}}[k] \leq \beta[k] \leq \beta^{\mathrm{ub}}[k]} \frac{1}{2}\rho A C_{\mathrm{P}}(\beta[k], K[k], v)v^3, \tag{3-42}$$

$$P_{\mathrm{w}}^{\mathrm{lb}}(v, K[k]; \beta[k-1]) = \min_{\beta^{\mathrm{lb}}[k] \leq \beta[k] \leq \beta^{\mathrm{ub}}[k]} \frac{1}{2}\rho A C_{\mathrm{P}}(\beta[k], K[k], v)v^3, \tag{3-43}$$

in which the superscripts 'lb' and 'ub' respectively signify lower and upper bound. Both of these definitions are dependent on the previous pitch angle because of the definition of the lower and upper bounds of the pitch angle (β^{lb} and β^{ub} respectively):

$$\beta^{\mathrm{lb}}[k] = \max\{\beta[k-1] - \dot{\beta}_{\max}\Delta t_{\mathrm{s}}, \beta_{\min}\}, \tag{3-44}$$

$$\beta^{\mathrm{ub}}[k] = \min\{\ \beta[k-1] + \dot{\beta}_{\max}\Delta t_{\mathrm{s}}, \beta_{\max}\}. \tag{3-45}$$

The attentive reader will note that since the pitch angles are determined from the aerodynamic powers as described in Section 2-2-5, the above definitions would require an iterative solution

approach. This is because Eq. (3-44) and Eq. (3-45) are needed to define the bounds of the aerodynamic powers based on the pitch solution trajectory, which is itself dependent on the aerodynamic power solutions. Inspired by [41][8], the solution approach taken in this thesis is to perform three iterations for the first solution. For subsequent solutions, no iterations are used. Instead, an estimate of the pitch angle at the previous time step is used from the previous solution $\hat{\beta}[k-1]$. The resulting implemented pitch constraints then become

$$\hat{\beta}^{\mathrm{lb}}[k] = \max\{\hat{\beta}[k-1] - \dot{\beta}_{\max}\Delta t_{\mathrm{s}}, \beta_{\min}\}, \tag{3-46}$$

$$\hat{\beta}^{\mathrm{ub}}[k] = \min\{\hat{\beta}[k-1] + \dot{\beta}_{\max}\Delta t_{\mathrm{s}}, \beta_{\max}\}. \tag{3-47}$$

An example of a resulting available power and minimum aerodynamic power characteristic are provided by Figure 3-4. Despite significantly limiting the range of pitch angles that are used in the new definitions of the available aerodynamic power and the minimum aerodynamic power, it is apparent that these curves retain their nearly concave shape, as was the case in [33] with the existing available power description.

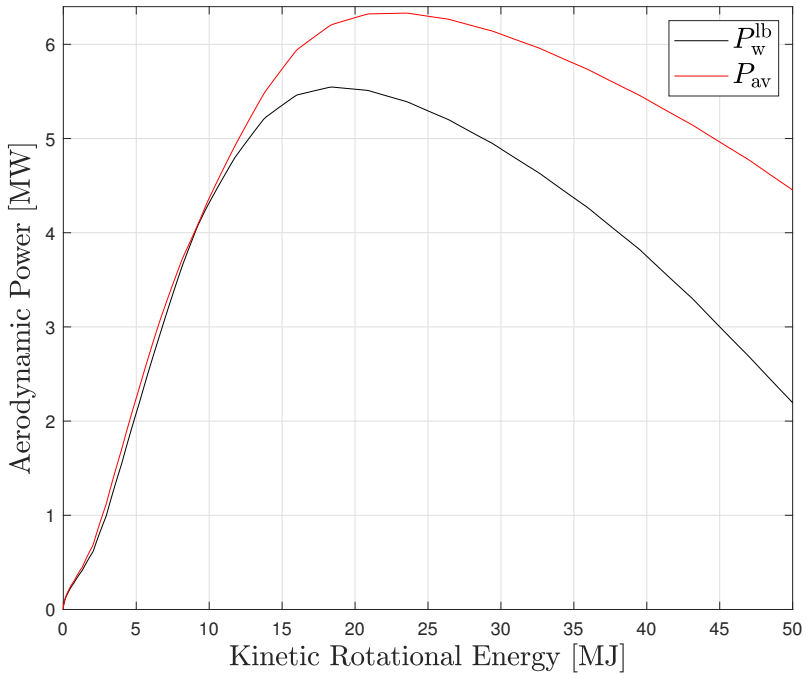

Figure 3-4: An example of a minimum aerodynamic power $P_{\mathrm{w}}^{\mathrm{lb}}$ and available aerodynamic power P_{av} characteristic as defined by Eq. (3-42) to Eq. (3-45) for a wind speed of 16 m/s, a previous pitch angle $\beta[k-1]$ of 11.5°, an MPC time step of $\Delta t = 0.1$ s, and a maximum absolute pitching rate of 8°/s.

Note that if an approximation of the available and minimum aerodynamic power is to be

[8]The principal idea of this source is that iterations are only needed for the first solution step in order to achieve convergence since, for sufficiently small time steps, consecutive solutions should not differ very much. Hence, iterations are not needed for subsequent solution steps. The difference of the problem described here with respect to this source is that not the system dynamics but the constraints are subject to a scheduling variable.

made using characteristics as shown in Figure 3-4, these approximations would need to be scheduled not only on the wind speed (as is the case in the classical CEMPC framework), but also on the previous pitch angle. To simplify this scheduling mechanism, the subject of the existing fitting approach is reconsidered.

Fitting to the Aerodynamic Power Coefficient Instead of the Aerodynamic Power

Let's temporarily revisit the existing CEMPC framework. By consideration of Eq. (2-23) and Eq. (2-24) one can see that for the available power, the piecewise-linear fitting approach essentially provided a fit to describe the nonlinearity of the maximum power coefficients found at a certain wind speed and different kinetic rotational energies. In fact, one may notice that the different normalized available powers depicted in Figure 2-2 appear very similar. To understand this similarity, consider that the relationship between the kinetic rotational energy, the tip speed ratio, and the wind speed is given by

$$K = \frac{JN^2}{2R^2}\lambda^2 v^2. \tag{3-48}$$

Since the aerodynamic power coefficient is dependent directly on the pitch and tip speed ratio, one can infer from Eq. (3-48) that a single more important characteristic is at the heart of all of the relationships $P_{\mathrm{av}}(v,K)/v^3$ shown in Figure 2-2:

$$C_{\mathrm{P}}^{\mathrm{ub}}(\lambda^2) = \max_{\beta_{\min}\leq\beta\leq\beta_{\max}} C_{\mathrm{P}}(\beta,\lambda^2). \tag{3-49}$$

In other words, by knowing the shape of the $C_{\mathrm{P}}^{\mathrm{ub}}(\lambda^2)$ characteristic, one could easily determine the shape of the $P_{\mathrm{av}}(v,K)$ characteristic for a specific wind speed using Eq. (3-48). Hence, it makes sense to fit to a single $C_{\mathrm{P}}^{\mathrm{ub}}(\lambda^2)$ characteristic instead of $P_{\mathrm{av}}(v,K)/v^3$ for several different wind speed values, as is done in the existing CEMPC framework.

This insight can also be applied to the newly defined available power and minimum aerodynamic power. Changing the relevant pitch constraints in Eq. (3-49), to find approximations of Eq. (3-42) and Eq. (3-43), one then essentially fits to the lower and upper bound aerodynamic power coefficient characteristics ($C_{\mathrm{P}}^{\mathrm{lb}}$ and $C_{\mathrm{P}}^{\mathrm{ub}}$ respectively) given by

$$C_{\mathrm{P}}^{\mathrm{ub}}(\hat{\lambda[k]^2};\beta[k-1]) = \max_{\hat{\beta}^{\mathrm{lb}}[k]\leq\beta[k]\leq\hat{\beta}^{\mathrm{ub}}[k]} C_{\mathrm{P}}(\beta[k],\lambda[k]^2), \tag{3-50}$$

$$C_{\mathrm{P}}^{\mathrm{lb}}(\hat{\lambda[k]^2};\beta[k-1]) = \min_{\hat{\beta}^{\mathrm{lb}}[k]\leq\beta[k]\leq\hat{\beta}^{\mathrm{ub}}[k]} C_{\mathrm{P}}(\beta[k],\lambda[k]^2), \tag{3-51}$$

using the newly introduced, bounded approximation method. This gives rise to the piecewise-linear approximations of the minimum and maximum aerodynamic power coefficient ($\hat{C}_{\mathrm{P}}^{\mathrm{ub}}$ and $\hat{C}_{\mathrm{P}}^{\mathrm{lb}}$ respectively)

$$\hat{C}_{\mathrm{P}}^{\mathrm{ub}}(\lambda[k]^2;\hat{\beta}[k-1]) = \min\{a_{\mathrm{c},k,1}^{\mathrm{ub}}\lambda[k]^2 + b_{\mathrm{c},k,1}^{\mathrm{ub}},\ldots,a_{\mathrm{c},k,n_{\mathrm{w}}}^{\mathrm{ub}}\lambda[k]^2 + b_{\mathrm{c},k,n_{\mathrm{w}}}^{\mathrm{ub}}\}, \tag{3-52}$$

$$\hat{C}_{\mathrm{P}}^{\mathrm{lb}}(\lambda[k]^2;\hat{\beta}[k-1]) = \min\{a_{\mathrm{c},k,1}^{\mathrm{lb}}\lambda[k]^2 + b_{\mathrm{c},k,1}^{\mathrm{lb}},\ldots,a_{\mathrm{c},k,n_{\mathrm{w}}}^{\mathrm{lb}}\lambda[k]^2 + b_{\mathrm{c},k,n_{\mathrm{w}}}^{\mathrm{lb}}\}, \tag{3-53}$$

in which $a_{\mathrm{c},k,i}^{\mathrm{lb}}$, $b_{\mathrm{c},k,i}^{\mathrm{lb}}$, $a_{\mathrm{c},k,i}^{\mathrm{ub}}$, and $b_{\mathrm{c},k,i}^{\mathrm{ub}}$ are constants that depend on the estimate of the previous pitch angle $\hat{\beta}[k-1]$, the subscript c indicates that these constants are used to express a

piecewise-linear approximation of their respective power coefficients, and the subscript k denotes that the constant is used for the k^{th} time step. The dependence of these constants on the estimated previous pitch angle is not shown for the sake of brevity and clarity.

By using Eq. (3-48) to replace the dependence of λ^2 in Eq. (3-52) and Eq. (3-53) with a dependence on K and $\hat{v}$ [9], and by subsequently applying these latter two equations to Eq. (3-42) and Eq. (3-43), one then finds the piecewise-linear approximations

$$\hat{P}_{\text{av}}(K[k];\hat{v},\hat{\beta}[k-1]) = \min\left\{a^{\text{ub}}_{k,1}K[k] + b^{\text{ub}}_{k,1},\ldots,a^{\text{ub}}_{k,n_{\text{w}}}K[k] + b^{\text{ub}}_{k,n_{\text{w}}}\right\}, \tag{3-54}$$

$$\hat{P}^{\text{lb}}_{\text{w}}(K[k];\hat{v},\hat{\beta}[k-1]) = \min\left\{a^{\text{lb}}_{k,1}K[k] + b^{\text{lb}}_{k,1},\ldots,a^{\text{lb}}_{k,n_{\text{w}}}K[k] + b^{\text{lb}}_{k,n_{\text{w}}}\right\}, \tag{3-55}$$

in which the number of affine inequalities n_{w} used is chosen to be 15, as is the case in Section 2-2-3, and the constants are defined by

$$a^{\text{ub}}_{k,i} = \left(\frac{\rho A R^2}{JN^2}\hat{v}\right) a^{\text{ub}}_{\text{c},k,i}, \tag{3-56}$$

$$b^{\text{ub}}_{k,i} = \left(\frac{1}{2}\rho A\hat{v}^3\right) b^{\text{ub}}_{\text{c},k,i}, \tag{3-57}$$

$$a^{\text{lb}}_{k,i} = \left(\frac{\rho A R^2}{JN^2}\hat{v}\right) a^{\text{lb}}_{\text{c},k,i}, \tag{3-58}$$

$$b^{\text{lb}}_{k,i} = \left(\frac{1}{2}\rho A\hat{v}^3\right) b^{\text{lb}}_{\text{c},k,i}. \tag{3-59}$$

Note that in the above definitions of the constants for Eq. (3-54) and Eq. (3-55), the resulting constants are dependent on both the previous pitch angle (because the original constants are), and the wind speed.

To ensure that $\hat{P}^{\text{lb}}_{\text{w}} \leq \hat{P}_{\text{av}}$, it is important to see to it that $\hat{C}^{\text{lb}}_{\text{P}} \leq \hat{C}^{\text{ub}}_{\text{P}}$. This is done by first finding a good piecewise-linear fit for $\hat{C}^{\text{ub}}_{\text{P}}$ and subsequently including it as an upper bound within the newly developed fitting method for the approximation of the minimum aerodynamic power coefficient $\hat{C}^{\text{lb}}_{\text{P}}$. This extra upper bound during the fitting procedure of the minimum aerodynamic power coefficient is particularly important, because, as one can see from Figure 3-4, the difference between the minimum and maximum aerodynamic power can be very small.

An Affine Lower Bound on the Aerodynamic Power

Ultimately, the idea of Eq. (3-54) and Eq. (3-55) is to provide suitable constraints for the CEMPC framework that take into account the pitching rate constraint. However, the concave lower bound of the aerodynamic power provided by Eq. (3-55) is incompatible with a convex optimization problem formulation. Hence, to approximate the minimum aerodynamic power, of the n_{w} affine constraints that form Eq. (3-55), only a single one is used. The piecewise-linear approximation of $\hat{P}^{\text{lb}}_{\text{w}}$ is described by the different affine constraints over specific intervals of $K[k]$. It makes sense to select the affine constraint $i = l_k$ that corresponds to the interval of $K[k]$ in which one expects the new solution for $K[k]$ to lie. To select the correct affine

[9] Note the use of an estimate here since this thesis in practice considers estimates of the wind speed.

constraint one can use the estimate provided by the previous solution $\hat{K}[k]$. The resulting, implemented minimum aerodynamic power is

$$\hat{P}_{\mathrm{w}}^{\mathrm{lb}}(K[k]; \hat{v}, \hat{\beta}[k-1], \hat{K}[k]) = a_{k,l_k}^{\mathrm{lb}} K[k] + b_{k,l_k}^{\mathrm{lb}}, \tag{3-60}$$

in which the choice of $i = l_k$ therefore depends on the estimate of the kinetic energy as provided by a previous solution $\hat{K}[k]$ and the different intervals of $K[k]$ that form the different 'pieces' of the piecewise-linear approximation as given by Eq. (3-55).

Compensating for Pitching Rate Constraint Violations Due to 'Pitch Drift'

Using the aerodynamic power constraints as developed above, there is still one problem with regards to pitching rate constraints within the prediction horizon. The issue stems from the fact that the implemented pitch constraints as given by Eq. (3-46) and Eq. (3-47) specify the lower and upper pitch bounds relative to an estimate $\hat{\beta}[k-1]$ instead of the actual previous pitch $\beta[k-1]$ (as is the case in Eq. (3-44) and Eq. (3-45)). As is demonstrated in Figure 3-5, the maximum deviation between consecutive pitch angles using this method is three times more than the desired quantity of $\dot{\beta}_{\max}\Delta t_{\mathrm{s}}$. Within this thesis the described issue will be referred to as 'pitch drift' because it stems from the drift that can be observed between consequtive pitch angle estimates.

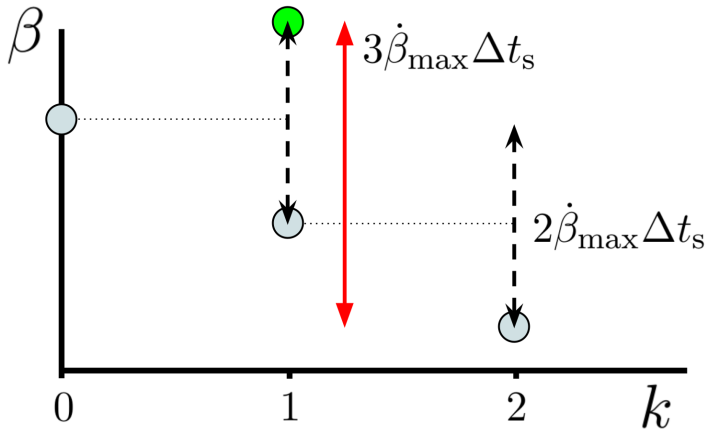

Figure 3-5: An illustration of the problem of 'pitch drift' whereby two consecutive pitch angles within the prediction horizon may adhere to the pitching rate constraint at one time step, but not during the next. The initial pitch estimates $\hat{\beta}$ from the previous solution are displayed in grey. The bounds of the new pitch angles are provided by Eq. (3-46) and Eq. (3-47) and are displayed by the black, dashed intervals. The pitch estimate at $k = 0$ reflects the measured pitch angle, which is assumed to have no uncertainty. Suppose that the resulting pitch solution that is found β only has a change (relative to $\hat{\beta}$) at $k = 1$, where the new pitch is given in green. The resulting change in pitch angle computed between $k = 1$ and $k = 2$ becomes $3\dot{\beta}_{\max}\Delta t_{\mathrm{s}}$, which clearly violates the lower bound pitch constraint formulated by Eq. (3-44) for $k = 2$.

At this point, it is useful to explain that since feedback is applied by means of pitch angle measurement as described in Section 3-7, the pitch angle estimate at $k = 0$ can be assumed to be perfect ($\beta[0] = \hat{\beta}[0] = \beta_{\mathrm{me}}$). As is visible from Figure 3-5, the pitch angle $\beta[1]$ should therefore always adhere to the new pitch constraints posed by Eq. (3-44) and Eq. (3-45).

However, the described problem does exist for other pitch angles further along in the prediction horizon. As such, allowing pitch constraint violations within the rest of the prediction horizon could decrease the model accuracy. One solution would be to simply apply a maximum absolute pitching rate that is one third of the actual desired maximum absolute pitching rate. However, this would likely introduce a considerable degree of conservatism since the example depicted in Figure 3-5 is arguably not likely to occur very often; solutions are assumed not to change very much between consecutive solution steps, which means that differences between $\hat{\beta}[k]$ and $\beta[k]$ should normally be fairly small. Nonetheless, one may still anticipate relatively small constraint violations where the original pitch estimates only just satisfy the constraints given by Eq. (3-44) or Eq. (3-45) (as is the case in Figure 3-5). Hence, an alternative is used whereby the pitch solution is first checked for any pitch constraint violations. If such violations are found, the pitch trajectory is subjected to an LP that performs pitch angle corrections. The optimization problem performed by this LP is:

$$\min_{\underline{\beta}_{\text{out}}} \sum_{k=1}^{N_\text{p}} z_\beta[k] \tag{3-61}$$

$$\text{s.t. } \beta_{\text{out}}[0] = \beta_{\text{in}}[0], \tag{3-62}$$

$$\beta_{\text{out}}[k] \geq \beta_{\min}, \qquad k \in \{1, 2, \ldots, N_\text{p}\}, \tag{3-63}$$

$$\beta_{\text{out}}[k] \leq \beta_{\max}, \qquad k \in \{1, 2, \ldots, N_\text{p}\}, \tag{3-64}$$

$$\beta_{\text{out}}[k] \geq \beta_{\text{out}}[k-1] - \dot{\beta}_{\max}\Delta t_\text{s}, \quad k \in \{1, 2, \ldots, N_\text{p}\}, \tag{3-65}$$

$$\beta_{\text{out}}[k] \leq \beta_{\text{out}}[k-1] + \dot{\beta}_{\max}\Delta t_\text{s}, \quad k \in \{1, 2, \ldots, N_\text{p}\}, \tag{3-66}$$

$$z_\beta[k] \geq \beta_{\text{out}}[k] - \beta_{\text{in}}[k], \qquad k \in \{1, 2, \ldots, N_\text{p}\}, \tag{3-67}$$

$$z_\beta[k] \geq -\beta_{\text{out}}[k] + \beta_{\text{in}}[k], \qquad k \in \{1, 2, \ldots, N_\text{p}\}, \tag{3-68}$$

in which the objective Eq. (3-61) seeks to minimize the sum of the absolute differences between the input pitch angles (β_{in}) and those given as an output of the LP (β_{out}). The parameter vector that is optimized $\underline{\beta}_{\text{out}}$ represents a vector that contains all of the $N_\text{p}+1$ output pitch angles. The absolute differences $|\beta_{\text{out}}[k] - \beta_{\text{in}}[k]|$ are represented by $z_\beta[k]$ due to Eq. (3-67), Eq. (3-68) and the convex problem formulation. Note the similarity with the representation of the absolute differences used in Section 3-5-1. The only equality constraint (Eq. (3-62)) ensures that $\beta_{\text{out}}[0]$ agrees with the measured pitch value. Minimum and maximum pitch angle constraints are implemented by Eq. (3-63) and Eq. (3-64) respectively, whilst a maximum pitching rate is ensured by Eq. (3-65) and Eq. (3-66).

3-9 Convex Economic Model Predictive Controller Implementation Overview

Given the various practical and theoretical considerations that have been described from Section 3-3 to Section 3-8, this section clarifies the resulting controller structure. Having read the above sections, it may be clear to the reader that there is more to the CEMPC block shown in Figure 3-1 than only a convex economic model predictive controller. The components of this block are shown in greater detail by Figure 3-6.

Convex economic model predictive control is performed using measurements of the pitch angle β_{me}, rotor speed $\omega_{\mathrm{r,me}}$, generator speed $\omega_{\mathrm{g,me}}$, a rotor effective wind speed estimate $\hat{v}$, and estimates of the kinetic energy trajectory $\hat{K}_k$ and pitch trajectory $\hat{\beta}_k$. The output of the convex economic model predictive controller consists of computed trajectories for the generator power $P_{\mathrm{g},k}$, rotational kinetic energy K_k, and aerodynamic power $P_{\mathrm{w},k}$. The computed kinetic energy trajectory is reused as an estimate for the subsequent MPC solution step. Using a pitch lookup table β_{lut} a pitch trajectory $\beta_{\mathrm{in},k}$ is calculated from the rotor-effective wind speed estimate and the kinetic energy and aerodynamic power trajectories. In the case that the computed pitch angles do not comply with the pitching rate constraint due to pitch drift, the pitch angles are corrected by an LP to arrive at the output pitch angles $\beta_{\mathrm{out},k}$. Similar to the kinetic energy, these pitch angles are reused as estimates $\hat{\beta}_k$ for the subsequent MPC solution step.

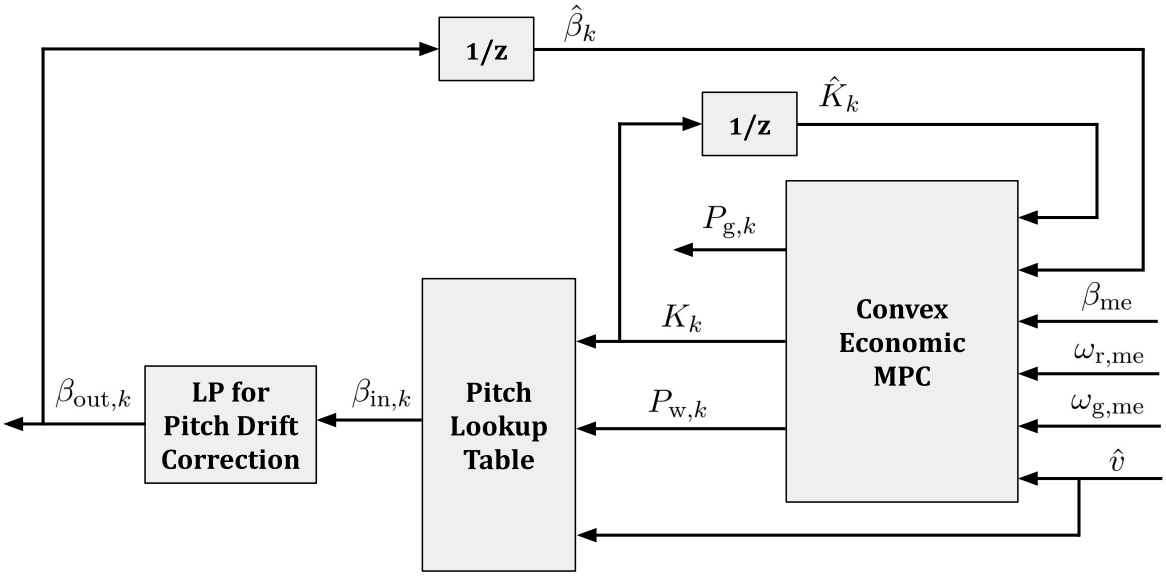

Figure 3-6: Design of the convex economic model predictive controller implementation for CPC. The convex economic model predictive controller uses pitch measurements β_{me}, rotor speed measurements $\omega_{\mathrm{r,me}}$, generator speed measurements $\omega_{\mathrm{g,me}}$, a rotor-effective wind speed estimate $\hat{v}$, estimates of the kinetic rotational energy trajectory $\hat{K}_k$ from the previous solution, and estimates of the pitch trajectory $\hat{\beta}_k$ from the previous solution to compute the trajectories of the generator power $P_{\mathrm{g},k}$, kinetic energy $\hat{K}_k$, and aerodynamic power $P_{\mathrm{w},k}$. A pitch lookup table β_{lut} is subsequently used to compute a possible pitch angle trajectory $\beta_{\mathrm{in},k}$ from the kinetic energy and aerodynamic power trajectories. If necessary, this pitch angle trajectory is then corrected by an LP problem to ensure that pitch constraints are satisfied despite pitch drift This results in the used pitch angle trajectory $\beta_{\mathrm{out},k}$, which also provides estimates of the pitch angle for the next MPC solution step.

3-10 Implemented Optimization Problem

Given the various alterations and additions to the existing CEMPC optimization problem presented previously in Section 3-2, the resulting optimization problem that has to be solved for each time step is now given below.

$$\begin{aligned}\min_{\underline{x}} \quad & \underbrace{-\alpha_1 \Delta t_\mathrm{s} c^\top \underline{P}_\mathrm{g}}_{\substack{\text{generator power}\\ \text{maximization}}} \underbrace{-\alpha_1 \eta_\mathrm{g} \left[K[N_\mathrm{p}] - \frac{K[N_\mathrm{p}] - K_\mathrm{rated} + z_\mathrm{K}[N_\mathrm{p}]}{2} \right]}_{\text{turnpike mitigation}} \\ & + \sum_{k=1}^{N_\mathrm{p}} \Bigg[\underbrace{\alpha_2 (P_\mathrm{g}[k] - P_\mathrm{g}[k-1])^2}_{\substack{\text{minimize generator}\\ \text{output power variations}}} + \underbrace{\alpha_3 \left(\frac{2}{\rho A \hat{v}^3} \right)^2 (P_\mathrm{w}[k] - P_\mathrm{w}[k-1])^2}_{\text{minimize } C_\mathrm{P} \text{ variations}} \\ & \underbrace{- \alpha_4 \frac{\Delta t}{2} \left(\hat{P}_\mathrm{av}[k] + \frac{P_\mathrm{rated}}{\eta_\mathrm{g}} - z_\mathrm{P}[k] \right)}_{\substack{\text{limited available}\\ \text{power maximization}}} + \underbrace{\alpha_5 \frac{K[k] - K_\mathrm{rated} + z_\mathrm{K}[k]}{2}}_{\substack{\text{minimize}\\ \text{overspeeding}}} \Bigg] \end{aligned} \tag{3-69}$$

$$\begin{aligned}
\text{s.t.} \quad & K[k] \geq 0, && k \in \{1, 2, \ldots, N_\mathrm{p}\}, && (3\text{-}3)\\
& K[k] \leq K_\mathrm{max}, && k \in \{1, 2, \ldots, N_\mathrm{p}\}, && (3\text{-}4)\\
& P_\mathrm{g}[k] \geq 0, && k \in \{1, 2, \ldots, N_\mathrm{p}\}, && (3\text{-}5)\\
& P_\mathrm{g}[k] \leq P_\mathrm{rated}, && k \in \{1, 2, \ldots, N_\mathrm{p}\}, && (3\text{-}6)\\
& \underline{K} = \mathcal{A} K[0] + \mathcal{B}_\mathrm{w} \underline{P}_\mathrm{w} + \mathcal{B}_\mathrm{g} \underline{P}_\mathrm{g}, && && (3\text{-}9)\\
& z_\mathrm{K}[k] \geq K[k] - K_\mathrm{rated}, && k \in \{1, 2, \ldots, N_\mathrm{p}\}, && (3\text{-}20)\\
& z_\mathrm{K}[k] \geq -K[k] + K_\mathrm{rated}, && k \in \{1, 2, \ldots, N_\mathrm{p}\}, && (3\text{-}21)\\
& z_\mathrm{P}[k] \geq \hat{P}_\mathrm{av}[k] - \frac{P_\mathrm{rated}}{\eta_\mathrm{g}}, && k \in \{1, 2, \ldots, N_\mathrm{p}\}, && (3\text{-}33)\\
& z_\mathrm{P}[k] \geq -\hat{P}_\mathrm{av}[k] + \frac{P_\mathrm{rated}}{\eta_\mathrm{g}}, && k \in \{1, 2, \ldots, N_\mathrm{p}\}, && (3\text{-}34)\\
& K[0] = \frac{1}{2} J N^2 \omega_\mathrm{r,me}^2, && && (3\text{-}36)\\
& P_\mathrm{w}[0] = \frac{1}{2} \rho A C_\mathrm{P}(\beta_\mathrm{me}, \lambda[0]) \hat{v}^3, && && (3\text{-}37)\\
& P_\mathrm{g}[0] = \eta_\mathrm{g} T_\mathrm{g,me} \omega_\mathrm{g,me}, && && (3\text{-}38)\\
& P_\mathrm{g}[k] \leq a_{\mathrm{g},i} K[k] + b_{\mathrm{g},i}, && k \in \{1, 2, \ldots, N_\mathrm{p}\}, \quad i \in \{1, 2, \ldots, n_\mathrm{g}\}, && (3\text{-}70)\\
& P_\mathrm{w}[k] \geq a_{k,l_k}^\mathrm{lb} K[k] + b_{k,l_k}^\mathrm{lb}, && k \in \{1, 2, \ldots, N_\mathrm{p}\}, && (3\text{-}71)\\
& P_\mathrm{w}[k] \leq \hat{P}_\mathrm{av}[k], && k \in \{1, 2, \ldots, N_\mathrm{p}\}, && (3\text{-}72)\\
& \hat{P}_\mathrm{av}[k] \leq a_{k,i}^\mathrm{ub} K[k] + b_{k,i}^\mathrm{ub}, && k \in \{1, 2, \ldots, N_\mathrm{p}\}, \quad i \in \{1, 2, \ldots, n_\mathrm{w}\}, && (3\text{-}73)
\end{aligned}$$

in which $\Delta t_\mathrm{s} = 0.1$ s, $N_\mathrm{p} = 100$, $n_\mathrm{g} = 5$, $n_\mathrm{w} = 15$, the relevant α constants have been reused from Eq. (3-1) for clarity, $\underline{x}$ is a column vector containing all of the relevant 'free' optimization variables: $\underline{P}_\mathrm{g}$, $\underline{P}_\mathrm{w}$, $\underline{\hat{P}}_\mathrm{av}$, $\underline{z}_\mathrm{K}$, and $\underline{z}_\mathrm{P}$, and c in the power maximization term of the objective is given by

$$c = \begin{bmatrix} \frac{1}{2} & 1 & 1 & \cdots & 1 & 1 & \frac{1}{2} \end{bmatrix}^\top. \tag{3-74}$$

With respect to the constraints, only Eq. (3-70) to Eq. (3-73) are new. The rest of the constraints are restated for the purpose of clarity. The kinetic rotational energy dynamics are described by Eq. (3-9). The equality constraints provided by Eq. (3-36) to Eq. (3-38) respectively prescribe the kinetic rotational energy, aerodynamic power, and generator output power at the current time step ($k = 0$). For all subsequent time steps within the prediction horizon the inequalities apply. Minimum and maximum bounds are prescribed for the kinetic rotational energies by respectively Eq. (3-3) and Eq. (3-4). The overspeeding variables $z_{\mathrm{K}}[k]$ are constrained by Eq. (3-20) and Eq. (3-21) in order to approximate the absolute values $|K[k]-K_{\mathrm{rated}}|$ as described in Section 3-5-1. Similarly, the overpower constraints are provided by Eq. (3-33) and Eq. (3-34). A non-negativity constraint is imposed on the generator power by Eq. (3-5). The maximum generator power is bounded by the rated power (Eq. (3-6)) and the piecewise-linear approximation described in Section 3-5-2 given by Eq. (3-70). To limit both the pitch and the pitching rate, appropriate upper and lower bounds of the aerodynamic power were developed in Section 3-8-2. The resulting lower bounds on $P_{\mathrm{w}}[k]$ are given by Eq. (3-71). The upper bound of the aerodynamic power is provided by the available power estimate $\hat{P}_{\mathrm{av}}[k]$ (Eq. (3-72)). Note that the available power estimate $\hat{P}_{\mathrm{av}}[k]$ is not described with an equality; since it is a nonlinear function according Eq. (3-54), such an equality would render the optimization problem non-convex. However, since the available power estimate is maximized by the objective, the equality can be replaced by an upper bounds that is equivalent to the original definition (see Eq. (3-73)).

Now consider the objective of the optimization problem (Eq. (3-69)). All objectives that only have N_{p} terms are simply summed, whilst the generator power maximization objective makes use of trapezoidal integration (as should be clear from the definition of c provided by Eq. (3-74)) to accurately approximate the integral from Eq. (3-1). The dependence on the time step length is only used within the generator and available power maximization objectives since the integral of these terms actually represent changes in energy, and thus have a clear physical interpretation. Moreover, note that the to be minimized objective is convex, and thereby is suitable for a convex optimization strategy. In fact, since the objective has a quadratic form, and all of the constraints are of a linear or affine form, the above optimization problem can be solved using a QP approach.

The inputs required to fully define this optimization problem are the rotor effective wind speed estimate $\hat{v}$, the right hand sides of Eq. (3-36) to Eq. (3-38), all constants for the minimum aerodynamic power constraints a^{lb}_{k,l_k} and b^{lb}_{k,l_k}, and all constants for the available power constraints $a^{\mathrm{ub}}_{k,i}$ and $b^{\mathrm{ub}}_{k,i}$. To exploit the fact that the QP problem setup (as provided above) remains the same between different MPC solutions, YALMIP [49] is used within MATLAB to create a tailor-made `optimizer` object. It takes the aforementioned inputs and efficiently solves the resulting (primal) QP problem using MOSEK's interior-point algorithm (which is particularly well-suited to large problem sizes) [50].

As was noted in Section 3-8, the constants $a^{\mathrm{ub}}_{k,i}$ and $b^{\mathrm{ub}}_{k,i}$ are dependent on pitch angle estimates, and the constants a^{lb}_{k,l_k} and $b_{\mathrm{g},i}$ are additionally dependent on rotational kinetic energy estimates. Hence, similar to the strategy outlined by [41], to obtain the first solution for use in MPC, the QP is solved three times in order to obtain an adequately converged solution. Thereafter, the QP is only solved once at each new MPC time step.

Chapter 4

Extending the Convex Economic MPC Framework to IPC

This chapter will extend the theory and implementation as developed in the previous chapter for collective pitch control (CPC) applications to the domain of individual pitch control (IPC) to facilitate wind turbine load mitigation. The loads that are considered in this chapter as an example are the out-of-plane blade root bending moment fatigue loads. Where relevant, changes with respect to the previously described CPC framework are discussed. Since model predictive control (MPC) is used as a control strategy, it is important to form an adequate model of the out-of-plane blade root bending moments. Moreover, the model that is used to mitigate out-of-plane blade fatigue loading also needs to be usable within a convex optimization problem (preferably with a quadratic programming (QP) structure, as is the case with CPC).

This chapter will first explain the convex economic model predictive controller implementation for IPC in Section 4-1. Next, in Section 4-2 a model for blade-effective wind speeds is developed. An essential component of the blade-effective wind speed model is the azimuth position, for which a model is subsequently developed in Section 4-3. The different blade-effective wind speeds for each of the three blades give rise to a slightly different description of the aerodynamic power and the kinetic rotational energy dynamics, respectively treated in Section 4-4 and Section 4-5. The new models of the kinetic rotational energy and the aerodynamic power are used in Section 4-6-2 to model the thrust that acts on each of the rotor blades using existing convex economic model predictive control (CEMPC) principles from Section 2-2-6. This thrust model is subsequently used to model out-of-plane blade root bending moments and the corresponding tilt and yaw bending moments in Section 4-6. Two different fatigue mitigation strategies are developed: one strategy aims to mitigate fatigue loading via the formalization of a relevant objective whilst another does so via the inclusion of output constraints.

4-1 Controller Implementation

In effect the convex economic model predictive controller implementation that is used in the case of IPC - as shown by Figure 4-1 - is very similar to its CPC counterpart in Section 3-1. The controller obtains measurements from the NREL 5 MW wind turbine and a rotor-effective wind speed estimate from the immersion and invariance (I&I) wind speed estimator. It uses these measurements and estimates to ultimately compute pitch and generator power outputs that are linearly interpolated. The generator torque is obtained from the generator power and rotational speed in the same fashion as was the case with CPC. The resulting pitch angles and generator torque are finally used as inputs to the wind turbine.

Important differences with respect to CPC are the controller's use of azimuth position and out-of-plane blade root bending moment measurements, as well as the individual pitch angle that is computed as an output for each blade. As will become clear later on in this chapter, the azimuth position is used to compute both the blade-effective wind speeds and plays a role in the implemented out-of-plane blade root bending moment fatigue load mitigation strategies. The out-of-plane blade root bending moments are measured to form a model with which to predict future out-of-plane blade root bending moments.

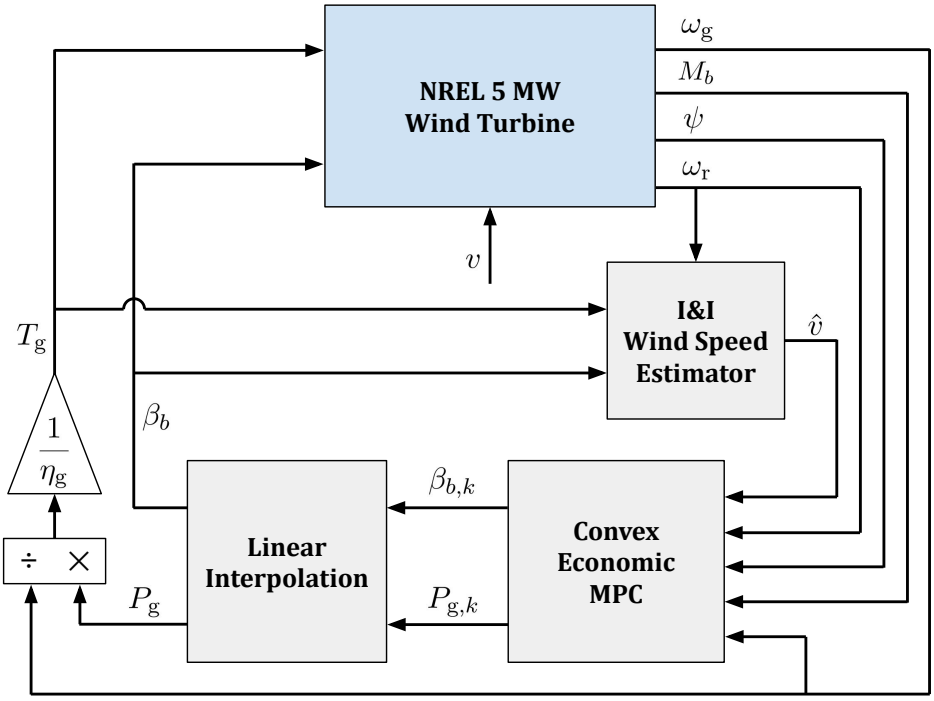

Figure 4-1: A control diagram that shows the dependencies between different control components and the investigated NREL 5 MW wind turbine in the case of IPC. A rotor-effective wind speed estimate $\hat{v}$ of the wind speed acting on the turbine v is provided to the CEMPC implementation by an I&I wind speed estimator. Other inputs to the convex economic model predictive controller consist of the measured rotational speeds of the generator and rotor (ω_g and ω_r), as well as the azimuth position ψ and the out-of-plane blade root bending moments M_b. The outputs of the CEMPC block consists of a solution trajectory for the pitch $\beta_{b,k}$ and generator power $P_{g,k}$. These are interpolated linearly to prevent any large transients of inputs to the generator. The applied generator torque is computed from the generator power and rotational speed as shown.

4-2 Blade-Effective Wind Speed Model

One of the main advantages of IPC is that it is able to account for the large spatial variability of loads that derive from the wind speed variations across the rotor disk [15]. Since MPC is used for the purpose of IPC it is important to be able to describe the spatial variability of the wind speed. To create a blade-effective wind speed model, the existing rotor-effective wind speed estimate obtained from the I&I estimator is augmented by the consideration of vertical wind shear. In this thesis, the vertical wind shear is modelled using the power law approximation given by [51]

$$v \propto h^{\alpha}, \tag{4-1}$$

in which h is the height from the ground, and α is the wind shear exponent. Both the software that will be used to model the wind turbine and wind conditions as well as the wind model considered here use a vertical wind shear exponent of $\alpha = 0.2$, which represents typical wind conditions [52].

As a result of Eq. (4-1), it is possible to calculate the wind speed v_2 given a reference wind speed v_1 from a corresponding reference height h_1 according to

$$v_2 = v_1 \left(\frac{h_2}{h_1}\right)^{\alpha}. \tag{4-2}$$

In practice, the reference wind speed v_1 is referred to as the (undisturbed) wind speed, and it corresponds to the wind speed at hub height $h_1 = h_{\text{hub}} = 90$ m. In the context of IPC, this wind speed at hub height is represented simply by v during the rest of this thesis.

To find the wind speed at some point on a blade, a radial distance r from the centre of the hub, consider that the height of this point is given by

$$h_2 = h_{\text{hub}} + r\cos(\psi_b), \tag{4-3}$$

in which ψ_b is the azimuth position of blade b. By combining Eq. (4-2) and Eq. (4-3) the wind speed at the previously described point on blade b then becomes

$$v_b(r) = v\left(1 + \frac{r}{h_{\text{hub}}}\cos(\psi_b)\right)^{\alpha}. \tag{4-4}$$

The variation of the wind speed along a blade, as described by Eq. (4-4) poses a problem for the models used for CEMPC up till this point. To see this consider

$$P_{\text{w}} = \frac{1}{2}\rho A C_{\text{P}}(\beta, \lambda)v^3, \tag{2-2}$$

which shapes the way in which the aerodynamic power has been modelled. There is only a single wind speed in this equation, and equally importantly, the power coefficient data used for modelling purposes also derives from a uniform input wind profile. A completely accurate solution would therefore incorporate the power law approximation above within the blade element momentum (BEM) theory that is used to find the power coefficient data. Whilst this integration would be interesting, it is beyond the scope of this research. In fact, likely due

to the complexity of the problem, an approximation that is often used is to assume that the wind only acts at one point on the blade, a radial distance $\frac{3}{4}R$ away from the centre of the hub [22, 53, 54]. The same approximation is made in this thesis, resulting in a blade-effective wind speed estimate $\hat{v}_b[k]$ that is described by

$$\hat{v}_b[k] = \hat{v}\left(1 + \frac{3R}{4h_{\text{hub}}}\cos(\hat{\psi}_b[k])\right)^{\alpha}. \tag{4-5}$$

Since the azimuth position ψ_b varies over time as the rotor turns, the blade effective wind speed also changes between time steps k. This is despite a rotor-effective wind speed estimate $\hat{v}$ that is assumed to remain constant throughout the prediction horizon. Within this IPC implementation, the rotor-effective wind speed obtained from the I&I estimator is taken to represent the wind speed at hub height.

4-3 Azimuth Model

The attentive reader will have noticed that Eq. (4-5) makes use of an *estimate* of the azimuth position from a previous solution $\hat{\psi}_b$. To understand why an estimate is used, consider the direct relationship between the kinetic rotational energy and the rotor speed given by

$$\omega_{\text{r}} = \frac{1}{N}\sqrt{\frac{2K}{J}}. \tag{4-6}$$

The direct relationship demonstrated by Eq. (4-6) between the kinetic energy K and the rotor speed ω_{r} demonstrates that since the kinetic energy is an output of the optimization problem, so will be the rotor speed. In turn, since the rate of change of the azimuth position is equal to the rotor speed, the azimuth position is also an output of the optimization problem. Hence, where the IPC framework requires information about the azimuth position (as is the case with blade-effective wind speeds), this information will be provided by azimuth position estimates that derive from the previous solution.

In order to form these estimates it is important to develop a model that describes the dynamics of the azimuth position. As mentioned earlier, by definition, the rate of change of the azimuth position is equal to the rotor speed. By considering the rotor speed as an input to the continuous-time state-space dynamics formulation

$$\dot{\psi}_b = (0)\psi_b + \omega_{\text{r}},$$

it is possible to arrive at a discrete state-space model of the azimuth position using the first-order hold discretization method as implemented by the MATLAB command

$$\texttt{c2d(ss(0,1,1,0),}\ \Delta t_{\text{s}}\ \texttt{,'foh').}$$

The resulting discrete state-space model can be used in the same way as is done in Section 3-4 to arrive at a linear matrix equality. In this case, this equality is given by

$$\underline{\psi}_b = \underline{1}\psi_b[0] + \mathcal{B}_{\psi}\underline{\omega}_r, \tag{4-7}$$

in which $\underline{\psi}_b$ and $\underline{\omega}_r$ respectively represent (ordered) vectors containing all of the azimuth positions and rotor speeds within the prediction horizon similar to, e.g., Eq. (3-10), $\underline{1}$ is an equally long vector composed of ones, and $\mathcal{B}_\psi$ represents a constant matrix that can be derived from the discrete state-space formulation.

Hence, to find azimuth estimates, one first finds estimates of the rotor speed. These can be obtained by applying estimates of the kinetic rotational energy from the previous solution to Eq. (4-6). By applying the resulting rotor speed estimates $\hat{\omega}_r$ to Eq. (4-7), estimates of the azimuth positions $\hat{\psi}_b$ are obtained. Note that since the three blades are spaced 120° apart, all azimuth positions can be described by the azimuth position of blade one according to

$$\psi_b = \psi_1 + \frac{2(b-1)\pi}{3}, \quad b \in \{1, 2, 3\}. \tag{4-8}$$

4-4 Aerodynamic Power

Within this IPC framework, the contribution of each blade to the total aerodynamic power is considered separately. Reusing the definitions developed within the CPC framework, for a 3-bladed turbine, this gives rise to

$$P_\mathrm{w} = \frac{1}{3}\sum_{b=1}^{3} P_{\mathrm{w},b}, \tag{4-9}$$

in which P_w is the total aerodynamic power, and $P_{\mathrm{w},b}$ represents the CPC-equivalent aerodynamic power of blade b (i.e., the amount of aerodynamic power that would have been developed by the entire rotor if all three blades were to operate under the same conditions as blade b). The aerodynamic power contribution of each blade is in effect assumed to be one third of what its CPC-equivalent aerodynamic power would be.

Note that the blade-specific pitch angle β_b that corresponds to each blade-specific aerodynamic power $P_{\mathrm{w},b}$ can still be obtained in the same fashion as in the CPC framework. However, the upper and lower bounds of the aerodynamic powers do have to be redefined in the case of IPC because of the use of blade-specific wind speeds and pitch angles. In fact, the resulting upper and lower bounds of the blade-specific aerodynamic powers $P_{\mathrm{w},b}$ are given by

$$\hat{P}_{\mathrm{av},b}(K[k]; \hat{v}_b[k], \hat{\beta}_b[k-1]) = \min\left\{a^{\mathrm{ub}}_{k,b,1}K[k] + b^{\mathrm{ub}}_{k,b,1}, \ldots, a^{\mathrm{ub}}_{k,b,n_\mathrm{w}}K[k] + b^{\mathrm{ub}}_{k,b,n_\mathrm{w}}\right\}, \tag{4-10}$$

$$\hat{P}^{\mathrm{lb}}_{\mathrm{w},b}(K[k]; \hat{v}_b[k], \hat{\beta}_b[k-1]) = a^{\mathrm{lb}}_{k,b,l_{k,b}}K[k] + b^{\mathrm{lb}}_{k,b,l_{k,b}}, \tag{4-11}$$

in which the constants $a^{\mathrm{ub}}_{k,b,i}$, $b^{\mathrm{ub}}_{k,b,i}$, $a^{\mathrm{lb}}_{k,b,l_{k,b}}$, and $b^{\mathrm{lb}}_{k,b,l_{k,b}}$ can be determined in a similar fashion as their CPC counterparts in Section 3-8. The principal difference is that the individual pitch angle estimates $\hat{\beta}_b[k-1]$ are used to arrive at the lower and upper bound C_P approximations (instead of the collective pitch estimate $\hat{\beta}[k-1]$), and that the blade-effective wind speed $\hat{v}_b[k]$ is used to subsequently find the lower and upper bounds of the aerodynamic power given by $\hat{P}_{\mathrm{av},b}$ and $\hat{P}^{\mathrm{lb}}_{\mathrm{w},b}$ (instead of the rotor-effective wind speed estimate $\hat{v}$).

4-5 Kinetic Rotational Energy Dynamics

The kinetic rotational energy dynamics are discretized in much the same way as in Section 3-4. With reference to Eq. (4-9), the continuous state-space dynamics provided by Eq. (2-18) are discretized using a first-order hold approximation. Using the MATLAB command

$$\texttt{c2d(ss(0,[1/3 1/3 1/3 -1/}\eta_{\mathrm{g}}\texttt{],1,[0 0 0 0]),}\ \Delta t_{\mathrm{s}}\ \texttt{,'foh')}$$

one obtains a discrete state-space formulation that is given by

$$x_{\mathrm{d}}[k+1] = A_{\mathrm{d}} x_{\mathrm{d}}[k] + B_{\mathrm{d}}^{\mathrm{IPC}} \begin{bmatrix} P_{\mathrm{w},1}[k] & P_{\mathrm{w},2}[k] & P_{\mathrm{w},3}[k] & P_{\mathrm{g}}[k] \end{bmatrix}^{\top}, \tag{4-12a}$$

$$K[k] = C_{\mathrm{d}} x_{\mathrm{d}}[k] + D_{\mathrm{d}}^{\mathrm{IPC}} \begin{bmatrix} P_{\mathrm{w},1}[k] & P_{\mathrm{w},2}[k] & P_{\mathrm{w},3}[k] & P_{\mathrm{g}}[k] \end{bmatrix}^{\top}, \tag{4-12b}$$

in which the superscript IPC is used to indicate that a vector or matrix is not equal to its CPC counterpart in cases where notation does not already illustrate this difference. By defining the vector with all aerodynamic powers such that

$$\underline{P}_{\mathrm{w}}^{\mathrm{IPC}} = \begin{bmatrix} P_{\mathrm{w},1}[0] & \cdots & P_{\mathrm{w},1}[N_{\mathrm{p}}] & P_{\mathrm{w},2}[0] & \cdots & P_{\mathrm{w},2}[N_{\mathrm{p}}] & P_{\mathrm{w},3}[0] & \cdots & P_{\mathrm{w},3}[N_{\mathrm{p}}] \end{bmatrix}^{\top}, \tag{4-13}$$

and the new matrix equality[1] that defines all kinetic energies within the prediction horizon is

$$\underline{K} = \mathcal{A} K[0] + \mathcal{B}_{\mathrm{w}}^{\mathrm{IPC}} \underline{P}_{\mathrm{w}}^{\mathrm{IPC}} + \mathcal{B}_{\mathrm{g}} \underline{P}_{\mathrm{g}}. \tag{4-14}$$

4-6 Out-of-Plane Blade Root Bending Moment Fatigue Load Mitigation

4-6-1 Modelling Approach

In order to mitigate out-of-plane blade root bending moment fatigue, these moments have to be modelled first. In literature, various ways of modelling the out-of-plane blade root bending moments have been used, not all of which are suitable for the CEMPC framework.

For example, in [22, 53], linearizations of aerodynamic moment data with respect to the blade-effective wind speed and pitch are used. Similar methods, as in [55], additionally perform a linearization with respect to the rotor speed. However, such an approach presents a problem since the pitch is not a free variable in the CEMPC framework. Instead, it derives from the aerodynamic power, blade-effective wind speed and kinetic rotational energy as described by Eq. (2-32).

An interesting alternative is given by the way the blade root bending moments are modelled in [40, 56]. Both sources model the variation of the thrust force per unit blade length as a quantity that increases linearly with the radial position away from the hub centre. Whilst [40] arrives at this distribution by assuming a constant aerodynamic efficiency across the radial

[1] By looking at Eq. (4-9), Eq. (4-13), and by comparing Eq. (3-9) and Eq. (4-14), it is possible to conclude that $\mathcal{B}_{\mathrm{w}}^{\mathrm{IPC}} = \frac{1}{3}\begin{bmatrix} \mathcal{B}_{\mathrm{w}} & \mathcal{B}_{\mathrm{w}} & \mathcal{B}_{\mathrm{w}} \end{bmatrix}$.

length of the blade as is done in [54], the authors of [56] verified this assumption by means of simulations. In any case, the linear distribution results in the following description of the out-of-plane blade root bending moment:

$$M_b[k] = \frac{2}{3} R F_{\mathrm{T},b}[k], \tag{4-15}$$

in which M_b and $F_{\mathrm{T},b}$ are respectively the out-of-plane blade root bending moment and thrust force exerted on blade b.

Since the thrust can be modelled using the existing CEMPC framework (see Section 2-2-6), the linear relationship between the thrust and out-of-plane blade root bending moment provided by Eq. (4-15) seems particularly useful. To be able to model the out-of-plane blade root bending moments using the thrust exerted on each blade, the existing way of modelling the thrust has to be adapted for use within an IPC framework.

4-6-2 Thrust Modelling

To model the thrust acting on each blade, the affine thrust approximation illustrated in Section 2-2-6 is adapted to IPC. Consider the affine approximation

$$\hat{F}_{\mathrm{T}}(P_{\mathrm{w}}, K; v, \beta^*, K^*) = Q_{\mathrm{T}}(v, \beta^*, K^*) P_{\mathrm{w}} + R_{\mathrm{T}}(v, \beta^*, K^*) K + S_{\mathrm{T}}(v, \beta^*, K^*), \tag{2-40}$$

from Chapter 2. By linearizing at the blade-effective wind speed, estimated pitch $\hat{\beta}[k]$, and estimated kinetic rotational energy $\hat{K}[k]$, the affine approximation for the thrust exerted on a single blade b becomes

$$\begin{aligned}\hat{F}_{\mathrm{T},b}(P_{\mathrm{w},b}[k], K[k]; \hat{v}_b[k], \hat{\beta}_b[k], \hat{K}[k]) = \frac{1}{3} Q_{\mathrm{T},b}(\hat{v}_b[k], \hat{\beta}_b[k], \hat{K}[k]) P_{\mathrm{w},b}[k] \\ + \frac{1}{3} R_{\mathrm{T},b}(\hat{v}_b[k], \hat{\beta}_b[k], \hat{K}[k]) K[k] + \frac{1}{3} S_{\mathrm{T},b}(\hat{v}_b[k], \hat{\beta}_b[k], \hat{K}[k]),\end{aligned} \tag{4-16}$$

in which $Q_{\mathrm{T},b}$, $R_{\mathrm{T},b}$, and $S_{\mathrm{T},b}$ are, in accordance with the theory discussed in Section 2-2-6, defined by

$$Q_{\mathrm{T},k,b} = Q_{\mathrm{T},b}(\hat{v}_b[k], \hat{\beta}_b[k], \hat{K}[k]) = \frac{\left.\dfrac{\partial C_{\mathrm{T}}}{\partial \beta}\right|_{\star}}{\hat{v}_b[k] \left.\dfrac{\partial C_{\mathrm{P}}}{\partial \beta}\right|_{\star}}, \tag{4-17}$$

$$R_{\mathrm{T},k,b} = R_{\mathrm{T},b}(\hat{v}_b[k], \hat{\beta}_b[k], \hat{K}[k]) = \frac{1}{2} \rho A \hat{v}_b[k]^2 \left(\left.\frac{\partial C_{\mathrm{T}}}{\partial K}\right|_{\star} - \left.\frac{\partial C_{\mathrm{P}}}{\partial K}\right|_{\star} \frac{\left.\dfrac{\partial C_{\mathrm{T}}}{\partial \beta}\right|_{\star}}{\left.\dfrac{\partial C_{\mathrm{P}}}{\partial \beta}\right|_{\star}} \right), \tag{4-18}$$

$$S_{\mathrm{T},k,b} = S_{\mathrm{T},b}(\hat{v}_b[k], \hat{\beta}_b[k], \hat{K}[k]) = \frac{1}{2} \rho A \hat{v}_b[k]^2 \left(C_{\mathrm{T}}|_{\star} - C_{\mathrm{P}}|_{\star} \frac{\left.\dfrac{\partial C_{\mathrm{T}}}{\partial \beta}\right|_{\star}}{\left.\dfrac{\partial C_{\mathrm{P}}}{\partial \beta}\right|_{\star}} \right), \tag{4-19}$$

in which $\star$ is used to represent the point defined by $\hat{v}_b[k], \hat{K}[k]$, and $\hat{\beta}[k]$.

By comparing Eq. (2-40) and Eq. (4-16) an important difference between the existing thrust model and the model used for IPC becomes clear. Unlike in Section 2-2-6, the affine thrust is found by means of multiple different pitch and kinetic energy linearization points, defined by the estimates $\hat{\beta}[k]$ and $\hat{K}[k]$. There are two important reasons for performing the relevant linearizations of the power and thrust coefficients (that ultimately define the matrices $Q_{\mathrm{T},b}$, $R_{\mathrm{T},b}$, and $S_{\mathrm{T},b}$) with respect to the estimates of the pitch and kinetic energy, instead of only the pitch and kinetic energy at $k = 0$, as is done with the existing CPC thrust model. Firstly, as was noted before, the accuracy of the affine approximation depends on how large the deviations of the pitch and kinetic energy are from their respective linearization points. Particularly for IPC applications, one may expect the pitch angle of a particular blade to change considerably throughout the prediction horizon. Secondly, the blade-effective wind speed changes considerably throughout the prediction horizon according to Eq. (4-5). This means that a new linearization of the power and thrust coefficient has to be performed anyways for each blade and time step within the prediction horizon. One may then just as well linearize these coefficients with respect to the available estimates of the pitch and kinetic energy.

Another difference with respect to the existing thrust model as developed in [34] and explained in Section 2-2-6 is that no maximum thrust constraint similar to Eq. (2-41) is implemented. The problem with such a constraint is that it may render the optimization problem infeasible. To see why this can happen, consider the definitions of $Q_{\mathrm{T},b}$, $R_{\mathrm{T},b}$, and $S_{\mathrm{T},b}$ provided by Eq. (4-17) to Eq. (4-19). As $\frac{\partial C_{\mathrm{P}}}{\partial \beta} \to 0$, each of these values goes to either positive or negative infinity. In turn, this causes $\hat{F}_{\mathrm{T},b}$ to violate any reasonable upper or lower bounds that may be posed in a similar fashion to what is done with Eq. (2-41).

In practice, as one may imagine from the C_{P} contours shown in Figure 2-1, $\frac{\partial C_{\mathrm{P}}}{\partial \beta}$ is only sufficiently small to cause numerical problems in fairly small regions of the β-λ plane[2]. Still, there is no guarantee that operation will not occur within these regions. Moreover, it appears as though the thrust constraint that is imposed in Section 2-2-6 serves to minimize model error, which ought to be considerably reduced by the use of multiple pitch and kinetic energy linearization points in the IPC thrust model. For these two reasons, thrust constraints like Eq. (2-41) are not used in the IPC framework.

4-6-3 Out-of-Plane Blade Root Bending Moments

By combining Eq. (4-15) with the thrust model provided by Eq. (4-16) it is possible to model the out-of-plane blade root bending moments. To see how well the modelled out-of-plane blade root bending moments correspond to their measured counterparts, several simulations are performed.

For these simulations, the MPC algorithm uses solves an optimization problem that looks very much like that of CPC as shown in Section 3-10, but includes the modifications described

[2]The minimum pitch of 0° happens to exclude a region where the maximum power coefficient would otherwise lie and where $\frac{\partial C_{\mathrm{P}}}{\partial \beta} \approx 0$. If this region were not to have been excluded by the minimum pitch, the described issue would be more problematic because to maximize power, the power coefficient needs to be maximized. Since this would entail operation in a region where $\frac{\partial C_{\mathrm{P}}}{\partial \beta} \approx 0$, one might expect problems to arise from an aerodynamic thrust constraint similar to Eq. (2-41) where operation around the maximum power coefficient is expected. For CPC applications such as those in [34] this would be an even larger problem because operation around this maximum aerodynamic power may be more prolonged.

in Section 4-2 to Section 4-6-2. In effect, the changes with respect to CPC are: different blade-effective wind speeds and aerodynamic power contributions, a slightly different discretized dynamics model of the kinetic rotational energy, and the implementation of a thrust model. The simulation results for a stepped wind speed that goes from 15 m/s to 16 m/s are shown in Figure 4-2. Note that to obtain these simulation results, perfect information on the rotor-effective wind speed provided directly as an output from the Fatigue, Aerodynamics, Structures, and Turbulence (FAST) simulation software (instead of the I&I estimate) was used[3].

By comparing the blue line to the measured out-of-plane bending moments shown by the black line, it becomes clear that the model provided by Eq. (4-15) is not very accurate. This prompts a more critical look at the used blade root bending model.

To arrive at another model that might work, consider that linearized diagonal blade root bending models that (besides their operating point) are dependent only on the pitch are also investigated in literature [14, 18, 57]. In the Laplace domain, these models take the form

$$\begin{bmatrix} M_1(s) \\ M_2(s) \\ M_3(s) \end{bmatrix} = \begin{bmatrix} g_{\mathrm{b}}(s) & 0 & 0 \\ 0 & g_{\mathrm{b}}(s) & 0 \\ 0 & 0 & g_{\mathrm{b}}(s) \end{bmatrix} \begin{bmatrix} \beta_1(s) \\ \beta_2(s) \\ \beta_3(s) \end{bmatrix}, \tag{4-20}$$

in which s is the Laplace operator, and $g_{\mathrm{b}}(s)$ is a transfer function that illustrates the relationship between the pitch of a certain blade and its own out-of-plane blade root bending moment.

Whilst, as explained earlier, the pitch in Eq. (4-20) is not a free optimization variable, it is strongly related to the aerodynamic power, which is used in the definition of the thrust (see Eq. (4-16)). Together with the original out-of-plane blade root bending moment model given by Eq. (4-15), this suggests that perhaps it might be useful to investigate a model given by:

$$\begin{bmatrix} M_1[k] \\ M_2[k] \\ M_3[k] \end{bmatrix} = \begin{bmatrix} a_{\mathrm{diag}} & 0 & 0 \\ 0 & a_{\mathrm{diag}} & 0 \\ 0 & 0 & a_{\mathrm{diag}} \end{bmatrix} \begin{bmatrix} \hat{F}_{\mathrm{T},1}[k] \\ \hat{F}_{\mathrm{T},2}[k] \\ \hat{F}_{\mathrm{T},3}[k] \end{bmatrix}, \quad k \in \{1, 2, \ldots, N_{\mathrm{p}}\}, \tag{4-21}$$

in which a_{diag} is a constant within the prediction horizon that depends on the rotor-effective wind speed v. Using linear least squares fitting of the model provided by Eq. (4-21) to the measured out-of-plane blade root bending moments, it is found that $a_{\mathrm{diag}} = 42.12$ m provides the best fit, which is shown in Figure 4-2 by the line with red circles. Upon observing this figure, it becomes clear that unfortunately, the new model given by Eq. (4-21) results in approximately the same modelled bending moments as is the case with Eq. (4-15)[4], thereby providing no significantly more accurate model.

Another model that is investigated in [57] considers a blade root bending model similar to Eq. (4-20), but accounts for coupling between the different blades. This model is given by

$$\begin{bmatrix} M_1(s) \\ M_2(s) \\ M_3(s) \end{bmatrix} = \begin{bmatrix} g_{\mathrm{b}}(s) & g_{\mathrm{p}}(s) & g_{\mathrm{n}}(s) \\ g_{\mathrm{n}}(s) & g_{\mathrm{b}}(s) & g_{\mathrm{p}}(s) \\ g_{\mathrm{p}}(s) & g_{\mathrm{n}}(s) & g_{\mathrm{b}}(s) \end{bmatrix} \begin{bmatrix} \beta_1(s) \\ \beta_2(s) \\ \beta_3(s) \end{bmatrix}, \tag{4-22}$$

[3] This was done to ensure that any resulting model errors are not due to considerable rotor-effective wind speed measurement errors.

[4] One may note that in fact, $a_{\mathrm{diag}} = 42.12$ m ≈ 42 m $= \frac{2}{3}R$.

in which the effect of pitching on respectively the preceding blade and the next blade is represented by $g_{\mathrm{n}}(s)$ and $g_{\mathrm{n}}(s)$. By means of the same reasoning that lead to Eq. (4-21), Eq. (4-22) warrants investigation of a model given by

$$\begin{bmatrix} M_1[k] \\ M_2[k] \\ M_3[k] \end{bmatrix} = \begin{bmatrix} a_{\mathrm{M}} & b_{\mathrm{M}} & c_{\mathrm{M}} \\ c_{\mathrm{M}} & a_{\mathrm{M}} & b_{\mathrm{M}} \\ b_{\mathrm{M}} & c_{\mathrm{M}} & a_{\mathrm{M}} \end{bmatrix} \begin{bmatrix} \hat{F}_{\mathrm{T},1}[k] \\ \hat{F}_{\mathrm{T},2}[k] \\ \hat{F}_{\mathrm{T},3}[k] \end{bmatrix}, \quad k \in \{1, 2, \ldots, N_{\mathrm{p}}\}, \tag{4-23}$$

in which a_{M}, b_{M}, and c_{M} are constants within the prediction horizon that depend on the measured rotor-effective wind speed[5]. By means of linear least squares fitting to the data shown in Figure 4-2, these constants are found to be $a_{\mathrm{M}} = 28.64$ m, $b_{\mathrm{M}} = 5.94$ m, and $c_{\mathrm{M}} = 8.08$ m. The relative size of these constants indicates the perceived contribution of the thrust acting on a certain blade to the out-of-plane blade root bending moments of the same blade and its two neighbours. The resulting best fit is shown in green, and clearly offers a significant improvement over the other two models given by Eq. (4-15) and Eq. (4-21).

Since the linear models used in, e.g., [18] represent linearizations at specific operating conditions, the same models are also applied to another operating point. Figure 4-2 represents operating conditions that correspond to wind speeds at hub height between 15 m/s to 16 m/s, which are above the rated wind speed of 11.4 m/s [37]. Hence, the new wind speed profile that is used is a stepped wind speed profile that goes from 8 m/s to 9 m/s, which is below rated. The resulting comparison between the measured and modelled out-of-plane blade root bending moments is shown in Figure 4-3.

The parameters obtained for the models given by Eq. (4-21) and Eq. (4-23) are illustrated for both wind speed profiles in Table 4-1. From the considerable difference between these parameters from one wind speed profile to the next, one can conclude that the implemented model corresponding to Eq. (4-23) that there is an important dependence of these parameters on the rotor-effective wind speed. To provide accurate estimates for these parameters, the static matrix is obtained by online linear least squares fitting to the out-of-plane blade root bending moments and modelled thrust forces that are respectively measured and modelled for the current time step ($k = 0$). This online identification provides a simple alternative to the use of a scheduling procedure.

Table 4-1: Parameter fits of two different out-of-plane blade root bending moment models (Eq. (4-21) and Eq. (4-23)) for two different wind speed ranges (8 m/s to 9 m/s and 15 m/s to 16 m/s).

stepped wind speed profile	Eq. (4-21)	Eq. (4-23)		
	a_{diag} [m]	a_{M} [m]	b_{M} [m]	c_{M} [m]
8 m/s - 9 m/s	45.64	30.15	3.44	12.42
15 m/s - 16 m/s	42.12	28.64	5.94	8.08

[5]System identification has also been tried to arrive at a more accurate state-space model. However, there is no significant improvement in accuracy and therefore such an approach does not warrant the increased model size and complexity.

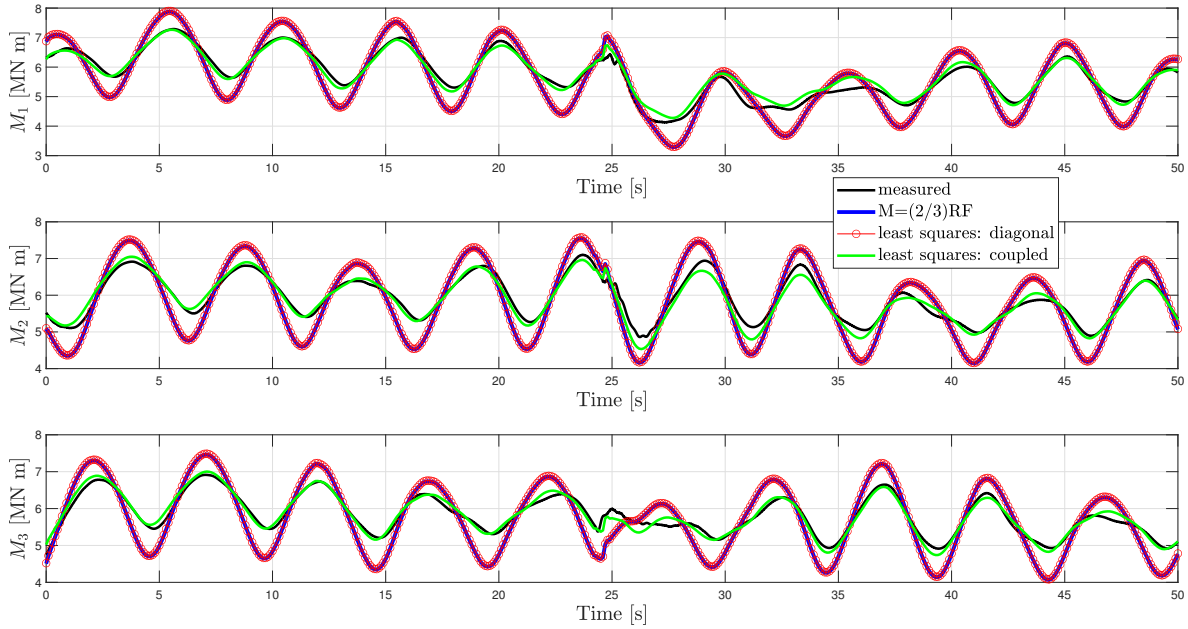

Figure 4-2: A comparison between measured and modelled out-of-plane blade root bending moments using a 15 m/s to 16 m/s stepped wind speed profile (the step occurs at 25 s). The moments corresponding to those that are measured, described by Eq. (4-15), Eq. (4-21), and Eq. (4-23) are respectively shown by the black line, the blue line, the line with red circles, and the green line.

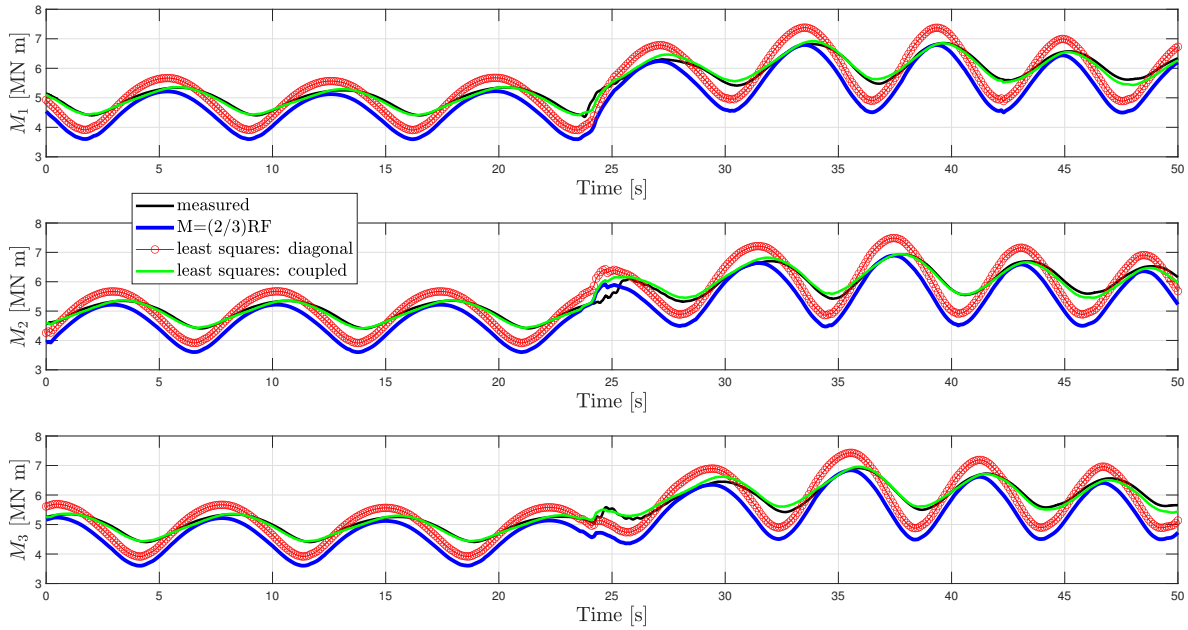

Figure 4-3: A comparison between measured and modelled out-of-plane blade root bending moments using a 8 m/s to 9 m/s stepped wind speed profile (the step occurs at 25 s). The moments corresponding to those that are measured, described by Eq. (4-15), Eq. (4-21), and Eq. (4-23) are respectively shown by the black line, the blue line, the line with red circles, and the green line.

4-6-4 Tilt and Yaw Bending Moments

Having found a model to describe the out-of-plane blade root bending moments, a strategy to perform the mitigation of out-of-plane blade root bending moment fatigue now has to be developed. Looking at the conventional IPC approach, this task is performed by reducing the tilt and yaw moments (M_{tilt} and M_{yaw} respectively) that result from the forward multi-blade coordinate (MBC) transformation [14]

$$\begin{bmatrix} M_{\text{tilt}}[k] \\ M_{\text{yaw}}[k] \end{bmatrix} = \frac{2}{3} \begin{bmatrix} \cos(\hat{\psi}_1[k]) & \cos(\hat{\psi}_2[k]) & \cos(\hat{\psi}_3[k]) \\ \sin(\hat{\psi}_1[k]) & \sin(\hat{\psi}_2[k]) & \sin(\hat{\psi}_3[k]) \end{bmatrix} \begin{bmatrix} M_1[k] \\ M_2[k] \\ M_3[k] \end{bmatrix}, \quad k \in \{1, 2, \dots, N_{\text{p}}\}, \tag{4-24}$$

in which the relationship between the different azimuth positions ψ_b is described by Eq. (4-8).

The tilt and yaw moments can be thought of as measures for the variability of the out-of-plane blade root bending moments as transposed on the tilt and yaw axes shown by Figure 1-3. Since out-of-plane blade root bending moment fatigue damage accumulates due to load cycles, it makes sense to mitigate these tilt and yaw loads.

4-6-5 Fatigue Mitigation Strategy: Objective Formulation

One way to mitigate these tilt and yaw loads is to minimize these loads within the objective function. An objective that can be minimized and that is consistent with the previously developed QP problem formulation is

$$\sum_{k=1}^{N_{\text{p}}} \left(M_{\text{tilt}}[k]^2 + M_{\text{yaw}}[k]^2 \right). \tag{4-25}$$

4-6-6 Fatigue Mitigation Strategy: Output Constraints

Another way to mitigate tilt and yaw bending moments is to limit them by means of output constraints. To prevent infeasibility of the optimization problem, these constraints are imposed as soft constraints. The resulting constraints are formulated as

$$M_{\text{tilt}}[k] \geq M_{\text{tilt}}^{\text{lb}}(\hat{v}) - \epsilon_{\text{tilt}}[k], \quad k \in \{1, 2, \dots, N_{\text{p}}\}, \tag{4-26}$$
$$M_{\text{tilt}}[k] \leq M_{\text{tilt}}^{\text{ub}}(\hat{v}) + \epsilon_{\text{tilt}}[k], \quad k \in \{1, 2, \dots, N_{\text{p}}\}, \tag{4-27}$$
$$M_{\text{yaw}}[k] \geq M_{\text{yaw}}^{\text{lb}}(\hat{v}) - \epsilon_{\text{yaw}}[k], \quad k \in \{1, 2, \dots, N_{\text{p}}\}, \tag{4-28}$$
$$M_{\text{yaw}}[k] \leq M_{\text{yaw}}^{\text{ub}}(\hat{v}) + \epsilon_{\text{yaw}}[k], \quad k \in \{1, 2, \dots, N_{\text{p}}\}, \tag{4-29}$$
$$\epsilon_{\text{tilt}}[k] \geq 0, \quad k \in \{1, 2, \dots, N_{\text{p}}\}, \tag{4-30}$$
$$\epsilon_{\text{yaw}}[k] \geq 0, \quad k \in \{1, 2, \dots, N_{\text{p}}\}, \tag{4-31}$$

in which the soft upper and lower bounds are respectively indicated by the superscripts ub and lb, and the variables ϵ_{tilt} and ϵ_{yaw} are used to relax the constraints. Since higher out-of-plane blade root bending moments may be anticipated at greater wind speeds, it makes sense to

schedule the lower and upper bounds according to the rotor-effective wind speed[6]. To make the violation of the soft lower or upper bounds unattractive, these two latter variables are penalized, for which a linear objective is chosen:

$$\sum_{k=1}^{N_\mathrm{p}} \left(\epsilon_\mathrm{yaw}[k] + \epsilon_\mathrm{tilt}[k]\right). \tag{4-32}$$

4-7 Feedback Changes for IPC

The formulation of new aerodynamic powers, and the use of the azimuth position, necessitates changes relative to the CPC framework regarding the use of measurements for feedback purposes.

Given the aerodynamic power definitions provided by Eq. (4-9), the constraint posed by Eq. (3-37) in the case of CPC is extended to multiple blades by

$$P_{\mathrm{w},b}[0] = \frac{1}{2}\rho A C_\mathrm{P}(\beta_{\mathrm{me},b}, \lambda_b[0])\hat{v}_b[0]^3, \quad b \in \{1,2,3\}, \tag{4-33}$$

in which $\beta_{\mathrm{me},b}$ represents the measured pitch angle of blade b, and λ_b represents the tip speed ratio of blade b (as computed by applying the blade effective wind speed $\hat{v}_b$ and the kinetic energy K to Eq. (2-31)).

Moreover, since both the blade-effective wind speed and the tilt and yaw moments are dependent on the azimuth position according to respectively Eq. (4-5) and Eq. (4-24), it is useful to also measure the azimuth position. In this IPC application, the azimuth position of the first blade $\psi_1[0] = \psi_{\mathrm{me},1}$ is measured, and the azimuth positions of the other blades at $k = 0$ can be calculated based on Eq. (4-8).

To form accurate predictions, it makes sense to use the updated kinetic energy predictions (as described in Section 3-7) as well as the measured azimuth position in the model provided by Eq. (4-7). The azimuth model that is used to form estimates of the azimuth position described in Section 4-3 is corrected by the azimuth measurement in the same way as was the case with, e.g., the update of CPC pitch angle estimates as described in Section 3-7.

[6] A suitable scheduling mechanism is not investigated here since only two different wind speed cases will be simulated in the next chapter, but it may warrant further investigation if operation under a greater range of wind speeds is to be simulated.

4-8 Implemented Optimization Problem

Given the changes of - and additions to - the CPC framework that are implemented within this IPC framework, the resulting optimization problem is provided in this section. A general optimization problem that encapsulates both tilt and yaw mitigation by means of an objective formulation and output constraints is given by

$$\begin{aligned}
\min_{\underline{x}^{\mathrm{IPC}}} \quad & \underbrace{-\alpha_1 \Delta t_{\mathrm{s}} c^\top \underline{P}_{\mathrm{g}}}_{\substack{\text{generator power}\\ \text{maximization}}} \underbrace{-\alpha_1 \eta_{\mathrm{g}} \left[K[N_{\mathrm{p}}] - \frac{K[N_{\mathrm{p}}] - K_{\mathrm{rated}} + z_{\mathrm{K}}[N_{\mathrm{p}}]}{2} \right]}_{\text{turnpike mitigation}} \\
& + \sum_{k=1}^{N_{\mathrm{p}}} \Bigg[\underbrace{\alpha_2 (P_{\mathrm{g}}[k] - P_{\mathrm{g}}[k-1])^2}_{\substack{\text{minimize generator}\\ \text{output power variations}}} + \underbrace{\frac{\alpha_3}{3} \sum_{b=1}^{3} \left(\frac{2}{\rho A} \right)^2 \left(\frac{P_{\mathrm{w},b}[k]}{\hat{v}_b[k]^3} - \frac{P_{\mathrm{w},b}[k-1]}{\hat{v}_b[k-1]^3} \right)^2}_{\text{minimize } C_{\mathrm{P}} \text{ variations}} \\
& \underbrace{- \frac{\alpha_4}{3} \sum_{b=1}^{3} \frac{\Delta t}{2} \left(\hat{P}_{\mathrm{av},b}[k] + \frac{P_{\mathrm{rated}}}{\eta_{\mathrm{g}}} - z_{\mathrm{P},b}[k] \right)}_{\substack{\text{limited available}\\ \text{power maximization}}} + \underbrace{\alpha_5 \frac{K[k] - K_{\mathrm{rated}} + z_{\mathrm{K}}[k]}{2}}_{\text{minimize overspeeding}} \\
& + \underbrace{\alpha_7 \left(M_{\mathrm{tilt}}[k]^2 + M_{\mathrm{yaw}}[k]^2 \right)}_{\substack{\text{minimize tilt and}\\ \text{yaw moments}}} + \underbrace{\alpha_8 \left(\epsilon_{\mathrm{yaw}}[k] + \epsilon_{\mathrm{tilt}}[k] \right)}_{\substack{\text{minimize violations of}\\ \text{tilt and yaw bounds}}} \Bigg]
\end{aligned} \tag{4-34}$$

$$\text{s.t.} \quad K[k] \geq 0, \qquad k \in \{1, 2, \ldots, N_{\mathrm{p}}\}, \tag{3-3}$$

$$K[k] \leq K_{\max}, \qquad k \in \{1, 2, \ldots, N_{\mathrm{p}}\}, \tag{3-4}$$

$$P_{\mathrm{g}}[k] \geq 0, \qquad k \in \{1, 2, \ldots, N_{\mathrm{p}}\}, \tag{3-5}$$

$$P_{\mathrm{g}}[k] \leq P_{\mathrm{rated}}, \qquad k \in \{1, 2, \ldots, N_{\mathrm{p}}\}, \tag{3-6}$$

$$z_{\mathrm{K}}[k] \geq K[k] - K_{\mathrm{rated}}, \qquad k \in \{1, 2, \ldots, N_{\mathrm{p}}\}, \tag{3-20}$$

$$z_{\mathrm{K}}[k] \geq -K[k] + K_{\mathrm{rated}}, \qquad k \in \{1, 2, \ldots, N_{\mathrm{p}}\}, \tag{3-21}$$

$$K[0] = \frac{1}{2} J N^2 \omega_{\mathrm{r,me}}^2, \tag{3-36}$$

$$P_{\mathrm{g}}[0] = \eta_{\mathrm{g}} T_{\mathrm{g,me}} \omega_{\mathrm{g,me}}, \tag{3-38}$$

$$P_{\mathrm{g}}[k] \leq a_{\mathrm{g},i} K[k] + b_{\mathrm{g},i}, \quad i \in \{1, 2, \ldots, n_{\mathrm{g}}\}, \qquad k \in \{1, 2, \ldots, N_{\mathrm{p}}\}, \tag{3-70}$$

$$\underline{K} = \mathcal{A} K[0] + \mathcal{B}_{\mathrm{w}}^{\mathrm{IPC}} \underline{P}_{\mathrm{w}}^{\mathrm{IPC}} + \mathcal{B}_{\mathrm{g}} \underline{P}_{\mathrm{g}}, \tag{4-14}$$

$$\begin{bmatrix} M_1[k] \\ M_2[k] \\ M_3[k] \end{bmatrix} = \begin{bmatrix} a_{\mathrm{M}} & b_{\mathrm{M}} & c_{\mathrm{M}} \\ c_{\mathrm{M}} & a_{\mathrm{M}} & b_{\mathrm{M}} \\ b_{\mathrm{M}} & c_{\mathrm{M}} & a_{\mathrm{M}} \end{bmatrix} \begin{bmatrix} \hat{F}_{\mathrm{T},1}[k] \\ \hat{F}_{\mathrm{T},2}[k] \\ \hat{F}_{\mathrm{T},3}[k] \end{bmatrix}, \qquad k \in \{1, 2, \ldots, N_{\mathrm{p}}\}, \tag{4-23}$$

$$\begin{bmatrix} M_{\mathrm{tilt}}[k] \\ M_{\mathrm{yaw}}[k] \end{bmatrix} = \frac{2}{3} \begin{bmatrix} \cos(\hat{\psi}_1[k]) & \cos(\hat{\psi}_2[k]) & \cos(\hat{\psi}_3[k]) \\ \sin(\hat{\psi}_1[k]) & \sin(\hat{\psi}_2[k]) & \sin(\hat{\psi}_3[k]) \end{bmatrix} \begin{bmatrix} M_1[k] \\ M_2[k] \\ M_3[k] \end{bmatrix}, \quad k \in \{1, 2, \ldots, N_{\mathrm{p}}\}, \tag{4-24}$$

$$M_{\mathrm{tilt}}[k] \geq M_{\mathrm{tilt}}^{\mathrm{lb}}(\hat{v}) - \epsilon_{\mathrm{tilt}}[k], \qquad k \in \{1, 2, \ldots, N_{\mathrm{p}}\}, \tag{4-26}$$

$$M_{\mathrm{tilt}}[k] \leq M_{\mathrm{tilt}}^{\mathrm{ub}}(\hat{v}) + \epsilon_{\mathrm{tilt}}[k], \qquad k \in \{1, 2, \ldots, N_{\mathrm{p}}\}, \tag{4-27}$$

$$M_{\mathrm{yaw}}[k] \geq M_{\mathrm{yaw}}^{\mathrm{lb}}(\hat{v}) - \epsilon_{\mathrm{yaw}}[k], \qquad k \in \{1, 2, \ldots, N_{\mathrm{p}}\}, \tag{4-28}$$

$$M_{\text{yaw}}[k] \leq M_{\text{yaw}}^{\text{ub}}(\hat{v}) + \epsilon_{\text{yaw}}[k], \qquad k \in \{1, 2, \ldots, N_{\text{p}}\}, \quad (4\text{-}29)$$

$$\epsilon_{\text{tilt}}[k] \geq 0, \qquad k \in \{1, 2, \ldots, N_{\text{p}}\}, \quad (4\text{-}30)$$

$$\epsilon_{\text{yaw}}[k] \geq 0, \qquad k \in \{1, 2, \ldots, N_{\text{p}}\}, \quad (4\text{-}31)$$

$$P_{\text{w},b}[0] = \frac{1}{2}\rho A C_{\text{P}}(\beta_{\text{me},b}, \lambda_b[0])\hat{v}_b[0]^3, \qquad b \in \{1, 2, 3\}, \quad (4\text{-}33)$$

$$P_{\text{w},b}[k] \geq a_{k,b,l_{k,b}}^{\text{lb}} K[k] + b_{k,b,l_{k,b}}^{\text{lb}}, \qquad b \in \{1, 2, 3\}, k \in \{1, 2, \ldots, N_{\text{p}}\}, \quad (4\text{-}35)$$

$$P_{\text{w},b}[k] \leq \hat{P}_{\text{av},b}[k], \qquad b \in \{1, 2, 3\}, k \in \{1, 2, \ldots, N_{\text{p}}\}, \quad (4\text{-}36)$$

$$\hat{P}_{\text{av},b}[k] \leq a_{k,b,i}^{\text{ub}} K[k] + b_{k,b,i}^{\text{ub}}, \ i \in \{1, 2, \ldots, n_{\text{w}}\}, \ b \in \{1, 2, 3\}, k \in \{1, 2, \ldots, N_{\text{p}}\}, \quad (4\text{-}37)$$

$$z_{\text{P},b}[k] \geq \hat{P}_{\text{av},b}[k] - \frac{P_{\text{rated}}}{\eta_{\text{g}}}, \qquad b \in \{1, 2, 3\}, k \in \{1, 2, \ldots, N_{\text{p}}\}, \quad (4\text{-}38)$$

$$z_{\text{P},b}[k] \geq -\hat{P}_{\text{av},b}[k] + \frac{P_{\text{rated}}}{\eta_{\text{g}}}, \qquad b \in \{1, 2, 3\}, k \in \{1, 2, \ldots, N_{\text{p}}\}, \quad (4\text{-}39)$$

$$\hat{F}_{\text{T},b}[k] = \frac{Q_{\text{T},k,b}}{3} P_{\text{w},b}[k] + \frac{R_{\text{T},k,b}}{3} K[k] + \frac{S_{\text{T},k,b}}{3}, \ b \in \{1, 2, 3\}, k \in \{1, 2, \ldots, N_{\text{p}}\}, \quad (4\text{-}40)$$

in which if α_7 and α_8 are new non-negative constants that provide the weighting of their respective objectives. Of the constraints, only Eq. (4-35) to Eq. (4-40) are new, the rest is simply restated for the sake of clarity. The vector that contains all 'free' optimization variables is given by $\underline{x}^{\text{IPC}}$, which (at least) consists of all relevant values of $P_{\text{g}}[k]$, $P_{\text{w},b}[k]$, $\hat{P}_{\text{av},b}[k]$, $z_{\text{K}}[k]$, $z_{\text{P},b}[k]$ within the prediction horizon. In the case that tilt and yaw moment mitigation is performed by means of the formulation of the objective corresponding to α_7, the constraints provided by Eq. (4-26) to Eq. (4-31) are not used, and $\alpha_8 = 0$. If however, the tilt and yaw moment mitigation is implemented by means of output constraints, $\alpha_7 = 0$, the aforementioned constraints are used in the optimization problem, and the vector with optimization variables $\underline{x}^{\text{IPC}}$ additionally also includes all relevant values of $\epsilon_{\text{yaw}}[k]$ and $\epsilon_{\text{tilt}}[k]$ within the prediction horizon.

Setting aside the extension to multiple blades, the implementation of the thrust and bending moment models, the IPC optimization problem looks very similar to its CPC counterpart from Section 3-10. For example, from the objective function provided by Eq. (4-34) and the constraints it is clear that, for both out-of-plane blade root bending moment fatigue load mitigation strategies, the optimization has a convex QP problem structure. Moreover, the same parameter values $n_{\text{g}} = 5$, $n_{\text{w}} = 15$, $N_{\text{p}} = 100$, $\Delta t_{\text{s}} = 0.1$ s are used within the IPC optimization problem in order to allow for a better comparison between the CPC and IPC CEMPC implementations. For the same reason, YALMIP is once again used within MATLAB to create a tailored QP-solver that makes use of MOSEK. The inputs that are needed to define the QP are all of the values of $Q_{\text{T},k,b}$, $R_{\text{T},k,b}$, $S_{\text{T},k,b}$, the right hand sides of Eq. (3-36), Eq. (3-38), and Eq. (4-33), the blade-effective wind speeds $\hat{v}_b$, the constants used for the minimum aerodynamic power approximation $a_{k,b,l_{k,b}}^{\text{lb}}$ and $b_{k,b,l_{k,b}}^{\text{lb}}$, the constants used for the available power approximation $a_{k,b,i}^{\text{ub}}$ and $b_{k,b,i}^{\text{ub}}$, the azimuth position predictions $\hat{\psi}_b$, the values of a_{M}, b_{M}, and c_{M}, and the soft lower and upper bounds $M_{\text{tilt}}^{\text{lb}}$, $M_{\text{tilt}}^{\text{ub}}$, $M_{\text{yaw}}^{\text{lb}}$, and $M_{\text{yaw}}^{\text{ub}}$. One may note that no scheduling method has been provided for these tilt and yaw upper and lower bounds. The next chapter will determine what these bounds should be based on simulation results.

Note that the blade-effective wind speed is dependent on the azimuth position estimates

according to Eq. (4-5). The components of the QP that rely on the blade-effective wind speed are lower and upper bounds of the aerodynamic power (Eq. (4-35) and Eq. (4-36)), the initial aerodynamic power (Eq. (4-33)), the thrust model (Eq. (4-40)), and the objective within Eq. (4-34) that aims to minimize C_{P} variations. The azimuth position hence acts as a scheduling variable for the dynamics of the thrust and tilt and yaw moment models. Since the azimuth position is function of the kinetic rotational energy according to Eq. (4-6), which is a state of the considered dynamics in the optimization problem, one may consider the relevant dynamics to resemble a quasi-linear parameter-varying (qLPV) system. As noted in Section 4-3, the dependency of, e.g., the blade-effective wind speed on the azimuth position requires an iterative solution process. Luckily, it is demonstrated in [41] that for such qLPV systems, multiple iterations of the QP are only required to achieve reasonable convergence for the first MPC solution step. For subsequent QP problems that arise within the model predictive controller, predictions of the azimuth position from the previous solution should suffice. The essential idea is that subsequent QP problems do not change considerably, and hence, multiple iterations of the QP are not required to achieve convergence[7]. As is the case with the CPC implementation, only three iterations are hence performed for the first MPC solution step.

With regards to the objective function, one may recognize most of the objectives from the objective function from the CPC framework. An objective that requires some additional justification in the IPC domain is the minimization of C_{P} variations. Within the domain of CPC, the objective stems from the observation that the changes in the tip speed ratio are fairly small between time steps, particularly when a steady optimal state is reached within the prediction horizon. Hence, if one also minimized changes in the C_{P}, the pitching rate is effectively reduced. However, in the IPC framework, the tip speed ratios are dependent on the blade-effective wind speed, and as such are much more variable. The reason that this objective is still included is that it appears to help to prevent the otherwise more erratic nature of the aerodynamic power solutions that result from the QP.

[7] One may note that not only the dynamics are scheduled on the azimuth position, but also the objective function and the available power constraints. Whilst the authors of [41] do not cover such dependencies, it still makes sense to use their approach to iterations because the QP problem should not change considerably between solution steps.

Chapter 5

Simulation Strategy and Results

The previous two chapters presented the modified collective pitch control (CPC) and the newly developed individual pitch control (IPC) frameworks for convex economic model predictive control (CEMPC) of wind turbines. This chapter illustrates how these frameworks are incorporated within simulations and presents the results that are obtained. To this end, the setup with which the CEMPC framework is simulated is first explained. Thereafter, benchmark controllers are introduced for both the CPC and IPC implementations. In the subsequent section, the weights of the derived quadratic programming (QP) optimization problems are presented. Two different wind cases are subsequently investigated. The first simulated wind conditions concern a large step in the wind speed. Since the purpose of this case is only to demonstrate several features of the convex economic model predictive controller, only CPC, and no benchmark controller will be used. The second simulated wind conditions concern a staircase wind profile that goes throughout the operating regime. Results for both CPC and IPC will be discussed and compared to the benchmark controllers here.

5-1 Simulation Strategy

To obtain results, the simulations are performed using the the control diagrams shown by Figure 3-1 and Figure 4-1 for respectively CPC and IPC. The NREL 5 MW wind turbine as described in [37] is simulated using Fatigue, Aerodynamics, Structures, and Turbulence (FAST) within MATLAB Simulink. FAST is a high-fidelity aeroelastic simulation tool for horizontal-axis wind turbines [58]. For simulation within MATLAB Simulink, FAST is implemented as an S-function block. In particular, the FAST version eight [59] is used to integrate the codes from the ElastoDyn, InflowWind, AeroDyn, and ServoDyn modules. The ElastoDyn module prescribes structural and drivetrain dynamics, and InflowWind governs the prevailing wind conditions. Similarly, as the names may suggest, the AeroDyn module is used to model the aerodynamics, whilst the ServoDyn module is used to model the actuator and generator dynamics.

5-2 Benchmark Controllers

To be able to say something meaningful about the performance of the developed CEMPC implementations, two benchmark controllers are used. Below the rated rotational speed, both benchmark controllers use an optimal torque controller (see, e.g., [60]) to track the tip speed ratio that maximizes the aerodynamic power coefficient at the optimal pitch angle. Above rated, both benchmark controllers keep the generator torque at the rated torque and apply a CPC feedback loop to regulate the generator speed to its rated value using a gain-scheduled pitch controller. This basic benchmark controller will be referred to as the CPC benchmark controller. The IPC benchmark controller additionally implements the conventional IPC framework shown in Figure 1-2, which is based on the multi-blade coordinate (MBC) transformations. The implemented IPC controller in the same Figure consists of a simple single-input single-ouput (SISO) integral controller with an integrator gain of $3 \cdot 10^{-6}$ acting on tilt and yaw moments provided in kN m.

5-3 Optimization Problem Weight Selection

The selection of the weights of the derived QP problems is no trivial task. In essence it has been performed by means of trial and error. To evaluate the weights, whilst the simulation is running one may plot the contributions of the different objectives to the equivalent QP maximization problem. An example hereof is given by Figure 5-2b. By also considering the obtained solution trajectories of the pitch, kinetic rotational energy, tip speed ratio, etc. at each time step it is then possible to critically evaluate the weights. For objectives whose contributions one seeks to minimize it is particularly important to critically asses whether the contribution is fairly low because it is adequately minimized or because the weighting it is given is too small. The resulting weights of both the CPC and IPC implementations of the convex economic model predictive controller are given by Table 5-1. Please note that the precision of the weights does not reflect the actual precision of the tuning process but rather normalization factors that were applied to ensure a better scaled optimization problem.

To further enhance the numerical scaling of the implemented QP, the QP that is fed to YALMIP's `optimizer` object in MATLAB is normalized. Since the hessian of the implemented QP problem depends on the rotor-effective wind speed or blade-effective wind speeds, this normalization is performed by dividing the entire cost function by the maximum absolute value of the linear part of the cost function - c_{qp} in

$$\min_x f(x) = \min_x \frac{1}{2} x^\top H_{\text{qp}} x + c_{\text{qp}}^\top x. \tag{3-13}$$

5-4 Wind Case 1: Large Step in Wind Speed

This section will present results that nicely illustrate several features of the CEMPC controller. Since the IPC-CEMPC framework uses largely the same methodology as its CPC counterpart, only results for CPC are shown. The simulated wind conditions are that of a stepped wind speed profile that goes from 5 m/s directly to 18 m/s, as shown by Figure 5-1a. Vertical wind

Table 5-1: Weights of the QP problem (before normalization) that is solved by the implemented convex economic model predictive controllers. α_1 is a weight for the generator power maximization and turnpike mitigation objectives, α_2 weights the minimization of generator output power variations, α_3 weights the minimization of C_{P} variations, α_4 weights the limited available power maximization, and α_5 weights the minimization of overspeeding. With regards to the out-of-plane blade root bending moment fatigue mitigation, α_7 weights the minimization of tilt and yaw moments in the case where an objective formulation is used as fatigue load mitigation strategy. α_8 represents the weight for the minimization of tilt and yaw moment upper and lower bound violations in the case that soft output constraints are used for fatigue load mitigation.

weight	α_1	α_2	α_3	α_4	α_5	α_7	α_8
value	$2.54{\cdot}10^{-8}$	$2.00{\cdot}10^{-13}$	$1.00{\cdot}10^{2}$	$2.40{\cdot}10^{-8}$	$2.54{\cdot}10^{-9}$	$1.00{\cdot}10^{-14}$	$1.00{\cdot}10^{-5}$

shear is implemented using Eq. (4-1) and a shear coefficient of $\alpha = 0.2$. The stepped input wind profile is provided to FAST via the InflowWind module, which implements this input wind speed profile. As a result, there is a noticeable difference between the rotor-effective wind speed obtained directly from FAST, and the input provided to the InflowWind module.

With reference to Figure 5-1b, the kinetic energy dynamics given by

$$\dot{K} = P_{\mathrm{w}} - \frac{P_{\mathrm{g}}}{\eta_{\mathrm{g}}} \tag{2-18}$$

are clearly visible. As a result of the observed increase in wind speed from 5 m/s to 18 m/s, the modelled aerodynamic power increases, which leads to an increase in the kinetic rotational

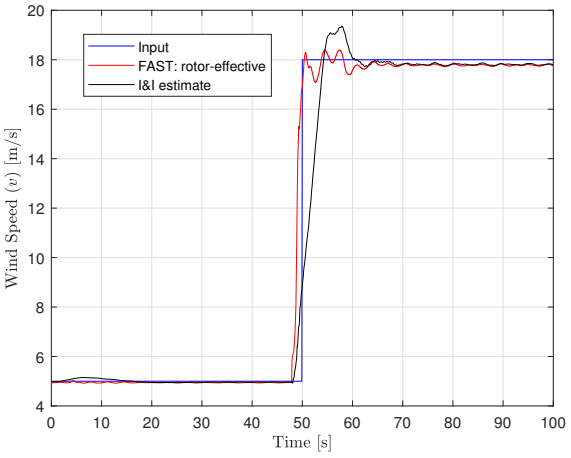

(a) Rotor-effective wind speed (estimate) and input wind speed.

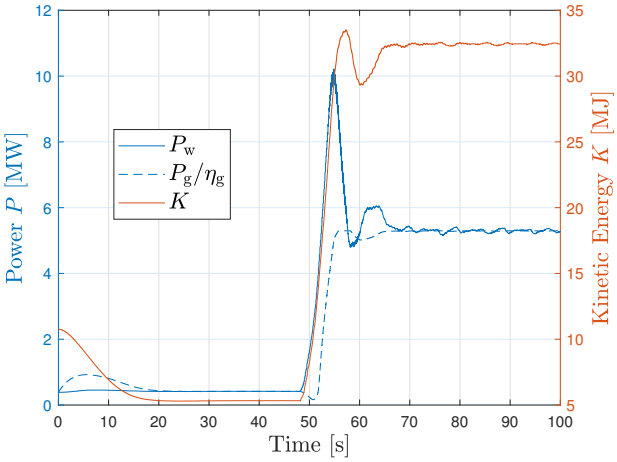

(b) Aerodynamic power, input generator power, and kinetic energy.

Figure 5-1: **(a)** Rotor-effective wind speed and its immersion and invariance (I&I) estimate corresponding to a stepped input wind speed that goes from 5 m/s directly to 18 m/s. **(b)** Modelled aerodynamic power P_{w}, input generator power $P_{\mathrm{g}}/\eta_{\mathrm{g}}$, and kinetic rotational energy K obtained using the CPC rendition of the convex economic model predictive controller for a wind speed that increases from 5 m/s directly to 18 m/s.

energy since the controller purposefully takes some time to also start increasing the input generator power.

5-4-1 Turnpike Mitigation

The used convex economic model predictive controller implements turnpike mitigation. As such, computed kinetic energy trajectories should not decrease drastically towards the end of the prediction horizon to allow for a greater power generation. To demonstrate that the CEMPC algorithms effectively implements turnpike mitigation, consider the example shown by Figure 5-2a, which shows the computed solution trajectories to the QP problem at 15.5 s into the simulation. It is clear that at the end of the prediction horizon, the kinetic energy does not decrease to allow for an increase in generator power. Judging by the contributions to the equivalent maximization optimization problem, shown by Figure 5-2b, the turnpike is indeed effectively mitigated because the controller also values the final kinetic rotational energy, which may be converted later by the generator with an efficiency of η_g.

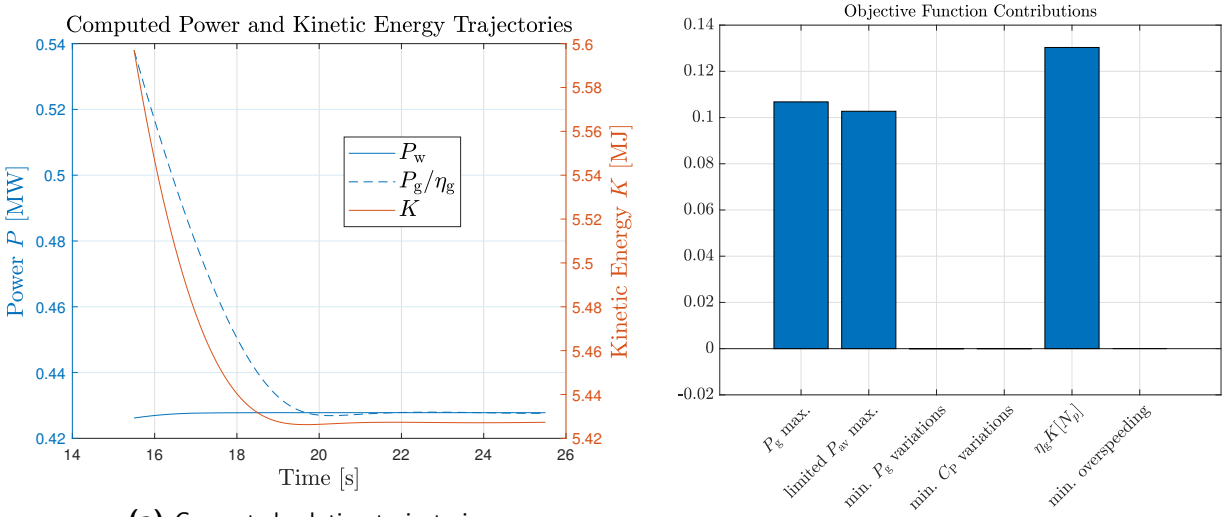

(a) Computed solution trajectories.

(b) Objective function contributions.

Figure 5-2: **(a)** Power and kinetic energy trajectories computed by the CPC rendition of the convex economic model predictive controller at a time of 15.5 s into the simulation of wind case one. The computed trajectories demonstrate that turnpike is effectively mitigated by the developed CEMPC framework. **(b)** Contributions of the various objectives to the equivalent maximization problem for the solution trajectories computed at 15.5 s by the CPC version of the convex economic model predictive controller for the first wind case. 'Max'. stands for 'maximization' and 'min.' is used as an abbreviation for 'minimize'.

5-4-2 Pitch and Pitching Rate Constraint Satisfaction

The reason for choosing the used wind speed profile is in large part to demonstrate the functioning of the pitching rate constraint. Figure 5-1a indicates that the I&I rotor-effective wind speed estimate lags behind the real rotor-effective wind speed during the step in wind

speed. This phenomenon was found to reduce the pitching rates that are used, which explains why such a large step in the wind speed has been used. To further highlight the pitching rate constraint, for the purposes of this section only, a maximum absolute pitching rate of $2^\circ/s$ has been used. The resulting collective pitch angle and pitching rate are shown in Figure 5-3. The pitching rate is clearly effectively limited to the maximum absolute pitching rate of $2^\circ/s$.

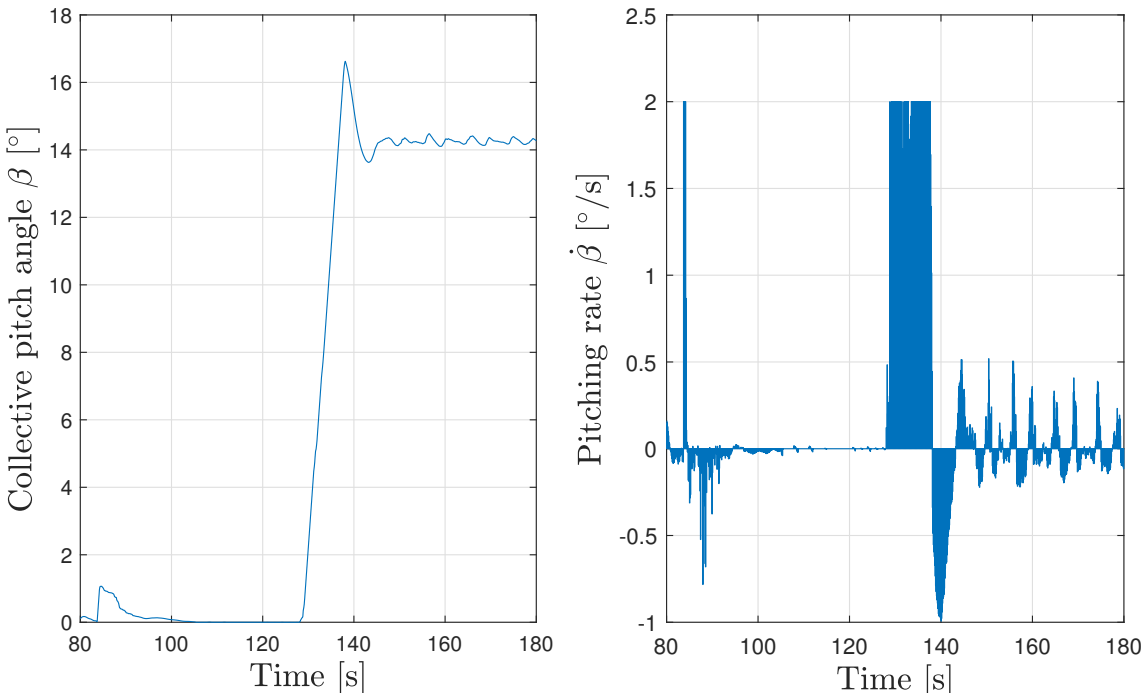

Figure 5-3: Collective pitch and pitching rates obtained using the CPC variant of the convex economic model predictive controller during a step in the wind speed from 5 m/s to 18 m/s. Note that the implemented maximum absolute pitching rate of $2^\circ/s$ is never exceeded.

As described in Section 3-8-2, the pitch and pitching rate constraints are enforced by solving a linear programming (LP) problem if such constraint violations are found. At a time of 1 s into the simulation, the LP-corrector is active. The input and outputs of the corrector (see also Figure 3-6 from Chapter 3) are illustrated by Figure 5-4. The measurement-updated pitch angle estimate $\hat{\beta}$ is shown because that is what the pitching rate constraints of the convex economic model predictive controller are based on. Note that around the relatively large increase in computed pitch angle at approximately 5 s, the pitch angle trajectory of β_{in} found by the lookup table violates the maximum absolute pitching rate. This is due to the lookup table implementation whereby, for the sake of computational efficiency, not all possible combinations of pitch angles are considered[1]. Pitch drift does not normally appear to be a very large problem for pitching rate constraint violations because subsequent pitch angles β_{in} typically move by a similar amount relative to the relevant, preceding pitch angle

[1]With reference to Figure 2-1 from Chapter 2 one may note that often, a particular combination of tip speed ratio and power coefficient can have two possible pitch angle solutions. To reduce the computational cost of the pitch lookup table, not all possible combinations of these pitch angles are considered. Instead, the pitch solution trajectory given by the pitch lookup table takes either the trajectory corresponding to all possible largest or smallest pitch angles.

estimate $\hat{\beta}$. As a result, the LP-corrector only needs to correct the pitch angles around 5 s to satisfy the maximum absolute pitching rate constraint of 2°/s.

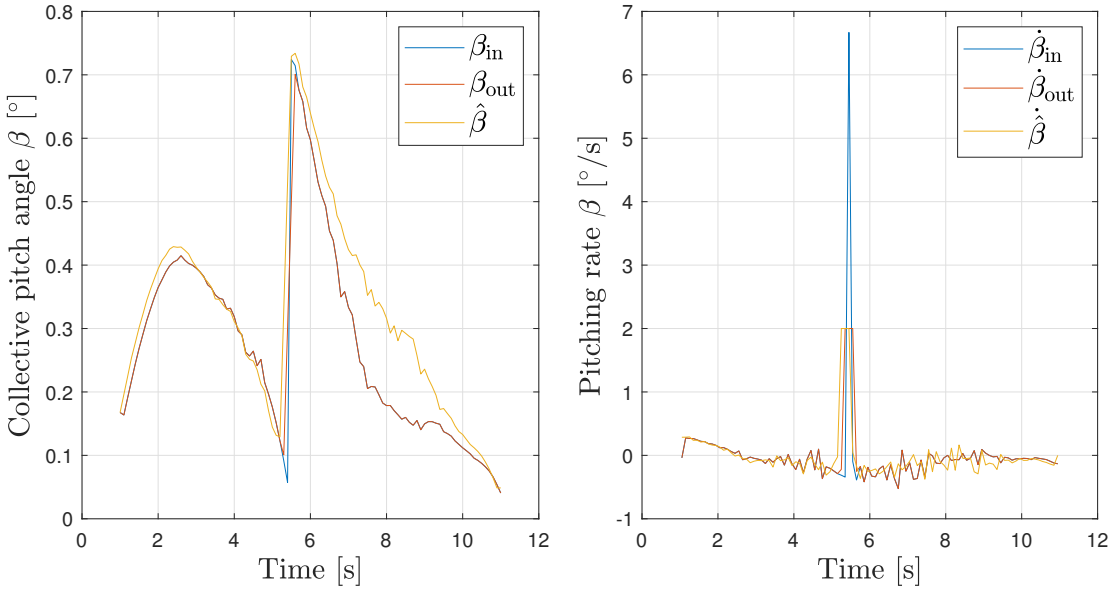

Figure 5-4: Input and output collective pitch and pitching rates of the LP-corrector obtained at 1 s into the simulation of the first wind case. The pitch estimate $\hat{\beta}$ is shown because the pitching rate constraints are implemented by the convex economic model predictive controller relative to these pitch angle estimates. Pitch and pitching rate constraint violations due to, e.g., pitch drift are corrected using an LP that has β_{in} as inputs, and provides β_{out} as outputs.

5-5 Wind Case 2: Staircase Throughout Operating Regime

Having shown several features of the CEMPC framework in the previous section, this section will investigate the performance of the convex economic model predictive controllers for both CPC and IPC, comparing the performance to the previously discussed benchmark controllers. For this purpose, an input wind speed profile that resembles a staircase that goes from 7 m/s to 18m/s in 600 seconds is used. This wind speed profile can be clearly seen from, e.g., Figure 5-5. As before, vertical wind shear is implemented in accordance with Eq. (4-1) and a vertical wind shear coefficient of $\alpha = 0.2$.

5-5-1 Collective Pitch Control

Qualitative Analysis

For the stepped wind speed profile shown in Figure 5-5, the actual rotor-effective wind speed and the I&I estimate thereof are also shown. It is clear that the I&I wind speed estimator is able to track the rotor-effective wind speed quite well. The oscillations of the rotor-effective wind speed that develop after 250 s are likely to result from increased pitching activity, which

causes, e.g., fore-aft tower oscillations and changes in the aerodynamic thrust exerted on the wind turbine.

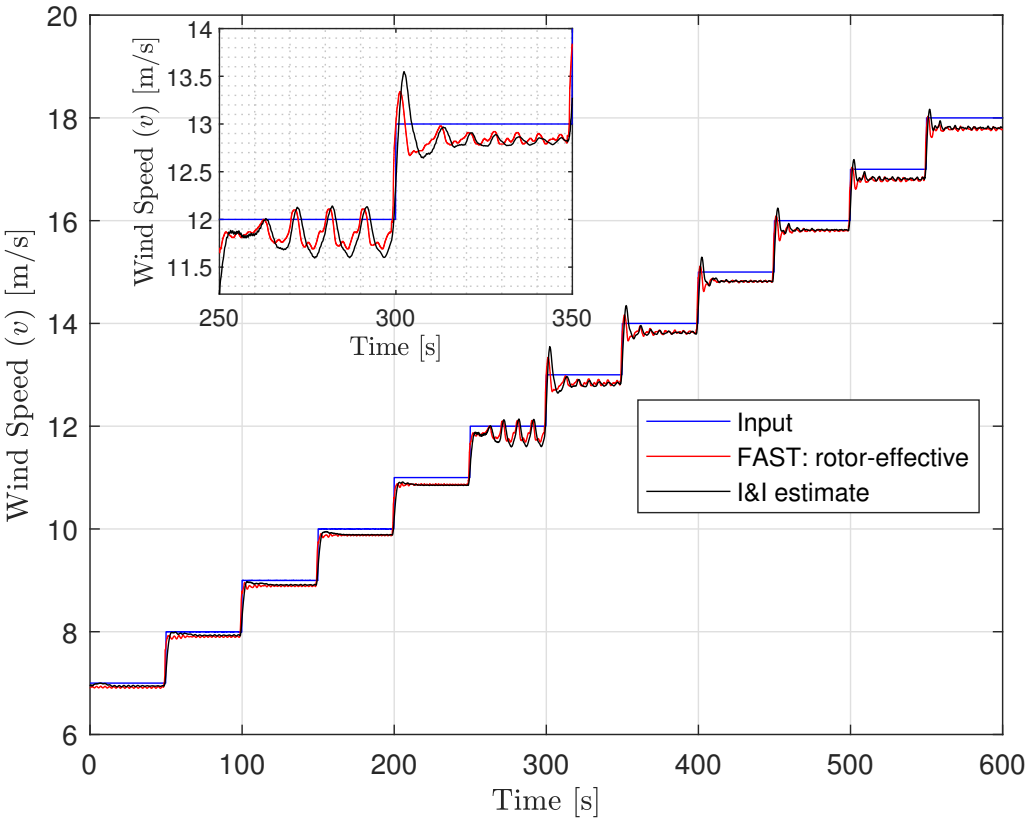

Figure 5-5: A stepped wind speed profile at hub height (starting at 7 m/s and ending at 18 m/s) with a vertical wind shear coefficient of $\alpha = 0.2$ (see Eq. (4-1)) is used to evaluate the performance of the collective pitch controllers. The rotor-averaged wind speed (in red, as obtained directly from FAST) may differ slightly from the input wind speed profile because of the InflowWind module implementation. As the inset axis shows more clearly, the I&I estimate, shown in black, tracks the rotor-averaged wind speed quite well.

The obtained generator output power and kinetic rotational energies are shown by Figure 5-6 whilst the generator torque and the collective pitch angles are illustrated by Figure 5-7. Below the rated wind speed of approximately 11.4 m/s (from the beginning to 250 s), it is clear that at the steady generator powers that are reached the CEMPC algorithm appears to generate less power than the benchmark controller. The greater kinetic energies at which the benchmark controller obtains these higher generator powers suggests that the benchmark controller finds a higher maximum power coefficient then the CEMPC-based controller. Since below rated the torque remains below the rated torque of approximately 43 kNm, as shown in Figure 5-7a, this cannot be due to the maximum torque constraint. Instead, the lower CEMPC generator powers derive from the way in which the available aerodynamic power is approximated by the CEMPC controller. The piecewise-linear approximation of the power coefficient as described in Section 3-8 is likely to underestimate the actual maximum attainable power coefficient

because the approximation is always smaller than (or equal to) the actual power coefficient. Moreover, a finite number of approximations of $n_{\mathrm{w}} = 15$ is used, and as a result there will typically always be some degree of error between the modelled and actual maximum power coefficient.

Above the rated wind speed (from 250 s onwards), the benchmark controller regulates the kinetic rotational energy to its rated value by means of pitch control whilst keeping the generator torque at the rated torque. This typically yields a rated generator output power except for when the wind speed increases, in which case overspeeding leads to the generator power to exceed its rated value. Likewise, the convex economic model predictive controller also attempts to regulate the kinetic rotational energy to its rated value. For CEMPC the reason for doing so is that K_{rated} is the only kinetic energy at which the rated generator power can adopt its rated value without incurring a penalty for overspeeding. In contrast to the benchmark controller, the CEMPC framework considers the rated power of 5 MW as a hard upper bound. As a result, the generator power is nearly never exceeded[2]. To ensure that the rated power is not exceeded, the convex economic model predictive controller decreases the generator torque from its rated value during overspeeding, and increases the pitch angle to reduce the aerodynamic power. To perform the desired regulation of the kinetic energy to its rated value, the convex economic model predictive controller depends on the I&I estimates of the rotor-effective wind speed. As one can see in Figure 5-5 these can oscillate a bit, particularly above rated, which explains the remaining oscillations of the pitch angle that are visible in Figure 5-7b. As noted before, the oscillations of the I&I rotor-effective wind speed are likely the result of changes in the pitch angle. This suggests an interesting interaction between the pitch angle and the rotor-effective wind speed.

To be able to compare CPC with IPC performance in terms of blade root bending moment fatigue load mitigation (and to determine the tilt and yaw moment bounds for the next section), results of the tilt and yaw moments as well as the individual out-of-plane blade root bending moments are shown in Figure 5-8. It is clear that the out-of-plane blade root bending moment oscillations are typically larger in magnitude with CEMPC than with the benchmark controller. This manifests itself in tilt and yaw moments that are also typically larger in magnitude with CEMPC than with the benchmark controller.

Performance Metrics

To summarize the above findings, several statistics are formulated to quantify the performance of the controllers in terms of pitching activity, out-of-plane blade root bending fatigue loading, and energy capture of the wind turbine. To asses the pitching activity, a measure called the actuator duty cycle (ADC) is often used [61]:

$$ADC = \frac{1}{T_{\mathrm{sim}}} \int_0^{T_{\mathrm{sim}}} \frac{\dot{\beta}}{\dot{\beta}_{\mathrm{max}}} dt, \tag{5-1}$$

[2]Due to some forms of model error this is not always the case. Suppose for example that whilst operating under rated conditions, the measured generator rotational speed turns out to be greater than what was predicted. As a result of Eq. (3-38) the implemented generator power may be larger than the rated power. However, given the small time step of $\Delta t = 0.1$ s, these errors are bound to remain small, just like the resulting increase in generator power above the rated power.

in which T_{sim} is the time length of the simulation or operation window that is under investigation. To asses the fatigue loading due to out-of-plane blade root bending moments, a metric called the damage equivalent loads (DEL) [62] is used:

$$DEL = \left(\sum_i \frac{S_i^m}{N_{\text{eq}}} \right)^{(1/m)}, \tag{5-2}$$

in which S_i is the range of of a particular load cylce i, m is the Wöhler coefficient, which is taken to be 10 for the NREL 5 MW wind turbine as based on typical values for composite wind turbine blades [63], and N_{eq} is the equivalent number of load cycles for which the DEL is computed (taken to be 10^7). Lastly, the total energy capture is calculated based on the integral of the generator power over time. The change in kinetic rotational energy between the start and end of a simulation may later also be converted to energy with an efficiency of η_g.

Figure 5-9 illustrates the obtained results using the above metrics of actuation duty cycle, DEL of out-of-plane blade root bending moment fatigue loading, and energy capture. It is clear that the CEMPC controller leads to approximately four times the amount of pitching activity compared to the benchmark controller, as measured by the ADC. Moreover, the CEMPC controller also leads to considerably higher damage equivalent out-of-plane blade root bending moment fatigue loading. As highlighted earlier, the CEMPC method does not manage to extract as much power as the benchmark controller, particularly below the rated wind speed. However, as Figure 5-9c illustrates, the decrease in generator power output is minimal. From the same figure it is clear that given the large time span of 10 minutes for which the simulation is run, the increase in kinetic energy that may later be used is negligible compared to the actual generator power output over time.

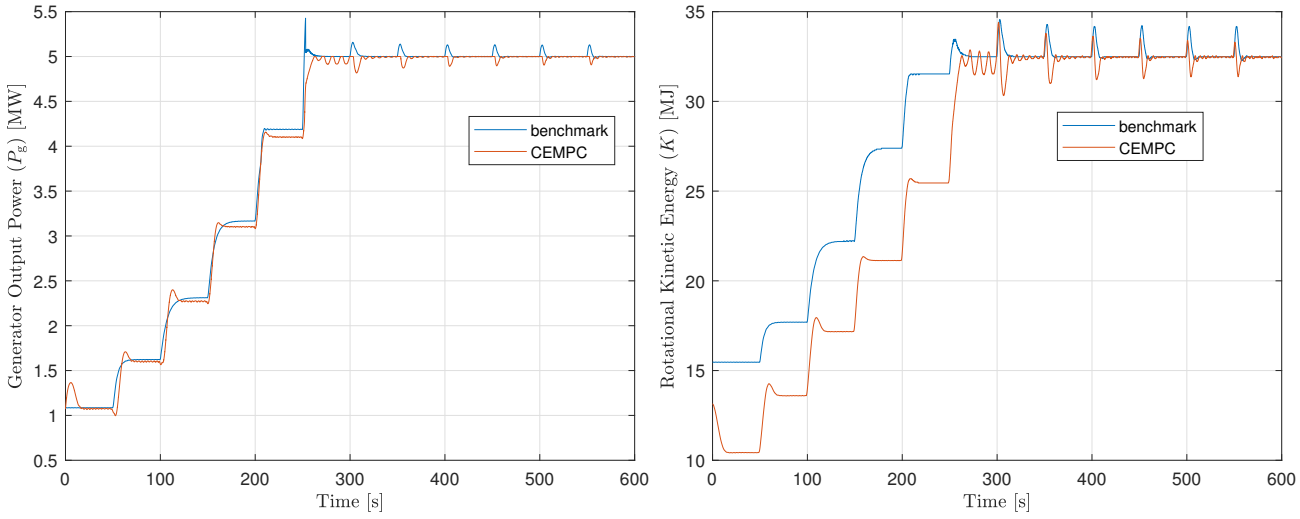

(a) Generator output power **(b)** Rotational kinetic energy

Figure 5-6: Generator power **(a)** and rotational kinetic energies **(b)** obtained using CPC for the stepped wind speed profile from Figure 5-5. Results for the benchmark and CEMPC controllers are shown in respectively blue and red.

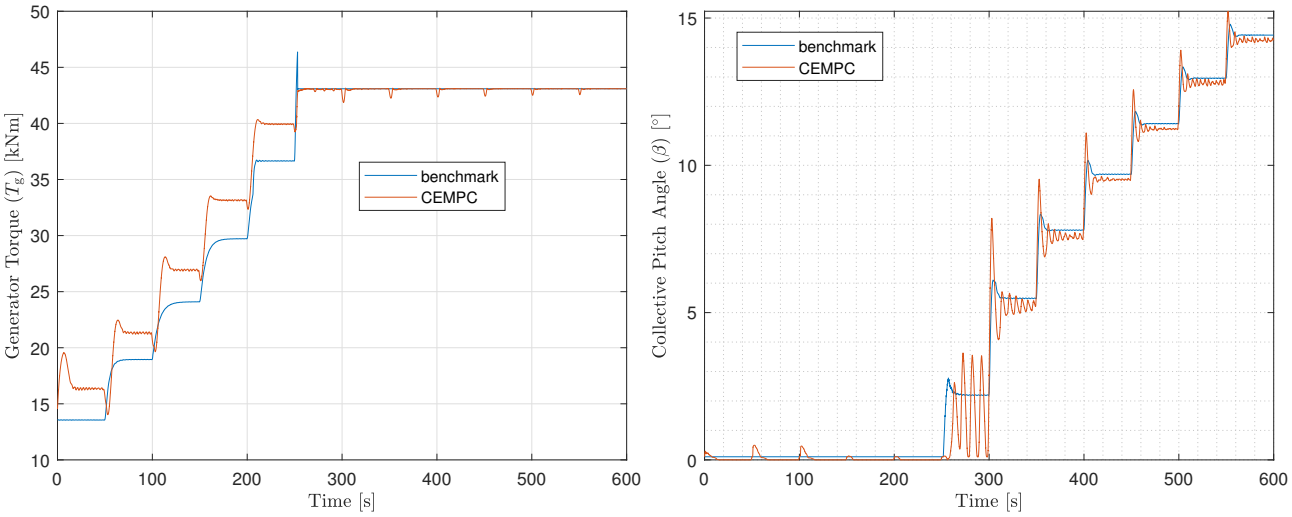

(a) Generator torque **(b)** Collective pitch angle

Figure 5-7: Generator torque **(a)** and collective pitch angles **(b)** obtained using CPC for the stepped wind speed profile from Figure 5-5. Results for the benchmark and CEMPC controllers are shown in respectively blue and red.

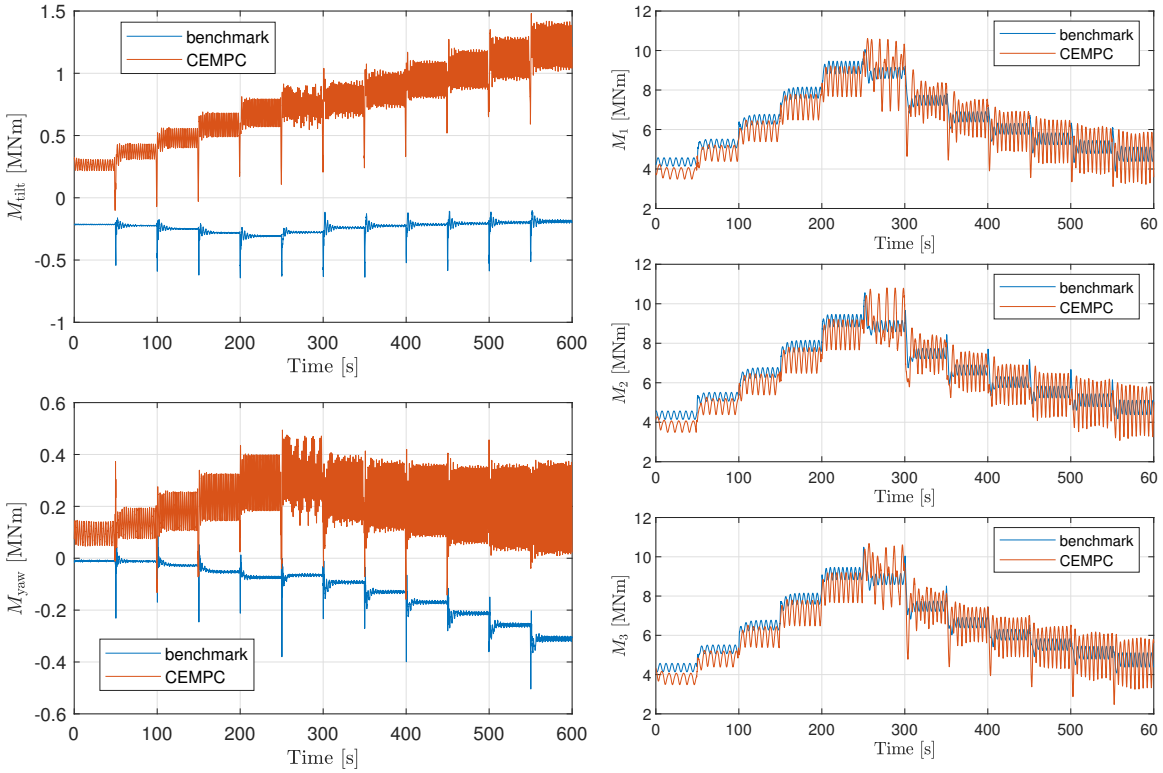

Figure 5-8: Tilt, yaw, and individual out-of-plane blade root bending moments obtained from CPC during a stepped wind speed profile going from 7 m/s to 18 m/s. Results obtained from the benchmark controller are indicated in blue whilst the results from the CEMPC controller are indicated in red.

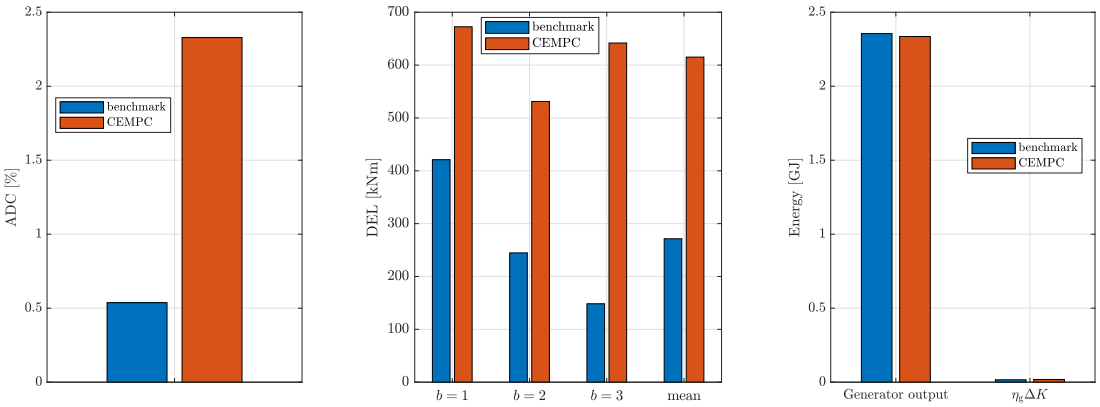

(a) Pitch actuation duty cycle **(b)** Damage equivalent load **(c)** Energy capture

Figure 5-9: Pitch actuation duty cycle **(a)**, damage equivalent out-of-plane blade root bending moment fatigue loading **(b)**, and total energy capture (both generator output power over time and the useful change in kinetic rotational energy $\eta_g \Delta K$ between the beginning and end of the simulation) **(c)** with CPC during a stepped wind speed profile from 7 m/s to 18 m/s. Benchmark results are shown in blue whilst CEMPC results are shown in red.

5-5-2 Individual Pitch Control

Determining Tilt and Yaw Moment Bounds for Output-Constrained IPC

Before moving on to the results obtained using IPC, the bounds for the tilt and yaw moments still have to be formulated for the output-constrained load mitigation method. To this end, consider the tilt and yaw moments obtained using CPC for both the benchmark and CEMPC controller, shown in Figure 5-8. As is visible from this figure, the tilt and yaw moments that are obtained using the CEMPC method are considerably more variable than those from the benchmark controller. Looking at the individual out-of-plane blade root bending moments one can similarly see that the variations of these moments are larger when using the CEMPC controller. Moreover, the tilt and yaw moments obtained using the CEMPC method typically appear larger in magnitude than those of the benchmark controller. These observations make it more difficult to select suitable upper and lower tilt and yaw moment bounds. Ultimately, based on the tilt and yaw moments shown in Figure 5-8, the tilt and yaw constraints were choosen as:

$$M_{\text{tilt}}^{\text{ub}} = -M_{\text{tilt}}^{\text{lb}} = 0.5 \text{ MNm}, \tag{5-3}$$

$$M_{\text{yaw}}^{\text{ub}} = -M_{\text{yaw}}^{\text{lb}} = 0.3 \text{ MNm}. \tag{5-4}$$

Whilst these constraints are not dependent on the rotor-effective wind speed (as was the case in Section 4-6), the idea is that the box constraints provided by Eq. (5-3) and Eq. (5-4) should suffice in motivating greater pitching activity - particularly above the rated wind speed - in order to reduce the tilt and yaw blade root bending moments.

Qualitative Analysis

The wind conditions for which the individual pitch controller are simulated are the same as those for which the collective pitch controllers were simulated. For completeness, as before, the resulting rotor-effective wind speed estimate that is obtained for the fatigue load mitigation strategy that makes use of an objective formulation is shown by Figure 5-10.

Figure 5-11 and Figure 5-12 bear a lot of similarities with their CPC counterparts, which were discussed previously. Once more, it is clear that the CEMPC controllers appear to typically favor a larger generator torque and a lower kinetic rotational speed than the benchmark controller. Moreover, it is clear that below rated, the CEMPC controllers are not able to extract as much power from the wind as the benchmark controller is able to do. This is again due to the limited accuracy of the piecewise linear approximations used to describe the (maximum) power coefficient. As is the case with CPC, above rated, the generator power is quite neatly regulated to the rated power of 5 MW.

When looking at the pitch angles shown in Figure 5-13 several observations can be made. As before, both CEMPC controllers react to a more pronounced observed oscillation of the rotor-effective wind speed (also visible in Figure 5-10) between 250 s and 300 s. Although the pitch angles are determined independently from one another in CEMPC, with the objective formulation, the pitch angles generally appear to oscillate more around a common (collective) pitch angle. This is in stark contrast to what is observed when output constraints are applied,

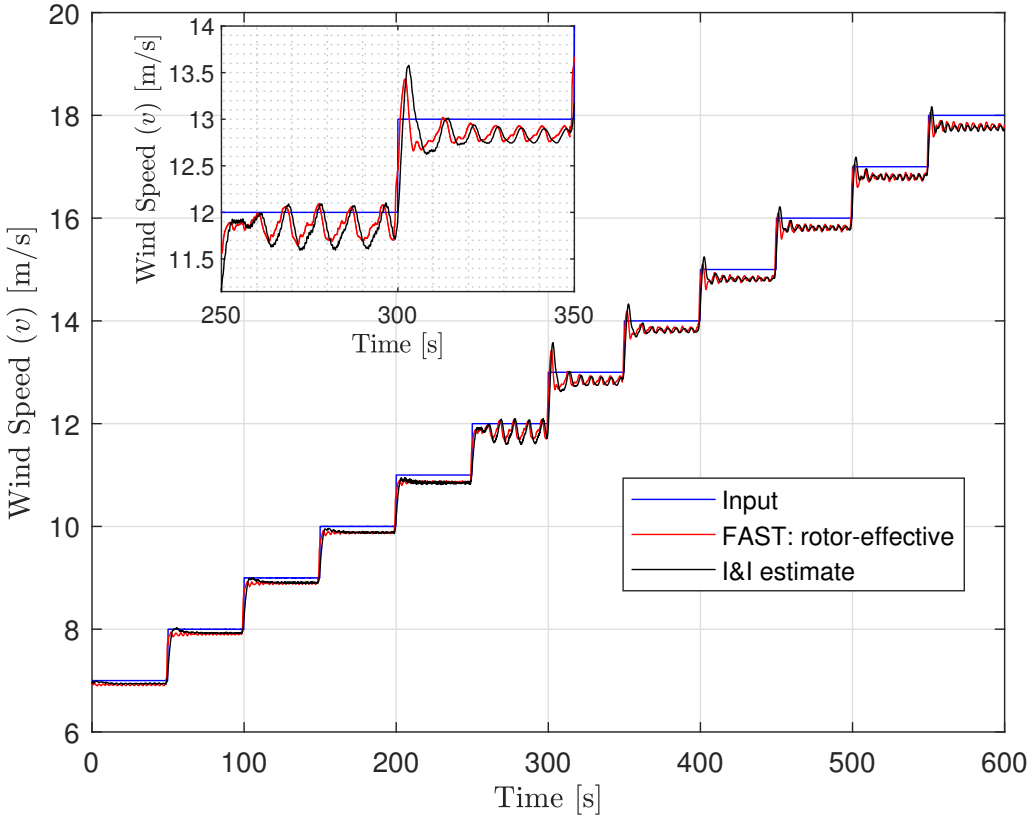

Figure 5-10: A stepped wind speed profile at hub height (starting at 7 m/s and ending at 18 m/s) with a vertical wind shear coefficient of $\alpha = 0.2$ (see Eq. (4-1)) is used to evaluate the performance of the individual pitch controllers. The rotor-averaged wind speed (in red, as obtained directly from FAST) may differ slightly from the input wind speed profile because of the InflowWind module implementation. As the inset axis shows more clearly, the I&I estimate, shown in black, tracks the rotor-averaged wind speed quite well. For clarity, only the I&I estimate of the CEMPC controller that makes use of the objective formulation to mitigate out-of-plane blade root bending fatigue loading is shown (the I&I estimate obtained for the output contraint implementation is very similar).

in which case the different blades do not necessarily appear to oscillate around a common pitch angle. An example hereof is clearly visible between, for example, 400 s and 450 s.

Given these pitch angles, the resulting tilt and yaw bending moments are shown in Figure 5-14. Whilst the benchmark MBC controller is able to effectively minimize the tilt and yaw moments, neither of the CEMPC controllers seem to offer as effective tilt and yaw bending load mitigation. By comparing Figure 5-14 with its CPC counterpart Figure 5-8 it does become clear that for CEMPC, at mostly high wind speeds (at which the CEMPC tilt and yaw bending moments were typically largest with CPC), the variability of the tilt and yaw bending moments seems to have increased whilst the average tilt and yaw bending moment seems to have decreased. Notice that when using output constraints, the box constraints defined by the bounds given by Eq. (5-3) and Eq. (5-4) are violated, and the average tilt and yaw moments per wind speed are larger than when using an objective formulation. For

both of the IPC-CEMPC applications it is clear that the average tilt and yaw moments are typically smaller than with its CPC counterpart. However, this does not seem to effectuate a noticeable decrease in the amplitude of the out-of-plane blade root bending moments relative to the CPC case.

When looking at Figure 5-14 there is a sharp decrease of the tilt and yaw moments at 18 m/s using the objective formulation to minimize fatigue. From Figure 5-13 one may infer that this is due to increased pitch actuation. Consider Figure 5-15, which indicates the one step ahead predictions made by the controller. Using a fatigue load mitigation strategy that makes use of an objective formulation, for a wind speed of 18 m/s the out-of-plane blade root bending moment prediction error increases considerably in magnitude. As a result, the controller thinks that it can attenuate the tilt and yaw moments to almost zero by using considerable pitching action.

With reference to the difference between the actual tilt and yaw moments shown in Figure 5-14 and the predicted tilt and yaw moments shown in Figure 5-15 it is important to make several observations. First of all, any tilt and yaw error is principally due to M_b errors since step ahead azimuth position errors are negligible. The small nature of these latter errors can be explained by the fact that both the azimuth position and the rotor speed are provided as feedback measurements. Secondly, the step ahead M_b prediction errors are significant. The absolute prediction errors shown amount to a typical prediction error that is in the order of 1%, which may be considered significant given the model predictive control (MPC) step size of only 0.1 s. Moreover, one may expect this prediction error to grow for more steps ahead into the prediction horizon.

Another issue that Figure 5-15 illustrates is the ineptness of the tilt and yaw moments as measures that are to be mitigated for out-of-plane blade root bending moment fatigue load mitigation. The step ahead predictions indicate that as long as the out-of-plane blade root bending moments of the three blades oscillate with a phase difference of approximately 120° with respect to one another, the resulting tilt and yaw moments are considered to be sufficiently attenuated by the controller. Now consider the MBC transformation matrix in Eq. (4-24); its nullspace is spanned by $[1\ 1\ 1]^\top$. Hence, if all out-of-plane blade root bending moments were to be equal, both the tilt and yaw moments would be zero. Suppose that the controller is able to ensure that all out-of-plane blade root bending moments are equal. In that case, contrary to what happens with MBC, these out of moments may still all vary by the same amount, nevertheless leading to fatigue damage. Whilst this is clearly not what happens (except when looking at the objective formulation predictions at a wind speed of 18 m/s), it demonstrates the unsuitability of tilt and yaw measures for out-of-plane blade root bending moment fatigue load mitigation when using the IPC-CEMPC framework developed in this thesis.

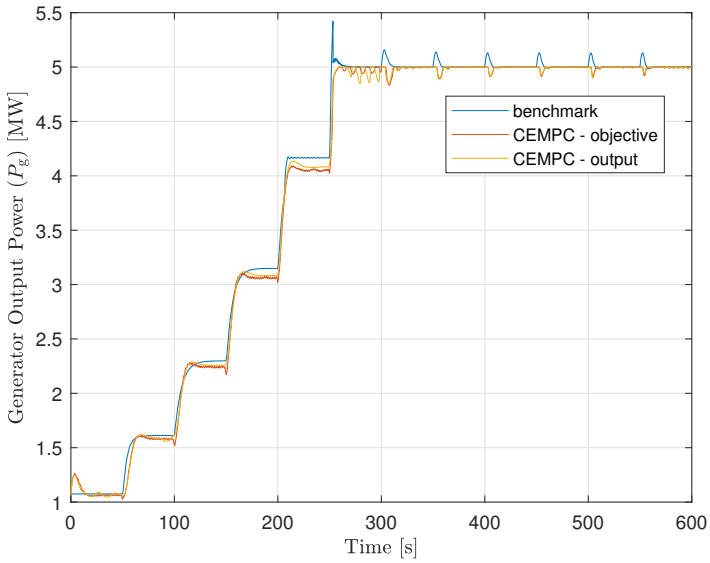

Figure 5-11: Generator output power of the different IPC controllers obtained from a stepped input wind profile going from 7 m/s to 18 m/s. The benchmark controller is shown in blue whilst the red line illustrates the CEMPC controller that makes use of an objective formulation to mitigate loads, and the yellow line indicates the results from the CEMPC controller that uses output constraints.

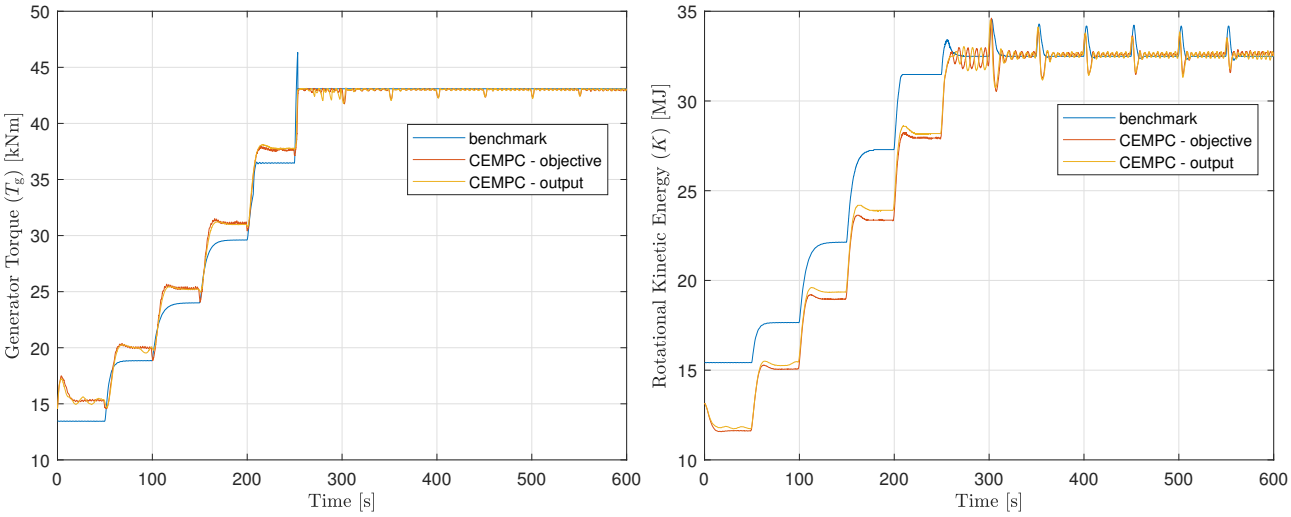

(a) Generator torque **(b)** Rotational kinetic energy

Figure 5-12: Generator torque **(a)** and rotational kinetic energies **(b)** obtained using IPC for the stepped wind speed profile from Figure 5-10. Results for the benchmark are shown in blue whilst results obtained using the objective formulation and output-constrained load mitigation methods are shown in respectively red and yellow.

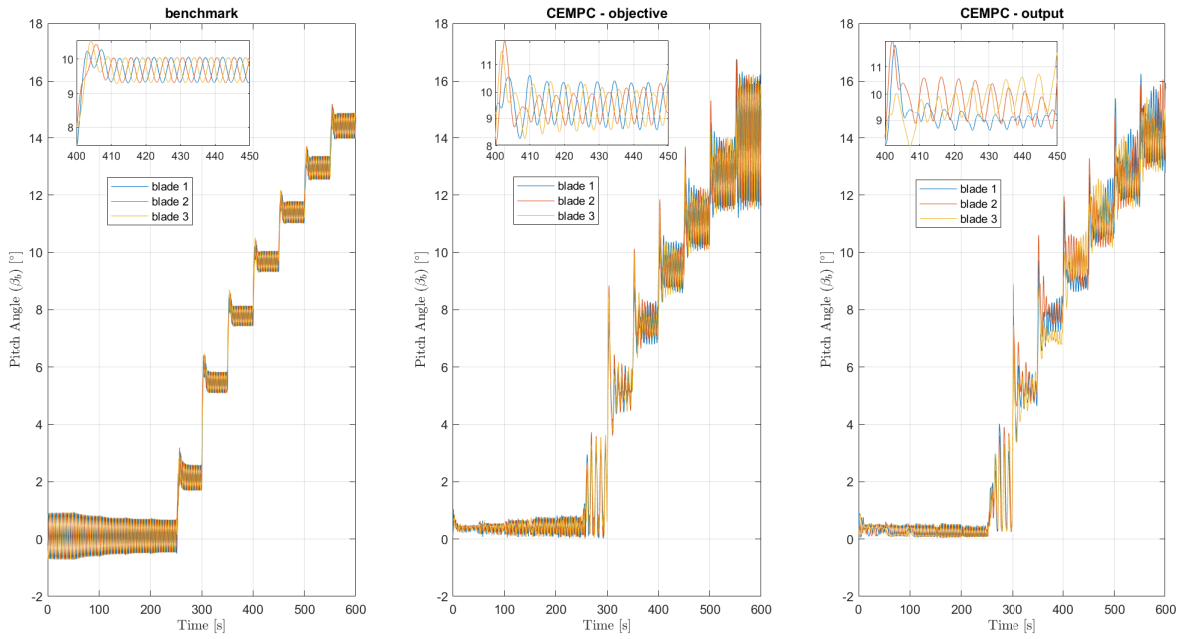

Figure 5-13: Individual pitch angles obtained using the three different IPC strategies and a stepped wind speed profile going from 7 m/s to 18 m/s. From left to right, the results of the benchmark, CEMPC using an objective formulation to mitigate loads, and CEMPC using an output constraints to mitigate loads are shown.

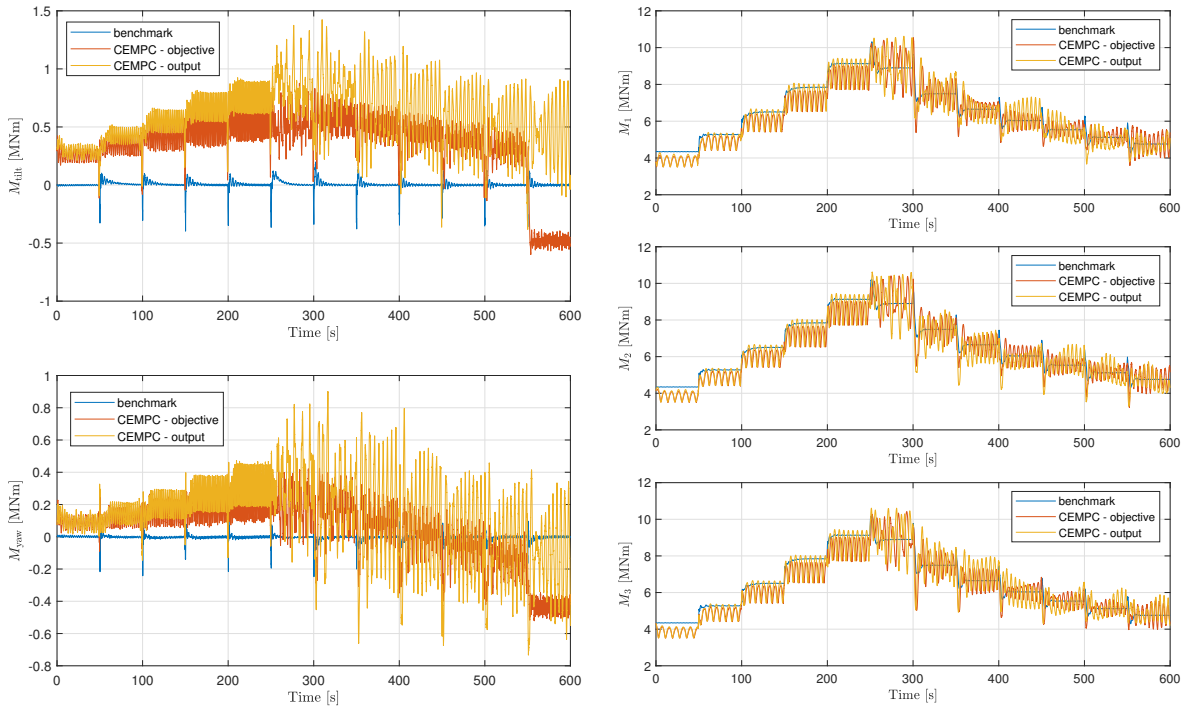

Figure 5-14: Tilt, yaw, and individual out-of-plane blade root bending moments obtained from IPC during a stepped wind speed profile going from 7 m/s to 18 m/s. Results obtained from the benchmark controller are indicated in blue whilst the results for the CEMPC controllers that make use of an objective formulation and output constraints are indicated in respectively red and yellow.

Performance Metrics

Once more, to be able to accurately compare the different control methods, use is made of the same metrics as those that were discussed in Section 5-5-1. With regards to the pitch actuator duty cycle, Figure 5-16a shows that the most pitching action is performed by the CEMPC controllers. The CEMPC controller that makes use of an objective formulation for load mitigation purposes on average performs about 3% more pitching activity than the output-constrained variant and about 4.5% more pitching activity than the MBC benchmark controller. As is to be expected, the individual pitch controllers all perform more pitch actuation than their CPC counterparts.

When looking at the damage equivalent loading, something becomes apparent. Whilst the average tilt and yaw moments at a particular wind speed may typically have appeared to be lower in Figure 5-14 when using an objective formulation than when using output constraints, the mean damage equivalent load does not reflect this. The mean damage equivalent out-of-plane blade root fatigue load is smallest with the MBC benchmark controller, followed by CEMPC using output constraints, and the greatest mean DEL is obtained using an objective formulation. The far greater DEL values of the CEMPC methods highlight the problems with the out-of-plane blade root bending model, and above all, the ineptitude of the tilt and yaw moments as measures for out-of-plane blade root bending moment fatigue load mitigation when using the IPC-CEMPC framework developed in this thesis.

Lastly, as was the case with CPC, the CEMPC methods both capture slightly less power than

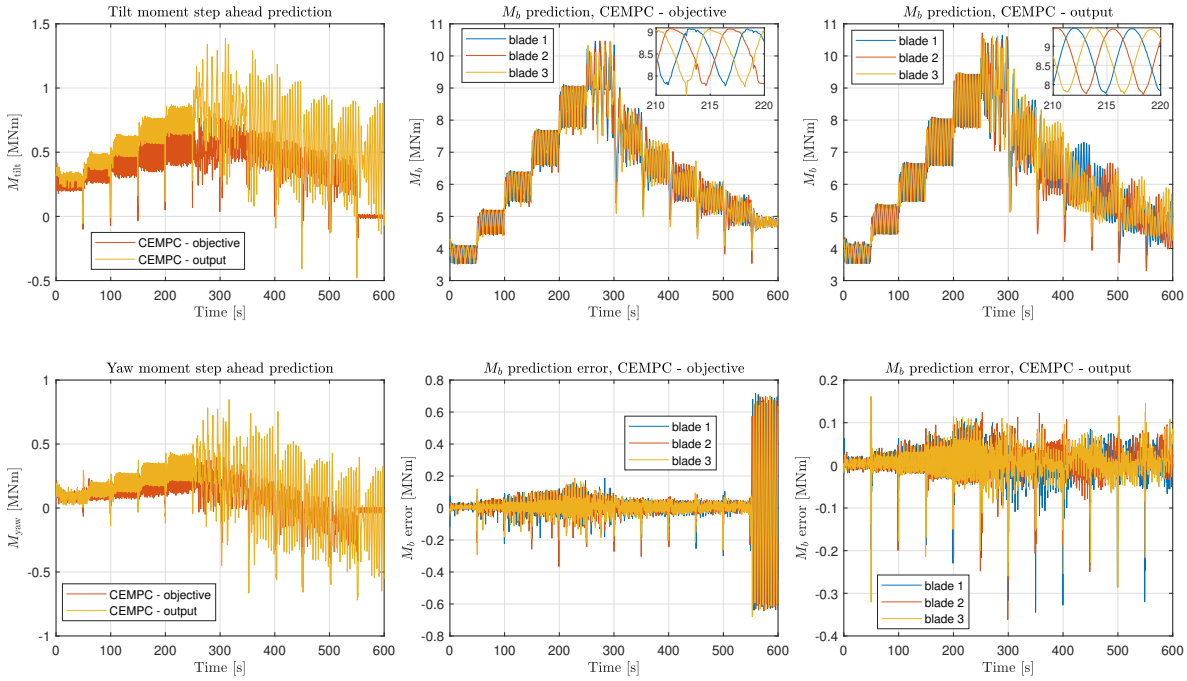

Figure 5-15: One step ahead predictions of the tilt (top left), yaw (bottom left), and out-of-plane blade root bending moments (top centre and top right) together with the step ahead out-of-plane blade root bending moment prediction error (bottom centre and bottom right) for both out-of-plane blade root bending moment fatigue load mitigation strategies.

the benchmark controller. This is for the most part due to the suboptimal power maximization below rated. However, it also reflects to a lesser degree that the rated power is a hard upper bound for the convex economic model predictive controllers, but not for the benchmark IPC controller. As before, the change in the kinetic rotational energy is negligible when compared to the actual energy capture due to the large simulation time.

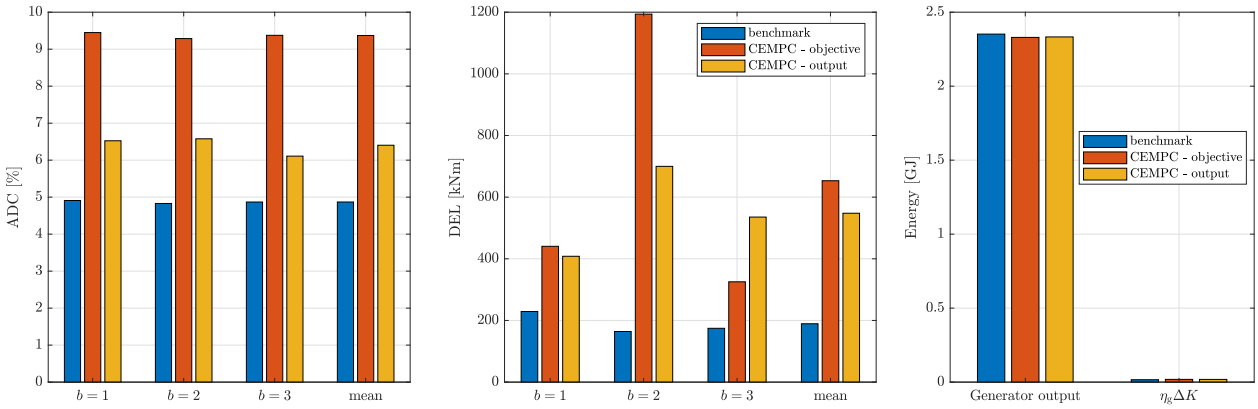

(a) Pitch actuation duty cycle **(b)** Damage equivalent load **(c)** Energy capture

Figure 5-16: Pitch actuation duty cycle **(a)**, damage equivalent out-of-plane blade root bending moment fatigue loading **(b)**, and total energy capture (both generator output power over time and the useful change in kinetic rotational energy $\eta_g \Delta K$ between the beginning and end of the simulation) **(c)** with IPC during a stepped wind speed profile from 7 m/s to 18 m/s.

Chapter 6

Conclusion

6-1 General Conclusion

This master thesis aims to answer a question that is yet unanswered within the existing literature. The convex economic model predictive control (CEMPC) framework for wind turbines appears promising, but in its existing form it is limited to collective pitch control (CPC). As a result, with regards to load mitigation, only fore-aft tower damping has yet been investigated. Since individual pitch control (IPC) offers particularly promising perspectives for load mitigation, this thesis aims to answer the following research question:

How can the existing CEMPC framework be extended to the domain of IPC for the purpose of wind turbine load mitigation?

This thesis has specifically considered out-of-plane blade root bending moment fatigue load mitigation since these loads are typically considered for mitigation by means of IPC. To answer the research question, answers to the following sub-questions were sought:

1. *How does the existing CEMPC method for wind turbine control work?*
   In Chapter 2 this sub-question was answered. The dynamics of a wind turbine are normally described in a nonlinear fashion. Hence, a typical optimization problem for model predictive control (MPC) applications gives rise to a nonlinear, non-convex optimization problem, even for simple objectives like power maximization. The CEMPC method makes use of a simple change of variables (exchanging the generator rotational speed, generator torque, and pitch angle for the kinetic rotational energy, generator output power, and aerodynamic power), which renders the dynamics linear. Moreover, the inequality constraints are all either rendered convex or can be approximated as such (notably the available power). Hence, a convex optimization problem arises for use in MPC.

2. *How may the existing CEMPC framework be altered to realize a both theoretically and practically suitable application for CPC?*
   Chapter 3 demonstrates that the existing CEMPC framework leaves sufficient room for improvement. Changes that have been performed include the application of: first-order hold discretization, a more truly *economic* optimization problem formulation, turnpike mitigation, and feedback constraints. A notable change concerns the reformulation of the optimization problem as a quadratic programming (QP) problem to reduce the problem complexity and thereby enable particularly efficient optimization algorithms. This reformulation is particularly relevant to the implementation of the maximum torque constraint, the minimization of overspeeding, and the (limited) maximization of available power. Another significant change concerns the inclusion of pitching rate constraints by means of the reformulation of the aerodynamic power constraints. Such pitching rate constraints are particularly relevant for typical MPC applications with fairly small time steps, as is the case in this thesis.

3. *How can the newly developed CPC implementation of CEMPC be extended to the domain of IPC?*
   Chapter 4 illustrates how the CEMPC framework can be extended to IPC. It is demonstrated that this extension is possible by considering a blade-effective wind speed and a resulting, independent CPC-equivalent aerodynamic power for each of the three blades. Using this approach, the principles developed for CPC-CEMPC can largely be reused. As a result the optimization problem is able to retain its QP form and, e.g., the ability to take into account pitching rate constraints.

4. *How can out-of-plane blade root bending moment fatigue load mitigation - a specific example of wind turbine loads - be incorporated within the developed IPC-CEMPC framework?*
   To model the out-of-plane blade root bending moment fatigue loads, it is important to be able to model the out-of-plane blade root bending moments. Finding a suitable model is difficult because widely used models make use of the pitch angle as an input. Such models are incompatible with the CEMPC framework wherein the pitch angle is an output that derives from the aerodynamic power, kinetic rotational energy, and the wind speed. Since alternative models in literature were found to be insufficiently accurate, a new model was developed. It relates the out-of-plane blade root bending moments with the thrust acting on each blade according to a coupled, static relationship that is updated at each time step based on the current blade root bending moment measurements and thrust model. To mitigate the out-of-plane blade root bending moment fatigue loading, two strategies are developed that aim to mitigate tilt and yaw moments. One strategy attempts to do so by the formulation of an objective that minimizes the tilt and yaw moments whilst the other places (soft) output constraints on these tilt and yaw moments.

5. *How do the developed CPC-based and IPC-based CEMPC frameworks perform compared to a respective benchmark controller when using a high-fidelity wind turbine simulator?*
   The performance of the controllers has been quantified according to three metrics, the actuator duty cycle (ADC), the damage equivalent loads (DEL), and the captured energy. With respect to the captured energy it is clear that particularly below the rated wind speed, the developed CEMPC frameworks capture less energy because of an

imperfect approximation of the available power. At and above the rated wind speed, the energy capture is fairly comparable, but still slightly less because of the rated power hard upper bound. As for the DEL, it is clear that the developed IPC-CEMPC framework in combination with the two load mitigation strategies are not able to realize a significant load reduction with respect to CPC. This is principally due to the unsuitability of the tilt and yaw moments as measures that are to be mitigated to effectuate fatigue load reductions, but a better out-of-plane blade root bending moment model would also be very useful. Regarding the actuation duty cycle it is clear that the CEMPC frameworks cause a greater degree of pitch actuation than their benchmark counterparts.

In summary, in light of the obtained results, it can be concluded that it is possible to extend the CEMPC framework to IPC by considering a blade-effective wind speed and a CPC-equivalent aerodynamic power for each blade. The CEMPC framework then does not change considerably with respect to the CPC implementation. This way of extending the CEMPC framework to IPC may not be the only feasible method, but has as a definite advantage that it is able to capitalize on the ability to also accommodate pitching rate constraints. However, as was demonstrated by the investigation of out-of-plane blade root bending moment fatigue loading, load mitigation in general may be difficult - but not necessarily impossible - using the IPC-CEMPC framework. This difficulty arises from the inability to directly use pitch angles as a free optimization variable with CEMPC. Moreover, care has to be taken when repurposing an existing load measure for use with CEMPC since the new features of this framework may render these measures less useful than expected. In addition, load models need to be sufficiently accurate, which has proven to be an obstacle to the effective implementation of load mitigation in this thesis.

6-2 Recommendations for Future Work

Given the problems that have arisen during this thesis, and the results that were obtained, a couple of recommendations for future work are formulated below.

1. *Develop a more efficient and accurate method to approximate the aerodynamic power constraints;*
   The obtained results indicate that below the rated wind speed, the power was not maximized as effectively as physically possible. This has to do with the fact that the piecewise-linear approximation of the power coefficient (and therefore available power) leads to an estimate of the maximum power coefficient that is slightly lower than the actual maximum power coefficient. To minimize this error, one can envision making use of a piecewise-linear power coefficient approximation that makes use of more affine segments. At the same time, less of these affine approximations that form the piecewise-linear approximation may be needed by exploiting estimates of the pitch and kinetic rotational energies from the previous solution. This latter suggestion would make use of the fact that most of the affine available power constraints, which together form the piecewise-linear approximation of the available power, are typically inactive.

2. *Further investigate how wind turbine loading can be accurately modelled and effectively mitigated within the developed IPC-CEMPC framework;*
   As discussed, the inability to directly use pitch angles as free optimization variables can make it difficult to mitigate certain forms of wind turbine loads such as out-of-plane blade root bending moment fatigue loads. It may therefore be useful to investigate whether it is possible to model the pitch angle in some way that is amenable to the CEMPC framework. One can, e.g., think of applying a linearization of the aerodynamic power in the same way as is done in [34]. Both data-driven and physics-driven models may be investigated.

   For the specific purpose of out-of-plane blade root bending moment modelling, perhaps linearization of the cone coefficient (which is a measure of the mean out-of-plane blade root bending moment as averaged over an entire rotor revolution [64]) can be used in a similar way as the linearization of the thrust coefficient in Section 2-2-6. Moreover, instead of using tilt and yaw moments, future work may consider simply minimizing the difference between subsequent out-of-plane blade root bending moments in a CEMPC framework. One may envision such an implementation by the inclusion of these differences in a quadratic or otherwise a linear objective (to represent the absolute value of these differences).

3. *Investigate the use of direct blade-effective wind speed estimation for the purpose of operation and load mitigation with IPC-CEMPC;*
   This thesis has made use of a rotor-effective wind speed that is augmented by a vertical wind shear model to arrive at blade-effective wind speeds, which were necessary for the IPC-CEMPC framework. It would be interesting to see whether direct estimation of these blade-effective wind speeds might improve the accuracy of predicted loads and kinetic rotational energies. An advantage of using the wind shear model in this thesis was that it is enabled the controller to easily make estimates of future blade-effective wind speeds based on the azimuth positions. Direct blade-effective wind speed estimation techniques will need to be augmented with some model that enables predictions to be formed of these blade-effective wind speeds. Perhaps the expected periodicity of such blade-effective wind speeds can be exploited using online subspace identification, as is done in, e.g., [65] for the purpose of Subspace Predictive Repetitive Control.

4. *Investigate the inclusion of actuator dynamics in the CEMPC framework*
   This thesis has not considered actuator dynamics. It would be interesting to see how it might be possible to incorporate or otherwise account for (particularly) pitch actuator dynamics within the CEMPC framework. If pitch actuator dynamics are impossible to incorporate within the CEMPC framework then the pitch angles provided by CEMPC might be considered a reference that another controller ought to track. In that case, model predictive controllers may be useful because they can incorporate information about anticipated future reference pitch angles from the CEMPC framework.

Appendix A

A bounded, convex, piecewise-linear fitting algorithm

As outlined in Section 3-8, there is need of a fitting procedure designed to find concave, piecewise-linear approximations of a function for which the function itself also acts as an upper bound. Whilst this appendix illustrates this optimization problem by referring to the maximization of the available power at a specific wind speed, as is relevant to Section 3-8, it is generally applicable to any similar bounded, concave, piecewise-linear fitting problem. A natural approach to find such a bounded, concave, piecewise-linear fit would be to impose concavity constraints on the affine elements of the approximation and try to maximize the area underneath it.

A-1 Non-convexity of the objective

Unfortunately, the resulting optimization problem is non-convex. To comprehend this, consider the objective, which consist of maximizing the sum of the areas underneath each of the n linear segments, which form trapezoids:

$$\max_{\underline{K}_{n+1}, \underline{\hat{P}}_{\text{av},n+1}} \sum_{i=1}^{n} \frac{\hat{P}_{\text{av},i+1} + \hat{P}_{\text{av},i}}{2}(K_{i+1} - K_i), \tag{A-1}$$

in which $\underline{K}_{n+1}$ and $\underline{\hat{P}}_{\text{av},n+1}$ are vectors containing the kinetic energy and available power optimization parameters.

To prove that this objective results in a non-convex optimization problem consider the equivalent objective

$$\min_{\underline{\Delta K}_n, \underline{S}_n} -\frac{1}{2}\sum_{i=1}^{n} S_i \Delta K_i, \tag{A-2}$$

in which $S_i = \hat{P}_{\text{av},i+1} + \hat{P}_{\text{av},i}$, $\Delta K_i = K_{i+1} - K_i$, and the vectors $\underline{\Delta K}_n$ and $\underline{S}_n$ represent vectors containing all of the optimization variables of ΔK_i and S_i respectively. Stacking the vector $\underline{\Delta K}_n$ on top of $\underline{S}_n$ to form a vector with all of the optimization parameters, one obtains a hessian that is given by

$$H = \begin{bmatrix} 0 & -\frac{1}{2}I_n \\ -\frac{1}{2}I_n & 0 \end{bmatrix}, \tag{A-3}$$

in which the matrix I_n is an $(n \times n)$ identity matrix. To show that this matrix is not positive semi-definite, consider that for H to be positive semi-definite the following has to be true:

$$\begin{bmatrix} \underline{\Delta K}_n^\top & \underline{S}_n^\top \end{bmatrix} H \begin{bmatrix} \underline{\Delta K}_n \\ \underline{S}_n \end{bmatrix} \geq 0, \quad \forall \underline{\Delta K}_n, \underline{S}_n. \tag{A-4}$$

By choosing the first elements of both $\underline{\Delta K}_n$, and $\underline{S}_n$ to be one, whilst the rest is zero, one can quickly verify that Eq. (A-4) is not true, meaning that H is not positive semi-definite, and therefore the quadratic objective function is not suitable for a convex optimization framework.

A-2 A new convex, piecewise-linear fitting algorithm

Since the maximization of the area underneath the piecewise-linear approximation consisting of a prescribed number of n constraints leads to a non-convex objective, it is desirable to consider a different approach. Moreover, since the available power is calculated from power coefficient data, it is impractical to try to describe the upper bound given by Eq. (3-41) analytically. This rules out a direct implementation of a nonlinear solver as is done in Section 3-5-2.

The method developed here is based on two steps. First, one maximizes the area under a concave, piecewise-linear approximation. Secondly the number of linear constraints used is reduced to the desired number n by iteratively removing the linear constraints that contribute the least to the area underneath the approximation.

A-2-1 Approximating the available power by solving a linear program

For a specific wind speed, one starts by obtaining a vector that contains all of the actual available powers $\underline{P}_{\text{av}}$ that corresponds to a vector composed of a given, regularly spaced set of kinetic energies $\underline{K}$. This gives rise to a linear programming (LP) problem:

$$\min_{\hat{\underline{P}}_{\text{av}}} -c^\top \hat{\underline{P}}_{\text{av}} \tag{A-5}$$

$$\text{s.t.} \quad \hat{\underline{P}}_{\text{av}} \leq \underline{P}_{\text{av}}, \tag{A-6}$$

$$A_{\text{con}} \hat{\underline{P}}_{\text{av}} \leq 0, \tag{A-7}$$

in which $\hat{\underline{P}}_{\text{av}}$ is the vector with approximated available powers that is to be optimized, c is a vector that reflects the trapezoidal integration method used to find the area underneath the

piecewise-linear approximation, as given by

$$c = \begin{bmatrix} \frac{1}{2} & 1 & 1 & \cdots & 1 & 1 & \frac{1}{2} \end{bmatrix}^\top, \tag{A-8}$$

and A_{con} is given by

$$A_{\text{con}} = \begin{bmatrix} 1 & -2 & 1 & & & \\ & 1 & -2 & 1 & & \\ & & \ddots & \ddots & \ddots & \\ & & & 1 & -2 & 1 \end{bmatrix}. \tag{A-9}$$

The key to understanding this optimization problem formulation is that the kinetic energies are regularly spaced. It explains why the concavity constraint is fully described by Eq. (A-7) and Eq. (A-9), and the objective as presented by Eq. (A-5) and Eq. (A-8) has been simplified to not feature the constant change in kinetic energies (ΔK) between adjacent elements.

The solution to this LP will provide a vector with approximations of the available power for the regularly spaced kinetic energies that adheres to the upper bounds given by Eq. (A-6).

A-2-2 Reducing the number of linear constraints used

In essence, consecutive points defined by consecutive elements of the vectors $\underline{\hat{P}}_{\text{av}}$ and $\underline{K}$ define a linear constraint that, in part, shapes the concave, piecewise-linear approximation. To reduce the number of linear constraints to the desired number n, a critical look is taken at the contribution of each point (excluding the beginning and end points) to the total area underneath the piecewise-linear approximation. Using the trapezoidal integration method, the contribution of the i^{th} point is given by

$$\Delta A_{\text{av,i}} = \frac{\hat{P}_{\text{av,i}} + \hat{P}_{\text{av,i}-1}}{2}(K_i - K_{i-1}) + \frac{\hat{P}_{\text{av,i}+1} + \hat{P}_{\text{av,i}}}{2}(K_{i+1} - K_i) - \frac{\hat{P}_{\text{av,i}+1} + \hat{P}_{\text{av,i}-1}}{2}(K_{i+1} - K_{i-1}). \tag{A-10}$$

To find an approximation with n linear constraints, $n+1$ points are needed. Hence, one may calculate the contribution of the various points, discard the point with the lowest contribution as given by Eq. (A-10), and repeat this procedure until only $n+1$ points are left. From these remaining points, one can easily distill the n linear inequality constraints that form the bounded, concave, piecewise-linear approximation.

A drawback of the method developed in this section is that unlike with Eq. (A-1), a discrete spectrum of kinetic energies is considered. Hence, to reduce the error of this approximation, one may increase the number of considered available powers and kinetic energies by means of interpolation of the original $\underline{P}_{\text{av}}$ and $\underline{K}$ vectors. Since the original, actual available power characteristic is not necessarily convex, it is important to include the original values of K in the new $\underline{K}$ vector. This can be accomplished by reducing the difference between consecutive

K values by an integer factor. The final algorithm then looks as shown by Algorithm 1.

Algorithm 1: Bounded, convex, piecewise-linear fitting algorithm

Result: n linear constraints that approximate the available power
Set desired number of linear constraints used for the approximation: n;
Obtain P_{av} data for the relevant K interval and wind speed;
if ΔK *is not small enough* **then**
    Reduce ΔK by an integer factor;
    Interpolate to find new P_{av} values;
end
Solve the LP problem posed by Eq. (A-5) to Eq. (A-7);
Compute contribution of all points (except the beginning and end points) to the area underneath the piecewise-linear approximation according to Eq. (A-10);
while *Number of points in* $\underline{\hat{P}}_{\text{av}} > n + 1$ **do**
    Determine the point with the lowest contribution: i;
    Remove the i^{th} point from $\underline{\hat{P}}_{\text{av}}$ and $\underline{K}$;
    Recalculate the contributions of the $(i-1)^{\text{th}}$ and (new) i^{th} points;
end
Determine the linear constraints formed by the remaining points in $\underline{\hat{P}}_{\text{av}}$ and $\underline{K}$;

Appendix B

Campbell Diagram

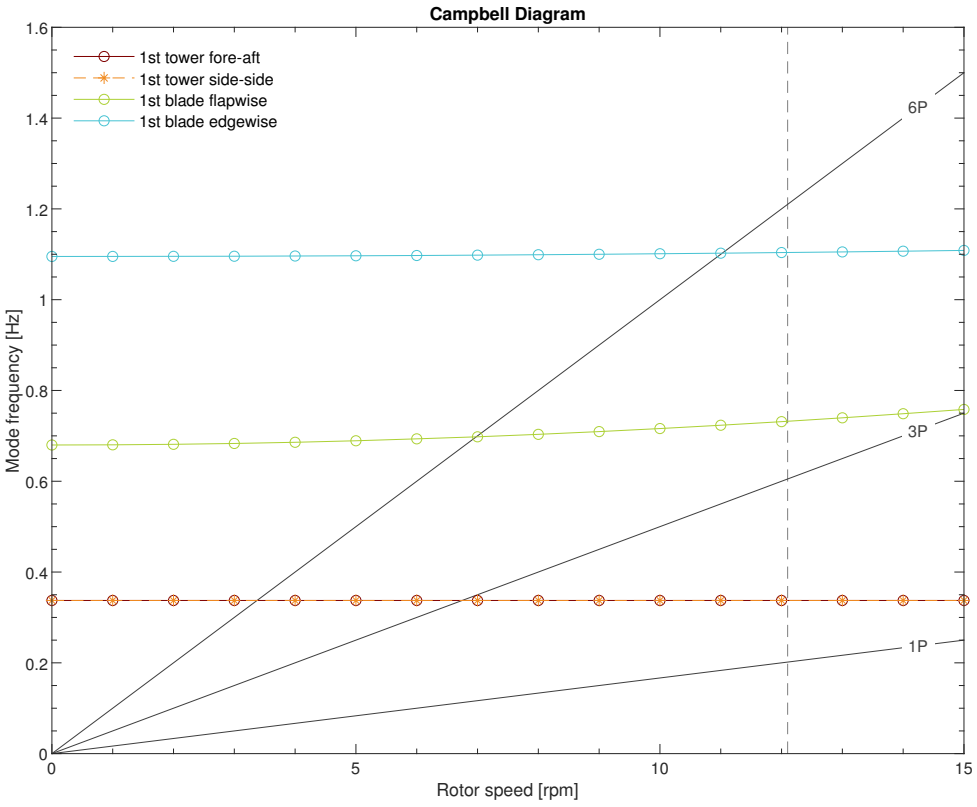

Figure B-1: A Campbell Diagram that demonstrates the natural frequencies of the NREL 5 MW turbine [37] as a function of the rotor speed. The vertical dashed line indicates the rated rotational speed. The 1P, 3P, and 6P lines illustrate the frequencies that correspond to, respectively, the rotor speed, three times the rotor speed, and six times the rotor speed.

Bibliography

[1] Core Writing Team, R. Pachauri, and L. Meyer, "Climate Change 2014: Synthesis Report," tech. rep., IPCC, Geneva, 2015.

[2] UNFCCC, "Paris Agreement," 2015.

[3] V. Masson-Delmotte, H.-O. Pörtner, J. Skea, P. Zhai, D. Roberts, P. R. Shukla, A. Pirani, W. Moufouma-Okia, C. Péan, R. Pidcock, S. Connors, J. B. R. Matthews, Y. Chen, X. Zhou, M. I. Gomis, E. Lonnoy, T. Maycock, M. Tignor, and T. Waterfield, "Global Warming of 1.5°C," tech. rep., IPCC, 2019.

[4] IRENA, "Future of Wind: Deployment, investment, technology, grid integration and socio-economic aspects (A Global Energy Transformation Paper)," tech. rep., International Renewable Energy Agency (IRENA), Abu Dhabi, 2019.

[5] D. L. Hoffman and T. S. Molinski, "How new technology developments will lower wind energy costs," in *2009 CIGRE / EEE PES Joint Symposium: Integration of Wide-Scale Renewable Resources into the Power Delivery System*, IEEE, 2009.

[6] "Offshore Wind Outlook 2019," tech. rep., IEA, 2019.

[7] T. K. Barlas and G. A. M. van Kuik, "Review of state of the art in smart rotor control research for wind turbines," *Progress in Aerospace Sciences*, vol. 46, no. 1, pp. 1–27, 2010.

[8] L. Y. Pao and K. E. Johnson, "Control of Wind Turbines: Approaches, Challenges, and Recent Developments," *IEEE Control Systems Magazine*, vol. 31, no. 2, pp. 44–62, 2011.

[9] E. A. Bossanyi, "Further Load Reductions with Individual Pitch Control," *Wind Energy*, vol. 8, no. 4, pp. 481–485, 2005.

[10] J. H. Laks, L. Y. Pao, and A. D. Wright, "Control of wind turbines: Past, present, and future," *Proceedings of the American Control Conference*, pp. 2096–2103, 2009.

[11] E. J. N. Menezes, A. M. Araújo, and N. S. B. da Silva, "A review on wind turbine control and its associated methods," *Journal of Cleaner Production*, vol. 174, pp. 945–953, 2018.

[12] M.-H. Chiang, "A novel pitch control system for a wind turbine driven by a variable-speed pump-controlled hydraulic servo system," *Mechatronics*, vol. 21, no. 4, pp. 753–761, 2011.

[13] J. G. Njiri and D. Söffker, "State-of-the-art in wind turbine control: Trends and challenges," *Renewable and Sustainable Energy Reviews*, vol. 60, pp. 377–393, 2016.

[14] Q. Lu, R. Bowyer, and B. L. Jones, "Analysis and design of Coleman transform-based individual pitch controllers for wind-turbine load reduction," *Wind Energy*, vol. 18, no. 8, pp. 1451–1468, 2015.

[15] E. A. Bossanyi, "Individual Blade Pitch Control for Load Reduction," *Wind Energy*, vol. 6, no. 2, pp. 119–128, 2003.

[16] A. K. Pamososuryo, "Enhancement of Conventional IPC Decoupling by Inclusion of an Azimuth Offset," Master's thesis, 2018.

[17] G. S. Bir, "User's guide to MBC3: Multi-Blade Coordinate Transformation Code for 3-Bladed Wind Turbines," Tech. Rep. September, NREL, 2010.

[18] S. P. Mulders, A. K. Pamososuryo, G. E. Disario, and J.-W. van Wingerden, "Analysis and optimal individual pitch control decoupling by inclusion of an azimuth offset in the multiblade coordinate transformation," *Wind Energy*, vol. 22, no. 3, pp. 341–359, 2019.

[19] S. P. Mulders and J.-W. van Wingerden, "On the averaging in the Multi-blade Coordinate transformations for wind turbines: an $\mathcal{H}_\infty$ model matching approach," in *2018 IEEE Conference on Control Technology and Applications (CCTA 2018)*, pp. 1631–1637, IEEE, 2018.

[20] M. Mirzaei, L. C. Henriksen, N. K. Poulsen, H. H. Niemann, and M. H. Hansen, "Individual Pitch Control Using LIDAR Measurements," in *Proceedings of the IEEE International Conference on Control Applications*, (Dubrovnik, Croatia), pp. 1646–1651, IEEE, 2012.

[21] Y. Liu, R. J. Patton, and S. Shi, "Wind turbine asymmetrical load reduction with pitch sensor fault compensation," *Wind Energy*, vol. 23, no. 7, pp. 1523–1541, 2020.

[22] K. Selvam, S. Kanev, J.-W. van Wingerden, T. van Engelen, and M. Verhaegen, "Feedback–feedforward individual pitch control for wind turbine load reduction," *International Journal of Robust and Nonlinear Control*, vol. 19, pp. 72–91, 2009.

[23] M. Vali, J.-W. van Wingerden, and M. Kühn, "Optimal Multivariable Individual Pitch Control for Load Reduction of Large Wind Turbines," *Proceedings of the American Control Conference*, vol. 2016-July, pp. 3163–3169, 2016.

[24] S. Schuler, D. Schlipf, P. W. Cheng, and F. Allgöwer, "ℓ_1-optimal control of large wind turbines," *IEEE Transactions on Control Systems Technology*, vol. 21, no. 4, pp. 1079–1089, 2013.

[25] A. Jain, G. Schildbach, L. Fagiano, and M. Morari, "On the design and tuning of linear model predictive control for wind turbines," *Renewable Energy*, vol. 80, pp. 664–673, 2015.

[26] E. F. Camacho and C. Bordons, *Model Predictive Control*. Springer, 2 ed., 2007.

[27] A. Bemporad, "Model Predictive Control Design : New Trends and Tools," in *Proceedings of the 45th IEEE Conference on Decision and Control*, pp. 6678–6683, IEEE, 2006.

[28] V. Petrović, M. Jelavić, and M. Baotić, "MPC framework for constrained wind turbine individual pitch control," *Wind Energy*, pp. 1–15, 2020.

[29] M. D. Spencer, K. A. Stol, P. Charles, J. E. Cater, and S. E. Norris, "Model predictive control of a wind turbine using short-term wind field predictions," *Wind Energy*, vol. 16, no. 3, pp. 417–434, 2013.

[30] A. Koerber and R. King, "Combined feedback-feedforward control of wind turbines using state-constrained model predictive control," *IEEE Transactions on Control Systems Technology*, vol. 21, no. 4, pp. 1117–1128, 2013.

[31] M. S. Mahmoud and M. O. Oyedeji, "Adaptive and Predictive Control Strategies for Wind Turbine Systems: A Survey," *IEEE/CAA Journal of Automatica Sinica*, vol. 6, no. 2, pp. 364–378, 2019.

[32] D. Schlipf, P. Grau, S. Raach, R. Duraiski, J. Trierweiler, and P. W. Cheng, "Comparison of Linear and Nonlinear Model Predictive Control of Wind Turbines Using LIDAR," in *Proceedings of the American Control Conference*, pp. 3742–3747, American Automatic Control Council, 2014.

[33] T. G. Hovgaard, S. Boyd, and J. B. Jørgensen, "Model predictive control for wind power gradients," *Wind Energy*, 2013.

[34] M. L. Shaltout, Z. Ma, and D. Chen, "An Adaptive Economic Model Predictive Control Approach for Wind Turbines," *Journal of Dynamic Systems, Measurement and Control, Transactions of the ASME*, vol. 140, no. 5, 2018.

[35] J. B. Rawlings, D. Angeli, and C. N. Bates, "Fundamentals of Economic Model Predictive Control," in *Proceedings of the IEEE Conference on Decision and Control*, pp. 3851–3861, IEEE, 2012.

[36] V. Petrović, M. Jelavić, and M. Baotić, "Advanced control algorithms for reduction of wind turbine structural loads," *Renewable Energy*, vol. 76, pp. 418–431, 2015.

[37] J. Jonkman, S. Butterfield, W. Musial, and G. Scott, "Definition of a 5-MW Reference Wind Turbine for Offshore System Development," tech. rep., NREL, 2009.

[38] T. van den Boom and B. De Schutter, *Optimization in Systems and Control*. TU Delft, 2018.

[39] A. Magnani and S. P. Boyd, "Convex piecewise-linear fitting," *Optimization and Engineering*, vol. 10, no. 1, pp. 1–17, 2009.

[40] M. Guadayol Roig, *Application of Model Predictive Control to Wind Turbines*. PhD thesis, ETH Zurich, 2017.

[41] P. S. Cisneros, S. Voss, and H. Werner, "Efficient Nonlinear Model Predictive Control via quasi-LPV representation," *2016 IEEE 55th Conference on Decision and Control, CDC 2016*, pp. 3216–3221, 2016.

[42] R. Ortega, F. Mancilla-David, and F. Jaramillo, "A globally convergent wind speed estimator for wind turbine systems," *International Journal of Adaptive Control and Signal Processing*, vol. 27, pp. 413–425, 2013.

[43] Y. Liu, A. K. Pamososuryo, R. Ferrari, and J.-W. van Wingerden, "The Immersion and Invariance Wind Speed Estimator Revisited and New Results." under review.

[44] A. Lasheen, M. S. Saad, H. M. Emara, and A. L. Elshafei, "Continuous-time tube-based explicit model predictive control for collective pitching of wind turbines," *Energy*, vol. 118, pp. 1222–1233, 2017.

[45] G. F. Franklin, J. D. Powell, and M. Workman, *Digital Control of Dynamic Systems*. Ellis-Kagle Press, 3 ed., 1997.

[46] F. D. Bianchi, H. De Battista, and R. J. Mantz, *Wind Turbine Control Systems*. Springer, 2009.

[47] S. Boyd and L. Vandenberghe, *Convex Optimization*. 7 ed., 2009.

[48] S. Gros, "An economic NMPC formulation for Wind Turbine Control," *Proceedings of the IEEE Conference on Decision and Control*, pp. 1001–1006, 2013.

[49] J. Löfberg, "YALMIP: A toolbox for modeling and optimization in MATLAB," in *Proceedings of the IEEE International Symposium on Computer-Aided Control System Design*, pp. 284–289, 2004.

[50] Mosek ApS, *MOSEK Rmosek Package*, 2021.

[51] T. Burton, D. Sharpe, N. Jenkins, and E. Bossanyi, *Wind Energy Handbook*. Wiley, 2001.

[52] E. Hau, *Wind Turbines: Fundamentals, Technologies, Application, Economics*. Heidelberg, Germany: Springer, 3 ed., 2013.

[53] T. G. van Engelen and E. L. van der Hooft, "Individual Pitch Control Inventory," tech. rep., ECN, Petten, the Netherlands, 2005.

[54] T. G. van Engelen, "Design Model and Load Reduction Assessment for Multi-rotational Mode Individual Pitch Control (Higher Harmonics Control)," in *European Wind Energy Conference and Exhibition 2006*, vol. 2, pp. 1335–1342, 2006.

[55] M. Geyler and P. Caselitz, "Individual blade pitch control design for load reduction on large wind turbines," *European Wind Energy Conference and Exhibition 2007, EWEC 2007*, vol. 1, no. May, pp. 141–150, 2007.

[56] V. Pascu, S. Kanev, and J.-W. van Wingerden, "Adaptive tower damping control for offshore wind turbines," *Wind Energy*, vol. 20, pp. 765–781, 2017.

[57] G. E. Disario, "On the effects of an azimuth offset in the MBC-transformation used by IPC for wind turbine fatigue load reductions," Master's thesis, Delft University of Technology, 2018.

[58] J. M. Jonkman and Buhl Jr. Marshall L., "FAST User's Guide," 2007.

[59] B. J. Jonkman and J. M. Jonkman, "Fast v8.16.00a-bjj," tech. rep., National Renewable Energy Laboratory (NREL), Golden, CO., 2016.

[60] E. A. Bossanyi, "The Design of Closed Loop Controllers for Wind Turbines," *Wind Energy*, vol. 3, no. 3, pp. 149–163, 2000.

[61] C. Bottasso, F. Campagnolo, A. Croce, and C. Tibaldi, "Optimization-based study of bend–twist coupled rotorblades for passive and integrated passive/activeload alleviation," *Wind Energy*, no. August 2012, pp. 1149–1166, 2013.

[62] H. B. Hendriks and B. H. Bulder, "Fatigue Equivalent Load Cycle Method," no. October, pp. 1–18, 1995.

[63] P. Ragan and L. Manuel, "Comparing estimates of wind turbine fatigue loads using time-domain and spectral methods," *Wind Engineering*, vol. 31, no. 2, pp. 83–99, 2007.

[64] J. Schreiber, C. L. Bottasso, and M. Bertelè, "Field testing of a local wind inflow estimator and wake detector," *Wind Energy Science*, pp. 867–884, 2020.

[65] S. T. Navalkar, J.-W. van Wingerden, E. van Solingen, T. Oomen, E. Pasterkamp, and G. A. M. van Kuik, "Subspace predictive repetitive control to mitigate periodic loads on large scale wind turbines," *Mechatronics*, vol. 24, pp. 916–925, 2014.

Glossary

List of Acronyms

MPC	model predictive control
EMPC	economic model predictive control
CEMPC	convex economic model predictive control
BEM	blade element momentum
IPCC	Intergovernmental Panel on Climate Change
IPC	individual pitch control
CPC	collective pitch control
LQR	linear quadratic regulator
LQG	linear quadratic Gaussian
MBC	multi-blade coordinate
LTI	linear time-invariant
SISO	single-input single-ouput
MIMO	multiple-input multiple-output
PI	proportional-integral
PID	proportional-integral-derivative
LIDAR	light detection and ranging
LP	linear programming
QP	quadratic programming
I&I	immersion and invariance
qLPV	quasi-linear parameter-varying
FAST	Fatigue, Aerodynamics, Structures, and Turbulence
ADC	actuator duty cycle
DEL	damage equivalent loads

List of Symbols

β	Pitch angle [deg]
η	Efficiency [-]
λ	Tip speed ratio [-]
ω	Rotational speed [rad s^{-1}]
$\mathbf{u}$	System inputs
$\mathbf{x}$	System states
A	Rotor area [m^2]
C	Coefficient [-]
d	Disturbance
J	Rotational inertia (of the drive train) [kg m^2]
K	Rotational kinetic energy [J]
N	Gearbox ratio [-]
R	Rotor radius [m]
T	Torque [N m]
t	Time [s]
v	Wind speed [m s^{-1}]
k	Time step number within the prediction horizon
m	MPC solution iteration counter
n	Number of piecewise-linear approximations
$_c$	Coefficient
$_d$	Discrete
$_g$	Generator
$_{max}$	Maximum
$_{me}$	Measured
$_{min}$	Minimum
$_{opt}$	Optimal
$_P$	Power
$_p$	Prediction horizon
$_{ref}$	Reference
$_r$	Rotor
$_s$	Sampling
$_v$	Scheduled based on the wind speed
$_w$	Wind
$_b$	Blade index
$_{lb}$	Lower bound
$_{ub}$	Upper bound
rpm	Rotations per minute